Time-Frequency and Fractal based analysis of EEG and sEMG signals under varying load conditions

A thesis submitted towards partial fulfilment of the requirements for the award of degree of

MASTER OF ENGINEERING

In

Biomedical Engineering

Submitted by

Anish Kumar Bardhan

Exam Roll No: **M4BMD22013**

Class Roll No. **002030201014**

Registration No. **154638 of 2020-2021**

Under the guidance of

Prof. (Dr.) Monisha Chakraborty

Professor

School of Bioscience and Engineering

Jadavpur University

Kolkata 700032

Course affiliated to:

Faculty of Engineering and Technology

Jadavpur University

Kolkata 700032

India

2022

M.E (Biomedical Engineering) course affiliated to
Faculty of Engineering and Technology
Jadavpur University
Kolkata - 700032

CERTIFICATE OF RECOMMENDATION

This is to certify that the thesis entitled "**Time-Frequency and Fractal based analysis of EEG and sEMG signals under varying load conditions**" is a bonafide work carried out by **ANISH KUMAR BARDHAN** under my supervision and guidance for partial fulfillment of the requirement for Post Graduate Degree of Master of Engineering in Biomedical Engineering during the academic session 2020-2022.

THESIS ADVISOR
Prof. (Dr.) Monisha Chakraborty
Professor
School of Bioscience and Engineering
Jadavpur University
Kolkata -700032

DIRECTOR
School of Bioscience and Engineering
Jadavpur University
Kolkata -700032

DEAN
Faculty Council of Interdisciplinary Studies, Law and Management
Jadavpur University
Kolkata -700032

M.E (Biomedical Engineering) course affiliated to
Faculty of Engineering and Technology
Jadavpur University
Kolkata - 700032

Certificate of Approval**

This foregoing thesis is hereby approved as a creditable study of an Engineering subject carried out and presented in a manner satisfactory to warrant its acceptance as a prerequisite to the degree for which it has been submitted. It is understood that by this approval the undersigned do not necessarily endorse or approve any statement made opinion expressed or conclusion drawn therein but approve the thesis only for the purpose for which it has been submitted.

Prof. (Dr.) MONISHA CHAKRABORTY
(Thesis Advisor)
Professor
School of Bio-Science and Engineering
Jadavpur University
Kolkata-700032

Signature of Examiner

** Only in case the thesis is approved

DECLARATION OF ORIGINALITY AND COMPLIANCE OF ACADEMIC ETHICS

I hereby declare that this thesis contains literature survey and original research work by the undersigned candidate, as part of his Master of Engineering in Biomedical Engineering studies during academic session 2020-2022.

All information in this document has been obtained and presented in accordance with academic rules and ethical conduct.

I also declare that, as required by this rules and conduct. I have fully cited and referred all material and results that are not original to this work.

NAME: **ANISH KUMAR BARDHAN**

CLASS ROLL NO. **002030201014**

EXAMINATION ROLL NO. **M4BMD22013**

REGISTRATION NO. **154638 of 2020-2021**

THESIS TITLE: **Time-Frequency and Fractal based analysis of EEG and sEMG signals under varying load conditions.**

SIGNATURE: **DATE:**

Anish thesis

ORIGINALITY REPORT

7%	4%	4%	2%
SIMILARITY INDEX	INTERNET SOURCES	PUBLICATIONS	STUDENT PAPERS

PRIMARY SOURCES

1	mafiadoc.com Internet Source	1%
2	dspace.jdvu.ac.in Internet Source	<1%
3	Submitted to University of Sydney Student Paper	<1%
4	Debanjan Parbat, Monisha Chakraborty. "A Novel Methodology to study the Cognitive Load Induced EEG Complexity Changes: Chaos, Fractal and Entropy based approach", Biomedical Signal Processing and Control, 2021 Publication	<1%
5	www.ncbi.nlm.nih.gov Internet Source	<1%
6	en.wikipedia.org Internet Source	<1%
7	Mahmoud Al-Kadi, Mamun Reaz, Mohd Ali. "Evolution of Electroencephalogram Signal	<1%

Analysis Techniques during Anesthesia", Sensors, 2013
Publication

8	Monisha Chakraborty, Debanjan Parbat. "Fractal analysis of sEMG signal under varying load conditions", 2016 2nd International Conference on Control, Instrumentation, Energy & Communication (CIEC), 2016 Publication	<1 %
9	K. Asaduzzaman. "A Study on Discrete Wavelet-Based Noise Removal from EEG Signals", Advances in Experimental Medicine and Biology, 2010 Publication	<1 %
10	HAMIDREZA NAMAZI. "DECODING OF HAND GESTURES BY FRACTAL ANALYSIS OF ELECTROMYOGRAPHY (EMG) SIGNAL", Fractals, 2019 Publication	<1 %
11	Mohd Nabil Bin Muhtazaruddin, Goro Fujita. "Distribution network power loss by using Artificial Bee Colony", 2013 48th International Universities' Power Engineering Conference (UPEC), 2013 Publication	<1 %
12	uwspace.uwaterloo.ca Internet Source	<1 %

13	dokumen.pub Internet Source	<1 %
14	SWETADRI SAMADDER, KOUSHIK GHOSH, TAPASENDRA BASU. "FRACTAL ANALYSIS OF PRIME INDIAN STOCK MARKET INDICES", Fractals, 2013 Publication	<1 %
15	HAMIDREZA NAMAZI. "FRACTAL-BASED CLASSIFICATION OF ELECTROMYOGRAPHY (EMG) SIGNAL IN RESPONSE TO BASIC MOVEMENTS OF THE FINGERS", Fractals, 2019 Publication	<1 %
16	Soudeh. H. Yaghouti, Sanika. S. Patankar, Jayant. V. Kulkarni. "Condition monitoring of rotary machinery using Continuous Wavelets", 2012 IEEE International Conference on Computational Intelligence and Computing Research, 2012 Publication	<1 %
17	Al-Kadi, Mahmoud, Mamun Reaz, Mohd Ali, and Chian Liu. "Reduction of the Dimensionality of the EEG Channels during Scoliosis Correction Surgeries Using a Wavelet Decomposition Technique", Sensors, 2014. Publication	<1 %
18	issuu.com Internet Source	<1 %

19	M. B. I. Reaz. "Techniques of EMG signal analysis: detection, processing, classification and applications", Biological Procedures Online, 12/2006 Publication	<1 %
20	Submitted to Queen Mary and Westfield College Student Paper	<1 %
21	www.scribd.com Internet Source	<1 %
22	www.tustin.k12.ca.us Internet Source	<1 %
23	André L.V. Coelho, Clodoaldo A.M. Lima. "Assessing fractal dimension methods as feature extractors for EMG signal classification", Engineering Applications of Artificial Intelligence, 2014 Publication	<1 %
24	jwcn-eurasipjournals.springeropen.com Internet Source	<1 %
25	doktori.bibl.u-szeged.hu Internet Source	<1 %
26	Varsha Harpale, Vinayak Bairagi. "An adaptive method for feature selection and extraction for classification of epileptic EEG signal in significant states", Journal of King Saud	<1 %

	University - Computer and Information Sciences, 2018 Publication	
27	hdl.handle.net Internet Source	<1 %
28	researchbank.rmit.edu.au Internet Source	<1 %
29	scholar.sun.ac.za Internet Source	<1 %
30	"Clinical Electroencephalography", Springer Science and Business Media LLC, 2019 Publication	<1 %
31	Submitted to Mahidol University Student Paper	<1 %
32	Submitted to University of Queensland Student Paper	<1 %
33	Amandeep Bisht, Preeti Singh, Chamandeep Kaur, Sunil Agarwal, Manisha Ajmani. "Progress and Challenges in Physiological Artifacts' Detection in Electroencephalographic Readings", Current Medical Imaging Formerly Current Medical Imaging Reviews, 2022 Publication	<1 %
34	Submitted to Derby College Student Paper	<1 %

35	Submitted to Liverpool John Moores University Student Paper	<1 %
36	Submitted to Mansoura University Student Paper	<1 %
37	"Biomedical Engineering and its Applications in Healthcare", Springer Science and Business Media LLC, 2019 Publication	<1 %
38	Submitted to University of Keele Student Paper	<1 %
39	eprints.usq.edu.au Internet Source	<1 %
40	Cornelius Borck. "Vital brains: On the entanglement of media, minds, and models", Elsevier BV, 2017 Publication	<1 %
41	Submitted to Jamia Milia Islamia University Student Paper	<1 %
42	V. R. Paramesura Rao, C. A. Hewawasam Puwakpitiyage, M. S. A. Muhammad Azizi, W. J. Tee, R. K. Murugesan, M. D. Hamzah. "Emotion Recognition in E-Commerce Activities using EEG-based Brain Computer Interface", 2018 Fourth International	<1 %

	Conference on Advances in Computing, Communication & Automation (ICACCA), 2018 Publication	
43	link.springer.com Internet Source	<1 %
44	silo.pub Internet Source	<1 %
45	www.cutr.usf.edu Internet Source	<1 %
46	www.dalescott.net Internet Source	<1 %
47	www.ijert.org Internet Source	<1 %
48	Banerjee, Anwesha, Monalisa Pal, Shreyasi Datta, D.N. Tibarewala, and Amit Konar. "Voluntary eye movement controlled electrooculogram based multitasking graphical user interface", International Journal of Biomedical Engineering and Technology, 2015. Publication	<1 %
49	Chi-Wen Hsieh, Hsiao-Chuan Liu, Chih-Yen Chen, Yi-Hong Chou, Chui-Mei Tiu, Ying-Che Hsu, Din-Yuen Chan. "An investigation of pixel resonance phenomenon in color imaging: the multiple interpretations of people with color	<1 %

vision deficiency", Multimedia Tools and Applications, 2014
Publication

50	Yangchicheng Shen. "Machine Learning Based Epileptic Seizure Detection for Responsive Neurostimulator System Optimization", Journal of Physics: Conference Series, 2020 Publication	<1 %
51	www.allsoporganicbutcher.com.au Internet Source	<1 %
52	www.comtechefdata.com Internet Source	<1 %
53	M.M. Tawfik, M.M. Morcos. "A novel approach for fault location on transmission lines", IEEE Power Engineering Review, 1998 Publication	<1 %
54	Manabu Aoyagi, Hiroyuki Watanabe, Yoshiro Tomikawa, Takehiro Takano. "Spurious-Mode Control of Same-Phase Drive-Type Ultrasonic Motor", Japanese Journal of Applied Physics, 2002 Publication	<1 %
55	Reza Sharbati, Faramarz Khoshnoudian, Mohammadreza Koopialipoor, M. M. Tahir. "Applying dual-tree complex discrete wavelet transform and gamma modulating function	<1 %

for simulation of ground motions", Engineering with Computers, 2019
Publication

56	ntnuopen.ntnu.no Internet Source	<1 %
57	www.frontiersin.org Internet Source	<1 %
58	www.researchgate.net Internet Source	<1 %
59	www.springerprofessional.de Internet Source	<1 %
60	www.statpearls.com Internet Source	<1 %
61	"Canine Sports Medicine and Rehabilitation", Wiley, 2018 Publication	<1 %
62	Akagi. "Combined Series and Shunt Power Conditioners", Instantaneous Power Theory and Applications to Power Conditioning, 02/02/2007 Publication	<1 %
63	Submitted to Colorado State University Fort Collins Student Paper	<1 %
64	M.S. Hussain. "Electromyography signal analysis using wavelet transform and higher	<1 %

order statistics to determine muscle contraction", Expert Systems, 02/2009
Publication

65	Oung, Qi, Hariharan Muthusamy, Hoi Lee, Shafriza Basah, Sazali Yaacob, Mohamed Sarillee, and Chia Lee. "Technologies for Assessment of Motor Disorders in Parkinson's Disease: A Review", Sensors, 2015. Publication	<1 %
66	acikbilim.yok.gov.tr Internet Source	<1 %
67	d-nb.info Internet Source	<1 %
68	docplayer.net Internet Source	<1 %
69	dspace.bracu.ac.bd:8080 Internet Source	<1 %
70	patents.google.com Internet Source	<1 %
71	repository.sustech.edu Internet Source	<1 %
72	tel.archives-ouvertes.fr Internet Source	<1 %
73	vdocument.in Internet Source	<1 %

74	www.biomeccon.org Internet Source	<1%
75	www.nat-hazards-earth-syst-sci.net Internet Source	<1%
76	Martin Furr, Stephen Reed. "Equine Neurology", Wiley, 2015 Publication	<1%

Exclude quotes	On	Exclude matches	Off
Exclude bibliography	On		

Dedicated for its purpose

ACKNOWLEDGEMENT

I want to thank my respected thesis adviser**, Professor (Dr.) Monisha Chakraborty, Professor, School of Bioscience and Engineering, Jadavpur University**, for all her help and guidance during this process, as well as for establishing chances for me to engage in an exciting area of research. Without her consistent support and advice, the thesis could not have been finished. Thanks to our respected director **Dr. Piyali Basak, Director, School of Bioscience and Engineering** and all other esteemed faculty members of the School of Bioscience and Engineering at Jadavpur University, I can pursue my academic goals.

I would also like to thank my respected senior **Nilotpal Das, PhD Scholar, CSIR senior research fellow (SRF) in Biomedical Instrumentation Laboratory which is under School of Bio-Science and Engineering department at Jadavpur University**, for his unconditional support and motivation which made this an enjoyable session.

Thanks to all my fellow classmates for their dedicated efforts in assisting me.

All members of the School of Bioscience and staffs are to be thanked for their kindness and cooperation throughout the thesis writing process.

Finally, I want to show my gratitude to my parents, who are a never-ending source of motivation, inspiration, and encouragement for me to continue my academic career.

DATE: ANISH KUMAR BARDHAN

PREFACE

Maintaining physical health is of utmost priority. Exercises keep human body fit and fine. So doing some physical exercises is very good for maintaining for physical health. There are many people who lift weights or dumbbells of different kilograms on a daily purpose for maintaining their physical fitness. As these dumbbells are of various weights, the person must apply different force for lifting different weights, that is, for lifting a weight of 1 kilogram the force applied will be different than when the person is lifting a weight of 5 kilogram. Brain is the main functional unit of the human body which controls the activities of various systems including the muscular system. So, there is a connection between brain and muscles. But what are the actual changes occurring in the muscles and simultaneously in the associated center of brain is the source of this work. For estimating the above-mentioned changes, feature extraction of EEG and EMG data are required. EMG and EEG data are non-stationary and transient, so, feature extraction is difficult process. For analyzing the changes of muscles and brain, frequency and time domain analysis of EMG and EEG signals under varying load condition is performed.

Chapter 1 starts with brief introduction which is helpful to understand about upcoming work motivation.

Chapter 2 presents work motivation as well as objective of this work.

Chapter 3 presents basic theory and knowledge which is helpful in making the working protocol of this experiment. This chapter starts with biomedical signal then cover brief idea about action potential, brain anatomy for EEG electrode placing, hand muscles anatomy for sEMG electrode placing, idea about EEG machine and acquisition techniques, idea about EMG machine and acquisition techniques and more.

Chapter 4 basically presents review of literature which is helping to leading to thesis. It starts from history of neuron which is the source of bio-signal generation followed by all previous research which are related to this work.

Chapter 5 consists of existing working methodology with designed protocol. This chapter basically covers EEG signal and sEMG signal acquisition processes. In denoising part wavelet transform has been used. Determination of power spectral density for both signals, and band power of both the signal have been calculated. For nonlinear studies fractal

dimension by Higuchi's algorithm have been used. And at last, correlation of both the signals has been performed.

Chapter 6 contains results of this experiment and shows pattern which is helpful for future research.

The discussion chapter presents the observed results from the preceding chapter, which are analyzed, and conclusions reached.

TABLE OF CONTENTS

List of Figures:

List of Tables:

CHAPTER 1

INTRODUCTION

Every physical activity in our body, be it voluntary or involuntary requires precise coordination between brain and muscles. While performing any voluntary activity, signals from brain is received by the muscles for which it contracts, and the activity is completed. Hence, when a person decides to perform a physical activity, a complex chain of processes occur inside the body including the brain. At every stage of this process, in the cells, action potentials (AP) are produced. These AP are transmitted through nerves to the other parts of the body, specially to different muscles which then coordinate together to perform the physical activity.

Suppose a person wants to stand up. For doing this activity, brain will generate AP which will stimulate the muscles in the locomotory parts of the body. Similarly, for performing every physical activity like walking, running, lifting objects, etc. brain stimulates different muscles of the respective regions to act in a coordinated manner. For this, the micro currents flow from the brain to the muscles. The bioelectric signal generated in the brain is known as the EEG signals which are picked up by scalp electrodes. The micro currents or AP generated in the muscles are known as the EMG signals which are picked up by surface electrodes. These bioelectric signals can then be studied to understand the working of brain and muscles while the physical activity is being performed. This is of particular interest, in the field of bio-signal analysis, as it gives an insight into the complex working of cells, nerves and muscles present inside the human body.

CHAPTER 2

MOTIVATION AND OBJECTIVE

EMG (Electromyography) and EEG (Electroencephalogram) signal analysis are performed for both clinical diagnosis and biological applications. EEG investigations are used to diagnose epilepsy, seizures, sleep disorders, brain tumors, and other conditions. EMG investigations are used to diagnose the fitness and functionality of the muscles. As there is a communication between the brain and spinal cord, so, the contraction of the muscles is possible. These muscle contractions help the human body in movement of different body parts and in locomotion. So, it is very much clear that for performing any kind of body activity there is a coordination between the brain and muscles. At present the biomedical industry is growing faster, and lots of prosthetic implementation are performed. The prosthetic hand and leg devices are artificial in nature. But when connected to the human body, they perform in a similar manner just as the original human hand or leg. Thus, it is clear that the signals from the brain and muscles reach the artificial limbs.

The main motivation for this thesis is to see the changes in brain dynamics and muscles dynamics when a person lifts various weights. In this study, EEG and EMG data of some subjects have been collected. A protocol is designed based on various weightlifting in which these data are utilized. For performing this experiment, a basic understanding of the working of nerves, brain, and muscles along with the methodologies involved in the analysis of bio-signals is required.

The primary objective of this study was finding out the changes in the brain and muscles dynamics. For this, frequency domain analysis was performed by evaluating the power spectral density. The band power of the muscles and the band power of EEG signals were evaluated. Fractal dimension analysis was done as both the physiological signals, EEG and EMG are nonlinear. With the help of this nonlinear analysis the change in the pattern of the EEG and EMG signals was observed with varying weights. Further, for statistical analysis, the correlation established between brain waves and muscle impulses was observed.

CHAPTER 3

THEORY AND BASIC KNOWLEDGE

3.1. Biomedical signal:

Any signal that can be continuously detected and monitored in living organisms is referred to as a "Biomedical signal or Biological signal". A biological signal might be electrical or nonelectrical. Electrical bio-signals, or bioelectrical time signals, are the result of an applied potential differential across a particular tissue, organ, or cell system, such as the nervous system [1]. EEG, EMG, ECG, EOG, and GSR are all well-known bioelectrical signals. Using a differential amplifier, which monitors the difference in voltage between two electrodes pressed against the skin, EEG and EMG data may be collected [2].

3.2. Working of neurons for generating bioelectric signal:

The working of neurons should be understood prior to acquisition of EEG and EMG signals. Neurons communicate with each other via electrical signals [3]. The electrical signal is generated due to some chemical reaction. The term "ions" refers to substances in the body that carry an electrical charge. Positively charged ions like sodium, potassium, calcium, and chloride play a crucial role in the neurological system [4]. Some protein molecules have a negative charge. The membrane that encircles nerve cells allows certain ions to pass, while preventing others. Such membranes are called semi-permeable membranes.

Now a better understanding of the resting potential and the action potential is discussed [5]. "At rest" refers to the state of a neuron when it is not firing. During rest, the inner of a neuron is negative compared to the exterior of the neuron, and vice versa. Although the concentrations of various kinds of ions try to equalize on both sides of membranes still it is not possible due to the cell membrane's restriction of the passage of certain kinds of molecules via channels (ion channels). While the membrane is not in use, (K+) ions may easily travel through it. It's more difficult for sodium ions (Na+) to pass through chloride ions (Cl-) if the cell is in a relaxed state. Negatively charged proteins cannot cross the membrane. With every two (K+) ions it takes in, the channel pumps three (Na+) out of the neuron. Resting potential is determined once all these pressures have been equalized and when the voltage difference between both the neuron's interior and exterior is measured. In a neuron's

membrane potential, there are approximately 70 mV (mV = millivolt) of difference between the interior and exterior. There are more sodium ions outside of the cell than (K+) ions inside of it, as seen in the graph below (Fig 1.2).

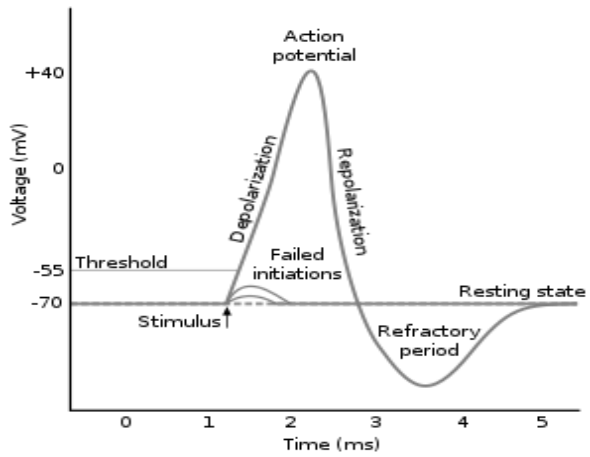

Fig.3.1 Voltage versus time curve for action potential [6]

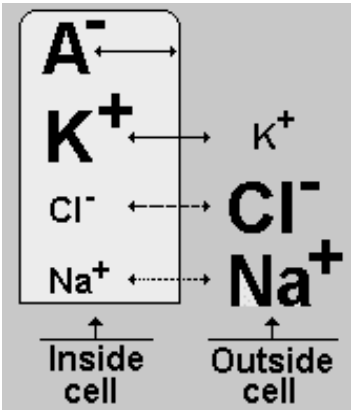

Fig.3.2 Inside and Outside of cell chemical reaction [7].

A spike or an impulse is a term used by neuroscientists to describe action potentials. Neurons create action potentials when depolarizing currents flow through them [8]. At a specific voltage, a human's resting potential is at its lowest level. For neuronal depolarization to be functional, it must be lower than the threshold value which is -55 mV. This threshold value must be crossed for the cell to create an action potential [9]. When the minimum threshold is attained, individual neurons will always fire an action potential, this is true for all action potentials. Consequently, the "ALL OR NONE" principle states that a neuron must fire a full action potential to pass the threshold.

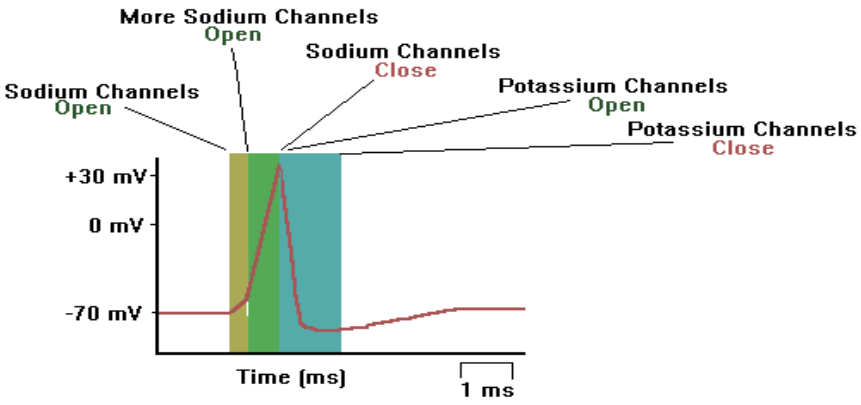

Fig.3.3 Working function of sodium and potassium channel [10].

When ions enter and leave the neuronal membrane, they cause an action potential, which is a transient burst of electrical activity. An external stimulus opens sodium channels because there are considerably more sodium ions outside than within the cell, so, they rush in [11]. Because sodium has a positive charge, these neurons become very positive and depolarized [12]. A surge of potassium causes the depolarization to be reversed [13]. This is the point at which sodium ions begin to shut down. It drops to -70 mV (millivolts) in the action potential (repolarization). Due to excessive open time of the potassium channels, the action potential is greater than 70 mV (hyperpolarization). The ion concentrations eventually revert to baseline, as well as the cell potential drops to -70 mV.

3.3. Bio-signal processing:

Physiological processes, chemical mechanisms and responses that occur in the human body when it is not performing optimally are explained by bio-medical signal processing. It includes simulating signals of interest, analyzing them, and comparing them to regular signals to better understand physiological systems.

The picture below depicts the stages involved in bio-medical signal processing:

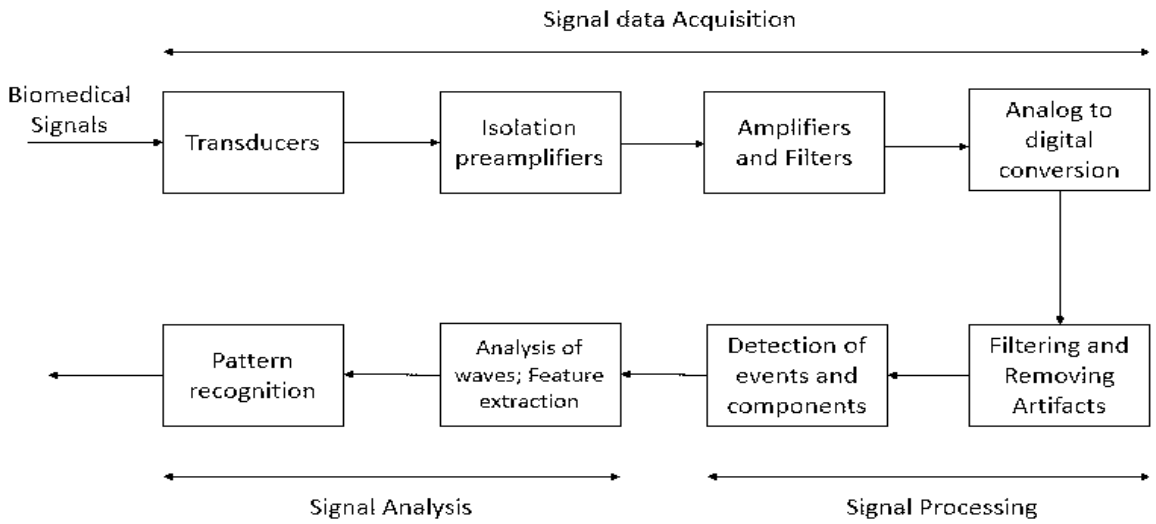

Fig.3.4 Picture shows that biomedical signal processing

There is basic four steps to follow bio-signal processing:

- It starts from acquiring of signal.
- Amplification and conversion of the signals.
- Examining the signal's important components.
- Analyzing the signal.

3.4. Electroencephalography (EEG):

Electroencephalography (EEG) is a technique for examining the electrical activity of neurons in the brain [14]. The EEG recordings are classified as scalp EEG, electrocorticography, or depth EEG. The EEG interpretation depends on the correct recording process [15]. A vast number of channels have been added to EEG machines during the previous 60 years, replacing vacuum tube amplifiers, paper recording, and computer storage. However, despite of its long history, numerical EEG analysis and brain mapping are still not routinely used in therapeutic settings. An EEG machine schematic is given in Fig.1.5

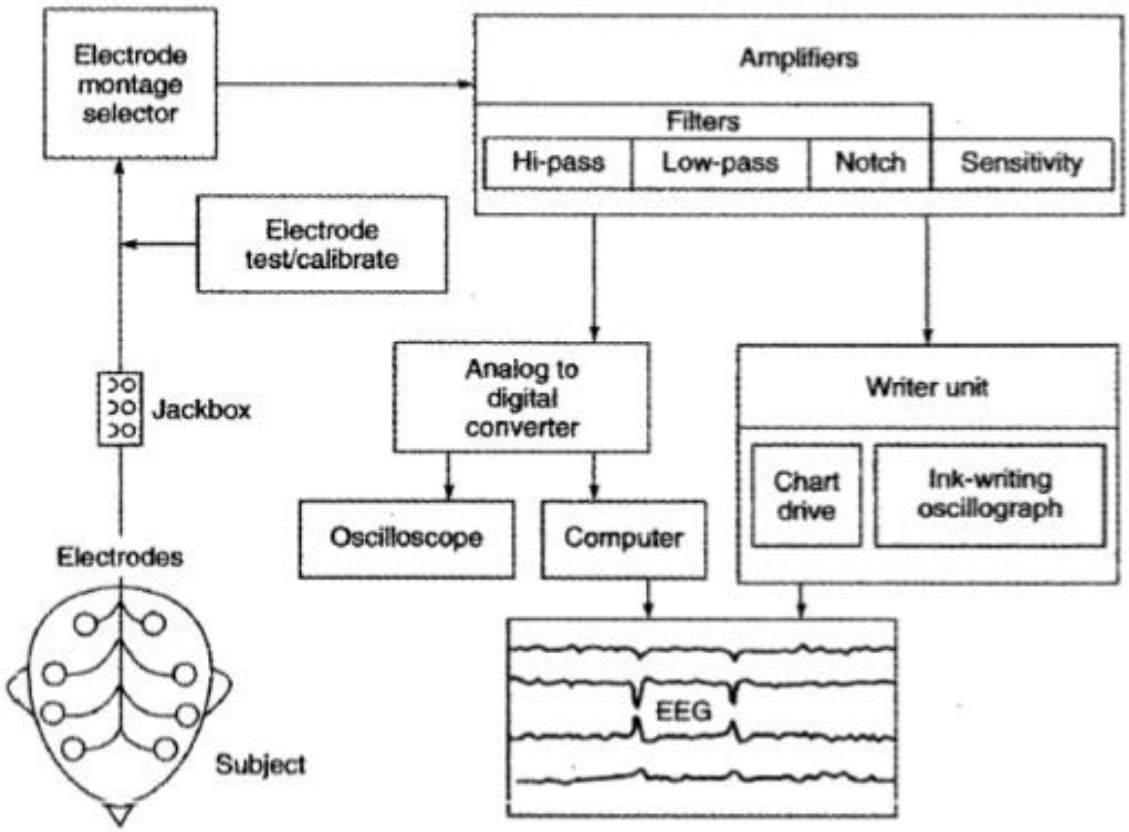

Fig.3.5 Schematic diagram for EEG machine [16]

3.5. About brain:

All our actions are coordinated by the brain. Its role is to receive, process, and reply to communications. We can think, learn, move, breathe, talk, express our emotions, and regulate most of our physical processes due to the brain's amazing capabilities.

3.6. Brain structure:

In case of brain structure there are two types of tissue like gray matter and white matter. Dendrites and cell bodies comprise the bulk of grey matter. Its function is to analyze and interpret data. On the surface of the brain, there is a large amount of grey matter. In the brain, there is a layer of white matter that is present underneath the grey. White matter consists of the long cell fibers of brain which transmit and receive information between the grey and white matter. Grey and white matter interact together to enable a man to do his everyday tasks.

Now coming to next part of human brain which is the brain lobe. The placement of EEG electrodes are done after selection of a particular brain lobe.

Basically, there are four lobes in human brain which are Frontal lobe (F), Temporal lobe (T), Parietal lobe (P), Occipital lobe (O). Along with these lobes, other lobes are also present which are Frontopolar (Fp), Central (C).

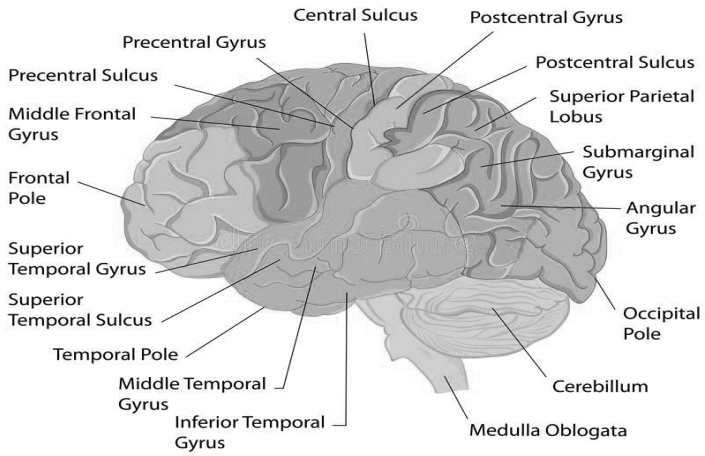

Fig.3.6 Simple human brain anatomy [17].

In previously section, it is seen that lobes are the four sections of the brain that make up one half of the brain.

3.6.1. Frontal lobe (F):

Basically, Frontal lobe is located at front part of the human brain. Executive functions are regulated by the frontal lobes. The ability to solve issues, plan, make choices, and manage one's behavior all rely on these talents. In this way, the frontal lobes are like the director of an orchestra, ensuring that every instrument plays in perfect unison.

3.6.2 Temporal lobe (T):

Temporal lobe is basically located on the side of human brain just above human ears. One of its major functions is to help in interpreting and comprehending sounds such as melodic and speech. Emotional control and facial recognition are two other functions of this lobe. The Hippocampus, a structure in the temporal lobe, is crucial for memorizing.

3.6.3. Parietal lobe (P):

This lobe is basically located above the temporal lobe and behind the frontal lobe. For example, they help us discern whether an item is smooth or sharp, hard, or soft, or something in between.

3.6.4 Occipital lobe (O):

It's found in the rear portion of the brain, in the Occipital Lobes. They play a vital function in vision because they help us make sense of what we see. Known as visual perception, this is how the brain processes visual information.

The **Central sulcus (C)** is a critical part of the cerebral cortex's anatomical map. Motor and sensory control are controlled by structures located nearby in the pre- and post-central gyri. That’s why the central lobe is used in this experiment.

3.7. Different types of EEG waves:

The electroencephalogram (EEG) of a brain shows complicated nonlinear dynamic behavior [18]. In an EEG device, the electrodes record electrical activity represented in a variety of EEG frequency bands. The raw EEG data may be classified as discrete waves with various frequencies using a method called the Fast Fourier Transform (FFT). Electrical oscillations are recorded in cycles per second (Hz), and one Hz equals one cycle per second in frequency measurement. There are four basic kinds of brainwaves: Beta, Alpha, Theta, and Delta; they are all classed by frequency.

The functions linked with the four primary brain frequencies are discussed in the following paragraphs. These functions are just linked with distinct brain frequencies there is no direct linear relationship between a frequency range and a specific brain function [19].

3.7.1. Beta wave (13-30hz):

Being aware or awake, attentive, and alert is the most common state linked with beta waves. A busy or agitated state of mind relates to low-amplitude beta waves. Besides this, beta waves are associated with the process of motor decision-making [20]. EEG beta waves are often called to when they are measured with an EEG instrument.

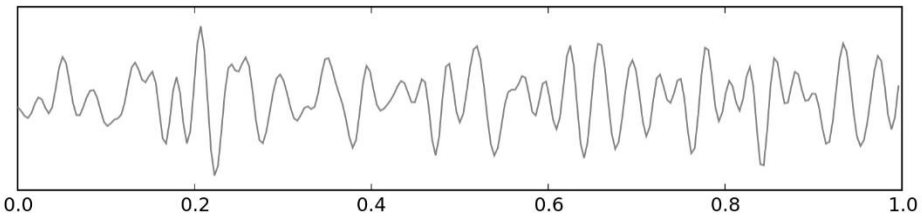

Fig.3.7 Figure of beta band pattern [21].

3.7.2. Alpha wave (8-12 Hz):

The relaxation, calm, and clear state of mind associated with alpha waves is well-known. The brain's occipital and posterior regions create alpha waves [22]. While it is possible to create alpha waves by shutting your eyes and relaxing, these waves are absent during cognitive tasks such as thinking and problem solving. Adults often experience alpha wave frequencies ranging from 9 to 11 Hz [23]. EEG alpha waves are often called to when they are measured with an EEG instrument.

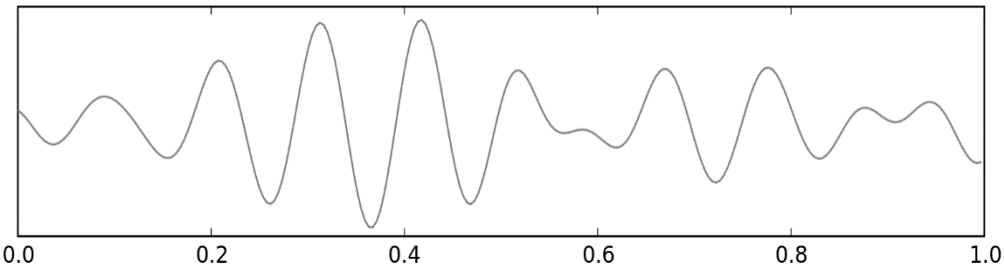

Fig.3.8 Figure of alpha band pattern [24]

3.7.3. Theta wave (4-8 Hz):

Theta activity is characterized as brain activity between 4 and 7 Hz [25]. While hyperventilation may lead to theta rhythm, it is more prevalent in young individuals, particularly in the temporal regions [26]. Theta activity larger than 30 mV is less prevalent in the elderly, even during slumber. These are known as EEG theta activity are recorded by an EEG instrument.

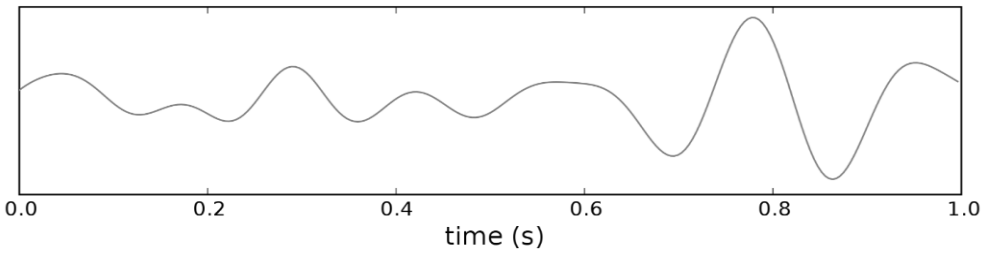

Fig.3.9 Figure of theta band pattern [27].

3.7.4. Delta wave (less than 4 Hz):

Delta activity is most common among babies. With ageing comes deep rest and delta waves. We've seen delta waves in absence seizures, which cause momentary attention lapses. Waves that have a high amplitude and a low frequency are called delta waves [28]. Eye-opening and hyperventilation may enhance delta rhythms, which are present throughout waking hours. These are known as EEG delta waves when measured using an EEG instrument.

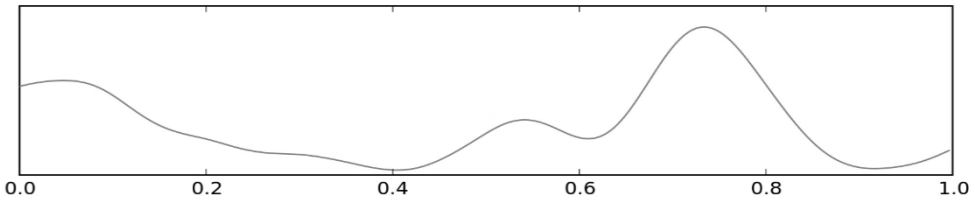

Fig.3.10 Figure of delta band pattern [29].

3.8. International 10-20 system:

The 10/20 method has made it commonplace to install scalp electrodes for a conventional EEG recording. The 10/20 range across Nasion-Inion and always for serves as the basis for this system's calculations. We designate the Fp, C, Parietal, O, and T as the frontal, central,

parietal, and temporal poles (T). In the middle of the electrodes, you'll see a subscript z, which is short for zero. Even numbers are employed as subscripts in the right hemisphere, whereas odd numbers are utilized in the left hemisphere [30].

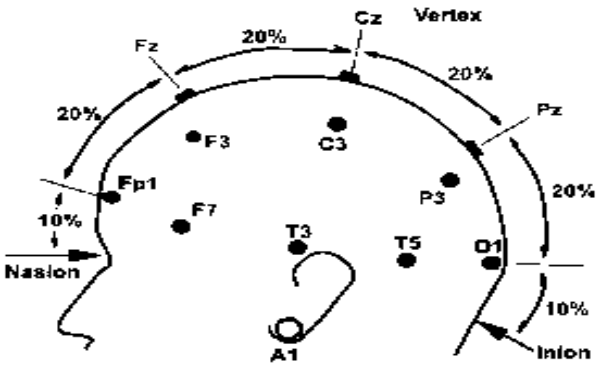

Fig.3.11 This figure shows that scalp electrode placement according to international 10/20 system (Side view) [31]

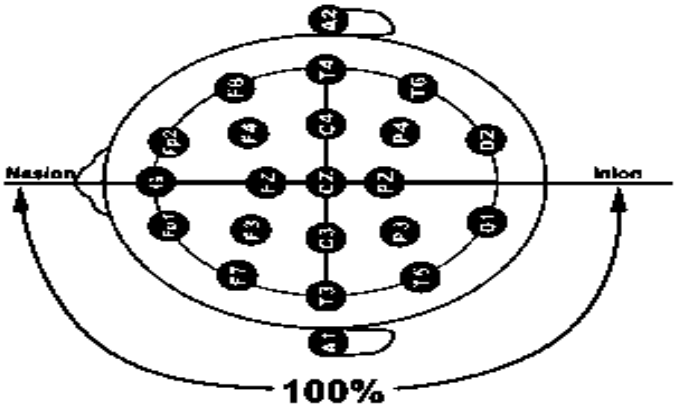

Fig.3.12 This figure shows that top view of international 10/20 system electrode placement [32].

3.9. Montages:

A bipolar or a referential montage may be used to observe an EEG's activity [33]. A reference electrode is included in each of the two electrodes that make up a bipolar channel [34]. In a referential montage, a single reference electrode is shared by all channels [35]. When taken directly from the scalp, an adult human EEG signal has an amplitude of 10 µV to 100 µV. Reading encephalographs have numerous options when it comes to setting up the display of

EEG voltages for the purposes of reading the EEG. A montage is a visual depiction of EEG channels.

3.9.1. Referential Montage:

The voltage difference between two electrodes may be seen in each of the channels[36]. Despite the fact that the "recording" electrodes aren't exactly in the same area as this reference electrode, it's near enough. Because midline placements do not enhance the signal in one hemisphere over the other, they are often employed online.

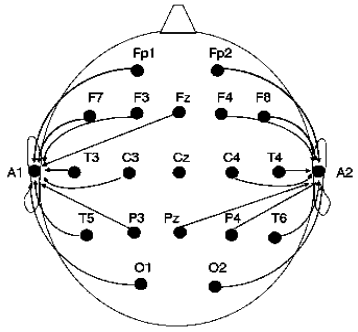

Fig.3.13 Sample image for referential montage [37]

Advantage of referential montage:

This reference montage helps record widely scattered potentials.

It also depicts the future change's shape.

Disadvantage of referential montage:

Using this montage makes finding an innocuous reference electrode challenging. As a result, all EEGs should be calibrated to the same standard [38].

Also, the reference electrode's potential may be so high that it affects every channel.

3.9.2. Bipolar montage:

The "double banana" bipolar montage, also known as the "bipolar longitudinal pattern," is a popular one. The parasagittal and temporal regions are covered bilaterally by a display with neighboring electrodes connected anterior to posterior in two lines.

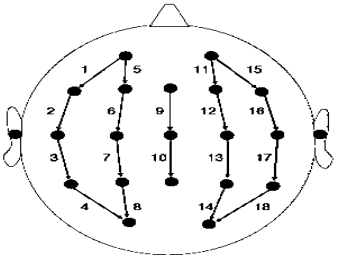

Fig.3.14 Sample image for bipolar montage [39]

Electrodes on each side of a bipolar transverse montage are linked together in a chain that goes from left to right. Each electrode is connected to a single reference point in a monopolar or referential montage. Conductive paste-coated disc electrodes are placed on the scalp of the subject (EEG).

Fig.3.15 Scalp surface disk type electrode [40].

3.10. Artifacts:

Artifact detection and eradication is the most difficult part of EEG monitoring. It's important to distinguish between artefacts that are patient-related [41] (e.g., movement, perspiration, ECG, eye movements) and those that are technical (e.g., cable movements, electrode paste-related). Finding the artefacts may be aided by several different methods. For example, a polluted signal may be detected using FEMG and impedance measurements. Other forms of interference may be discovered by examining various display settings.

Electrical signals are not discriminated by the electrodes used during EEG recordings. Extra-physiologic and physiologic artefacts are the two types of artefacts that may be found in recordings of activity that originates outside of the subject's brain.

Some common artifacts polluted EEG data which are EMG activity, eye movement, and skin artifact.

3.10.1. EMG Artifacts:

Myogenic potentials produced in the frontalis and temporalis muscles (clenching of the jaw muscles) are shorter in length than those generated in the brain, which is a frequent artefact of EMG activity. The duration, morphology, and rate of firing may all be used to identify these artefacts (frequency). Parkinson's disease may create EMG abnormalities with a frequency of 4 to 6 Hz [42].

3.10.2. Ocular Artifact:

Negative and positive poles may be found on either side of the eyeball, with the cornea at the front and the retina at the back of the eyeball (retina). The enormous amplitude alternative current field generated as the globe spins around its axis may be detected by any of electrodes placed near the eye. Even as positive pole moves toward frontopolar electrodes FP1 and FP2, it produces symmetrical downward deflections [43].

3.10.3. Skin Artifact:

This is complicated by the skin's characteristics. Stratum corneum-granulosum DC potential is substantial and changes with local skin deformation. Skin cleaning (alcohol swab) is the only reliable approach to remove artefacts from the source. As well, sweating sodium chloride interacting with electrode metals might cause a steady baseline drift.

3.11. About electromyography (EMG)

Electromyography (EMG) signals may be used in clinical and biological settings [44]. Today, the EMG signal is most often used for measuring the muscle's activation time, assessing its strength, and calculating its fatigue index by analyzing its frequency spectrum. These three applications are by far the most prevalent uses for EMG signals today.

3.12. Anatomical position of hand muscles:

Biceps, triceps, and forearms are the three major muscular groups in our human arms [45]. Extensors help stretch the arm and raise the joint angle, whereas flexors assist flex the arm and lower the joint angle. The biceps are an upper arm muscle. The biceps have two heads: a small head and a long head. Tendons connect the biceps to the arm bones. These are the

proximal biceps tendons. The distal biceps tendon connects the biceps to the forearm bones (radius and ulna) [46]. By contracting the biceps, the forearm is pushed up and rotated outwards. The forearm connects the elbow to the wrist in the upper extremity [47]. The forearm is made up of two bones: the radius and ulna. It has two parts: anterior (flexor) and posterior (extensor). Both compartments include 20 muscles each.

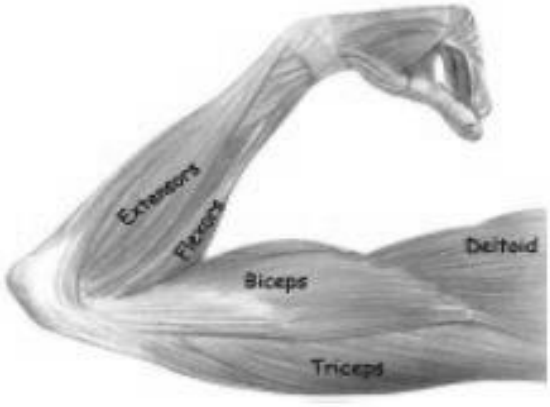

Fig.3.16 Anatomical position of hand muscles [48]

3.13. Electrical noise affects EMG data:

When the EMG signal is not amplified, it has a maximum amplitude range of 10 mV (+5 to -5). As they travel through different tissues, EMG signals gather up noise [49]. Electrical noise has distinct properties, and it is crucial to know them.

EMG signals may be affected by electrical noise in the following ways:

1. Ambient noise,
2. Motion Artefacts,
3. Inherent noise in electronic equipment.

The following techniques may be used to improve the quality of an EMG signal:

1. The signal-to-noise ratio of EMG signals should be as low as possible [50].
2. Signal peaks should not be distorted, and notch filters should not be used.

During EMG signal processing, all positive EMG signals are considered [51]. Half-wave rectification retains just the positive data and discards the negative [52]. The absolute value of each data point is used in full-wave rectification [53]. Full-wave rectification is usually recommended for rectification.

3.14. EMG signal processing:

Raw EMG provides useful data in a meaningless format. Only quantifiable data is relevant. Raw EMG signals are subjected to signal processing methods to get accurate readings [54].

An EMG signal may be cleaned up using several techniques. Denoising approaches other than wavelet-based fall short, while wavelet-based is the best.

A discrete temporal filter bank may be used to create WT [55]. Wavelet Fourier transforms are WT filters. Classifying EMG signals using the WT is a great idea [56].

3.15. Nonlinear analysis:

Non-linear dynamic approaches such as Fractals, Chaos theory, and Entropy may be used to analyze EEG and EMG signals. Time series analysis using non-linear methods aids in both identifying system characteristics and predicting their behavior. Fractal patterns occur naturally in system dynamics, particularly in phase space. The examination of these structures is particularly beneficial for predicting the future behavior of complex systems because they reveal basic relationships between uncertainty and indeterminism.

3.16. Fractal:

An endless pattern that appears in various sizes is known as a fractal. It's a scientific term for this quality. There are several examples of fractals in nature. Our blood veins, brains, trees, lightning bolts and river networks all have the same branching patterns that we observe in nature. For example, I consider our lungs surface area. We have around 100 square meters of surface area in our airways, which are branching fractals. Trees and lungs both exchange oxygen and carbon dioxide via their huge surface areas, which makes the comparison clear. Scale is 30 cm = 3*10-1 m.

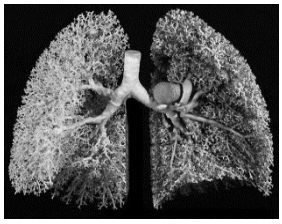

Fig.3.17 Human lungs [57]

CHAPTER 4

REVIEW OF LITERATURE

This chapter focuses on the EEG and EMG signal identification, capture, processing, and analysis. This section provides an overview of EEG and EMG research during the last few decades [58].

In the second part of the 18th century, Luigi Galvani, Lucia Galeazzi Galvani, and Giovanni Aldini discovered the function of electricity in nerves by dissecting frogs. Charles Bell and François Magendie established via dissection and vivisection between 1811 and 1824 that the spinal cord's ventral roots send motor impulses while the posterior roots receive sensory information (Bell-Magendie law) [59]. Jean Pierre Flourens developed the experimental approach of performing targeted brain lesions on animals and reporting their effects on motility, sensitivity, and behavior in the 1820s. Early 20th century research established that neurons were electrically excitable and that their activity altered the electrical state of nearby neurons. Camillo Golgi developed a staining process in the late 1890s that employed a silver chromate salt to expose the detailed architecture of single neurons. He defined the "in excitable" or "refractory period" between nerve impulses in 1899. His main interest was in how nerves influenced muscles and sight. The term "Neuroscience" may have been first used in 1962 by Francis O. Schmitt's "Neuroscience Research Program" at MIT [60].

Richard Caton (1842–1926), a Liverpool physician, published his results in the British Medical Journal in 1875 [61]. Adolf Beck, a Polish biologist, investigated rhythmic oscillations in the brains of rabbits and dogs in 1890 [62]. Beck began studying animal brain electrical activity. Beck used electrodes on the brain's surface to measure sensory input [63]. His findings of changing brain activity led to brain waves [64]. Cognition was first recorded in monkeys in 1912 by Russian researcher Vladimir Pravdich-Neminsky [65]. For the first time ever, a human EEG was recorded in 1924 by German scientist and psychiatrist Hans Berger (1873–41). A Beckman Instruments electroencephalograph equipment was used to monitor the brain waves of the astronauts on at least one of the Project Gemini human spaceflights (1965-1966). It was one of several Beckman Instruments designed specifically for NASA's needs.

The researchers used radio equipment to boost the brain's signal and then recorded it on graph paper [66]. It wasn't until Berger saw that the participants' levels of awareness fluctuated that he came up with the name for the EEG device. Using concentric needle electrodes, Franklin Offner created the first dedicated EEG recording device. In 1935, Gibbs et al. defined spike waves, which led to the creation of clinical encephalography. According to the study of Gibbs and Jasper, published the following year, interictal spikes are the focal markers of epilepsy. Electroencephalography underwent a sea change after World War II, as scientists developed new methods for detecting, denoising, and analyzing brain impulses. In the 1950s, 18 William Grey Walter pioneered EEG topography, or the mapping of electrical activity over the surface of the brain [67]. This was used in psychiatry until the 1980s. There have been advancements in EEG signal categorization via the use of Neural Network detection systems since 1996. Some of these advancements will be described more below. Scalp electrodes are placed to capture EEG signals [68]. Using the electrode signals, Equation (1) describes the whole signal.

$$X(t) = [X_1(t), X_2(t), \ldots, X_m(t)]^T \quad \text{---------- (1)}$$

Here X(t) represents the EEG signal. T stands for transposition and m for channel count. The rows represent EEG data from various electrodes and the columns show temporal variation. The EEG signal is filtered to remove unwanted disturbances, but this must be done carefully to avoid data loss. During the 1980s, digital filters were utilized to eliminate electrical disturbances from the sound. Analyzing EEG data with digital filters requires cross-multiplying data points from the raw signal and their neighbors with a set of weights, according to Nitschke and colleagues. Since the EEG data must be converted to a wavelet, a precise mother wavelet must be used. Equation (2) may be used to represent the wavelet decomposition of a signal x(t) [69].

$$x(t) = \sum_k c_{j_0 k} \varphi_{j_0 k}(t) + \sum_{j=j_0} \sum_k d_{jk} \psi(t) \quad \text{----------(2)}$$

in where x(t) the mother wavelet's scaling function is. Equation (2) has two parts: approximation coefficients and detailed coefficients. A biomedical signal is non-linear and non-stationary. Because of this, non-linear signal processing methods are appropriate for their investigation [70].

Nonlinear measurements like fractal dimensions may be used to assess EEG signal nonlinearity.

One of the fascinating properties of bio signals is their capacity for self-similarity, or the ability to evolve from a small-scale structure to a larger-scale one. Analysis of signals with self-similarity may produce discriminative characteristics straight from the signals utilizing fractal dimensions. Fractal dimension is a way to assess the inconsistencies in these kinds of signals that aren't integer or fractional but rather non-integer or fractional in nature [71]. Fractal dimensions may be calculated using the following methods [72]: Box counting, Hurst exponent, PSD, approach suggested by Higuchi, Sevcik and Katz, and two variations of Castiglioni. There are two essential criteria for every feature extraction [73] the mean squared error (MSE) provided by Equation (3) and the signal to noise ratio (SNR) given by Equation (4) [74]. Here, x(n) is raw EEG or EMG signal, $\hat{x}(n)$ is denoised EEG or EMG signal.

$$MSE = \frac{1}{N}\sum_{n=1}^{N}[x(n) - \hat{x}(n)]^2 \quad \text{----------(3)}$$

$$SNR = 10\log\left|\frac{\sum_n \hat{x}^2(n)}{\sum_n[x(n) - \hat{x}(n)]^2}\right| \quad \text{----------(4)}$$

Francesco Redi documented EMG in 1666, and the evolution of EMG began [75]. The text explains that the electric ray fish has a highly developed muscle that creates electricity. Early in the 19th century a scientist named Walsh demonstrated that muscular tissue from an Eel fish could produce an electrical spark in 1773. According to an article published in 1792, A. Galvani demonstrated that electricity could cause muscular contractions by demonstrating that it could be applied to muscle fibers [76]. More than half a century after that, in 1849, Dubios-Raymond demonstrated that electrical activity may be recorded while a voluntary muscular contraction is taking place [77]. Marey, who coined the term "electromyography" in 1890, was the first to make a recording of this activity. An oscilloscope was used by Gasser and Erlanger in 1922 to display the electrical impulses generated by muscle fibers. Because of the random character of the myoelectric signal, only a limited amount of information could be gleaned from its monitoring [78]. As electromyographic signal detection technology advanced from the 1930s to the 1950s, researchers were able to employ better electrodes to

examine muscles more extensively [79]. In the 1960s, doctors started using surface EMG in the treatment of increasingly occurring specific illnesses. In 1966, Hardyck and his team became the first to employ EMG in clinical settings. Early on, Cram and Steger established a clinical approach for scanning various muscles to use an EMG sensor device [80]. Electrodes had not yet improved enough to enable batch manufacture of compact and lightweight instruments and amplifiers necessary for this project until the mid-1980s. Till then, there were a few commercially available amplifiers that were appropriate for the task at hand. During the early 1980s, microvolt cables were made accessible that may generate desired artefacts. The characteristics of surface EMG recording have improved over the last 15 years because of study. Recently, surface electromyography has become more popular in clinical procedures for recording from the superficial muscles, but intramuscular electrodes are still employed exclusively for recording from deep muscles. The brain processes muscle contractions and other bodily functions [81]. The brain will then communicate with the spinal cord [82]. The axonal terminals formed by the division of motor neurons in the spinal cord are known as axonal [83]. Muscle fibers are linked to axonal terminals. There is an electrical signal in the muscle fibers [84]. Neurons in the spinal cord provide the fibers of muscle with electrical impulses [85]. Neuronal axons, or nerve fibers, exit the spinal cord and travel via the peripheral nervous system to the muscles and glands. As previously stated, each motor axon divides into several branches and innervates many muscles. A motor unit consists of a single motor neuron and all the muscle fibers that it controls [86]. Across all muscle fibers, the dispersed signal from a single motor unit is synchronized and equal. Action potentials in muscle fibers are the signal they generate [87]. The motor unit action potential (MUAP)is made up of the sum of the action potentials of all the muscle fibers in a single motor unit [88]. EMG signals that include MUAP information are an invaluable diagnostic tool for a variety of neuromuscular conditions. Each one of a motor unit's innervated muscle fibers gets a shot of adrenaline when it fires. The motor unit action potential train is a series of impulses generated by a recurrently firing motor unit [89]. For each active motor unit, a unique myoelectrical signal is generated [90]. Poisson processes may be used to represent the EMG signal, which seems to be random and is often treated as a filtered excitation process, in which the MUAP is the filter. A significant difficulty in motor system analysis is the precise identification of discrete events in the EMG. The time of the muscle's activation and deactivation has been studied using a variety of ways [91]. Exercising is becoming more popular. It's been utilized extensively in the domains of sports performance and rehabilitation. Muscular force is the maximal force that a muscle can create [92]. Muscle

force increases performance, prevents injuries, improves body composition, self-image, lifelong muscle, and bone health, and prevents chronic illness. Visual examination by experienced observers is the most prevalent approach for deciphering motor events from EMG data. "Single threshold approach," which compares EMG data to preset thresholds, is the most straightforward and widespread computer-based method for finding the commencement of muscle contraction activity [93]. Analyzed raw signals are compared to an amplitude threshold that is determined by the average power of the background noise. EMG signal decomposition has been accomplished using wavelet spectrum matching and wavelet coefficient principal component analysis [94]. According to Jianjung et al, many motor unit potentials will overlap at the same time, particularly during a powerful muscular contraction. For, the breakdown of EMG signals, Eric and Damjan developed a non-linear least mean square (LMS) optimization of higher order cumulants back in 2002 [95]. According to Guglielminotti and Merletti, the greatest feasible energy localization in the time-scale plane may be [96] achieved by using a wavelet analysis that is tailored to fit the MUAP's form[97]. For nonlinear analysis, Fractal dimension is used because FD (fractal dimension) and MFL (maximum fractal length) have been shown to be linked to the complexity and power of the muscular contractions connected with them. Many researchers have already spent a great deal of time building new algorithms, updating current methodology, and enhancing detecting methods to decrease noise and capture reliable EMG and EEG data.

CHAPTER 5

EXPERIMENTAL METHODOLOGY

The procedure of taking data with help of EEG and EMG machines is already mentioned in the previous section. In this chapter, the protocol set for this experiment is discussed. Before entering this protocol, a brief idea about the stimulus is touched upon and also the type of stimulus used in this experiment in discussed.

5.1. Stimulus:

Stimulus is something which arouses a specific reaction in the body of a person by acting from outside the body environment and changes the normal activities of the person for a short period of time. In this experiment, stimulus is given in form of different kind of weights which are given in increasing order from 0 to 5 kg with an interval of 1 min between each weightlifting.

5.2. Flow chart for entire experiment process:

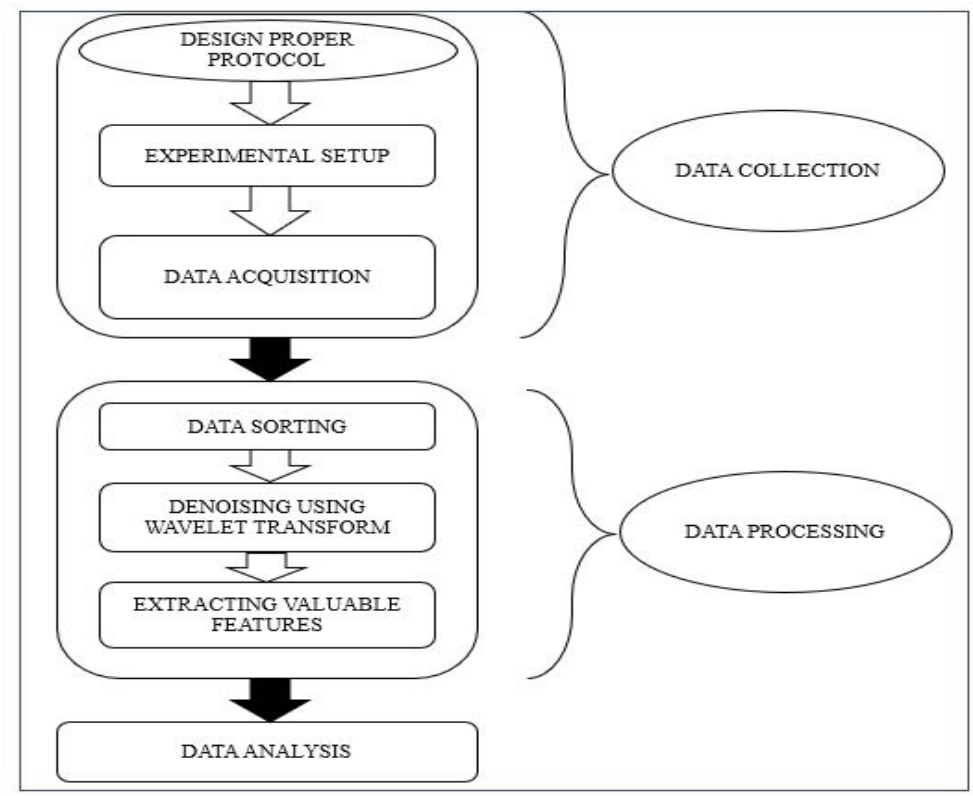

Fig.5.1 This flow chart shows that overview our entire experiment process.

5.3. Whole set-up before starting data recoding:

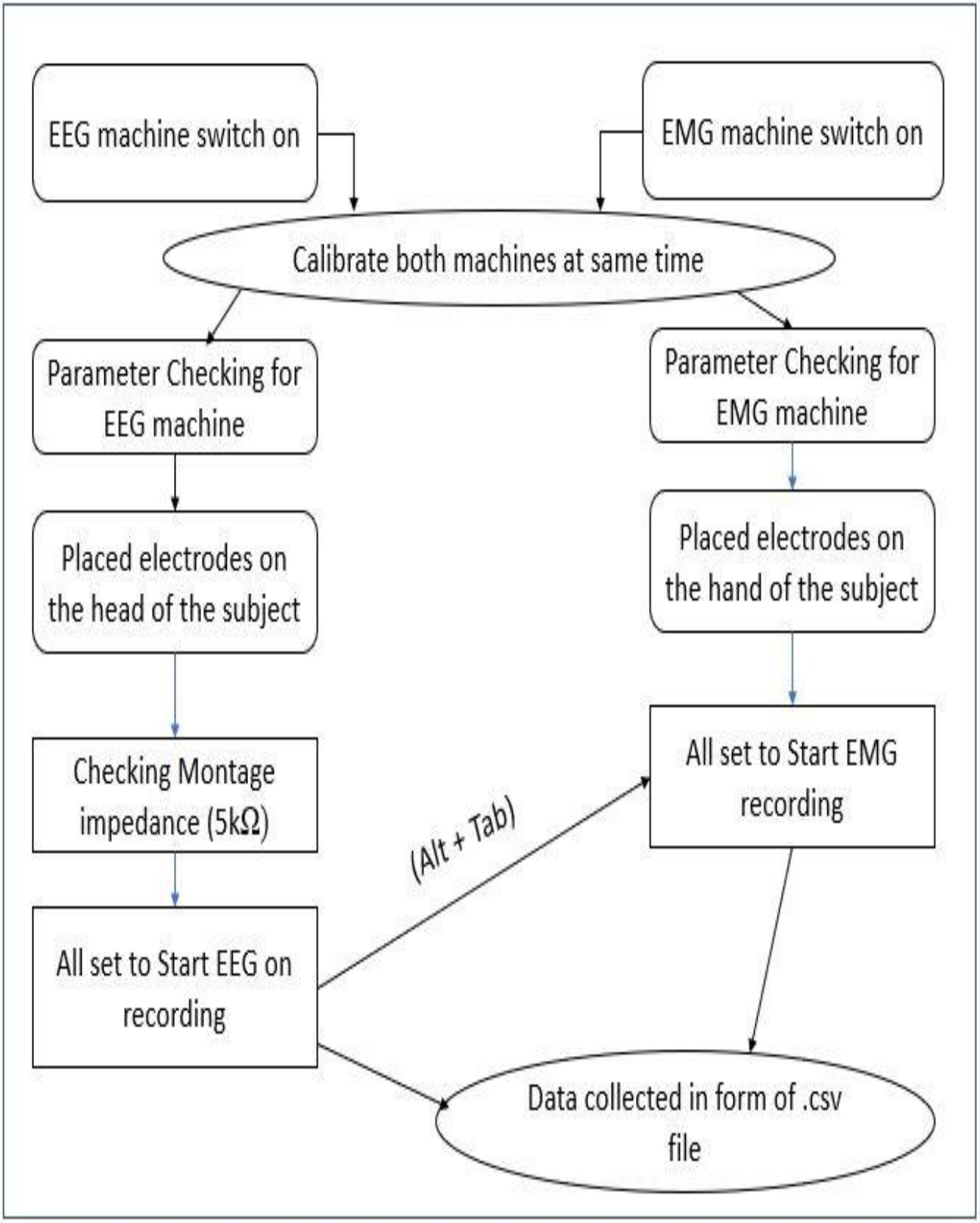

To record the EEG and EMG signal by varying different kind of weight stimulus, both EEG and EMG machines are switched on together. Then the electrodes of EEG and EMG are placed on subjects. Electrode of EEG placed on subject's scalp (central region) by the help of EEG conducting paste. And EMG electrodes were placed on hand (biceps and forearm) of the same subject. Then both EEG and EMG softwares calibrated at the same time.

Next the focus on EEG montage impedance. When impedance will be under 5kΩ then it is taken as perfect reading and saved it. At that time EMG window will not be in process. After saving the montage resistance we will check the other parameters like sensitivity, high pass filter (HPF), low pass filter (LPF), notch filter, and EMG filter. The sensitivity was set to 20μV/mm, LPF was set to 0.5 Hz, HPF was set to 5Hz, the notch filter and EMG filter were set on. After checking all parameters, recording of EEG is started. Then we will go to the EMG window without hampering EEG window which means EEG recording will be on. And parallelly EMG recording is started. For the 1st recording, the EMG window is set for the 1 min10 sec but recording time of data measurement is 10 sec. By the same process other weights like 0.5 kg, 1 kg, 1.5kg, 2kg, 2.5kg, 3kg, 3.5kg, and 5kg are recorded. After taking all readings, both the EMG window and EEG window are switched off. The recorded EMG and EEG data are collected in the form of .csv file.

5.4. Selection of montage:

Referential and bipolar transverse montage are employed for better EEG recording [98]. Intelligent montages are required for precise and detailed field assessment. Here referential and bipolar transverse montages are used to capture brain signal.

5.5. Calibration of signal:

A calibrating signal is a known voltage input. The user may set a calibration voltage (1μV to 10mV or more). In all levels of EEG signal processing, from amplification to pen output, this signal is conveyed. When calibrating a square wave pulse, changes in channels' amplitude might be seen. A voltage calibration signal for each filter and sensitivity level used while recording is required.

5.6. Impedance:

The resistance of a system to the flow of alternating current is expressed in units called ohms [99]. In terms of electrical conductivity, bigger numbers provide a greater obstacle. Reduced EEG signal amplitude is caused by increased electrode impedance [100]. In EEG research, a resistance of at least 100 ohms and a maximum of 5 kΩ should be used.

5.7. Electrodes:

These are small metal discs coated with silver chloride, which may be made of stainless steel, tin, or silver. These are placed on the scalp. To identify these locations, the International 10/20 method is applied. A letter and a number identify each electrode location. In the different brain lobes electrodes are placed [101]. Even numbers indicate the right side of the skull, whereas odd numbers represent the left side [102]. Conductive paste-coated disc electrodes are placed on the scalp of the subject (EEG) [103].

5.8. Electrical safety:

EEG is a safe treatment however, it might cause electrical harm, causing pain and burn. Electrical current delivered to the brain or scalp may cause seizures [104]. Ventricular fibrillation may be caused by current. Irritant metals used for depth measurement in the brain might cause local damage. The risk of damage varies among different patient groups. The first group consists of patients who do not touch an electrical equipment are the safest [105]. The second category comprises of people who have electrodes connected to their skin but no additional medical devices. The third category comprises of high-risk individuals including newborns and those with intravascular catheters or other medical devices.

It is possible for a person attached to an EEG machine to suffer from hazardous currents. These can be: -

1. Due to leakage current,
2. Due to improper grounding,
3. Due to double grounding.
4. Due to switch sparking.

5.9. EEG data acquisition:

Surface electrodes (Ag/AgCl) were put on the scalp of the subjects to capture the EEG data. The International 10/20 System of surface electrodes was used to put the electrodes. In this experiment seven electrodes were connected (C3, C4, CZ, A1, A2, Ground, and Reference). Here bipolar transverse montage and referential montage were used to capture the EEG signal (C3-CZ, C4-CZ, and CZ-REF). A clinical 24-channel computer-based EEG data collecting module (model: RMS Maximus 24, India Pvt. Ltd.) was utilized to collect the EEG signals. The 256 Hz sample rate is used to store the data.

5.10. EMG data acquisition:

The active electrodes E1, E2, E3, and E4 were inserted in the target muscle group namely the biceps muscles and forearm muscle. The reference electrode was put at the neutral point. Two electrodes E1 and E2 form Channel 1 (CH1), electrodes E2 and E3 form Channel 2 (CH2). After required skin preparation, the active electrodes were put roughly 2 cm apart using reusable clamp type metallic electrodes. The signal captured from these electrodes is amplified and filtered, and the output is recorded using the laptop, which has a 16-bit resolution and a 4.5KHz sampling rate. EMG recordings were acquired from 8 healthy right-handed subjects who participated for the study, consisting of 2 women and 6 men. During the trial, the subject was instructed to relax and breathe normally. The individual was instructed to lift weights of different denominations. The results of each trial were kept for subsequent examination.

Next step was denoising of EEG and EMG signals.

5.11. EEG and EMG signal denoising:

It is possible to think of transforms as an improvement over the original signal. As a result of the frequency information it gives, the Fourier transform is a good match for this concept. A waveform's frequencies can be accurately described using Fourier analysis, but its time cannot be tracked. Many biological signals include a significant amount of timing information that is of essential importance. It is possible to extract time and frequency information from a waveform in a variety of ways [106]. Many methodologies have been introduced to extract frequency and time information from waveforms. There are several

ways to represent a waveform's characteristics that vary over time, but one of the most common is to employ a technique known as a wavelet transform [107].

5.12. Why Wavelet Transform (WT) is important for denoising:

In case of Fourier transform, the waveform was compared to a sine function [108]. In fact, it was compared to a whole family of sine functions with the same frequency [109]. By multiplying the signal with sinusoidal functions and averaging where eq. (5) is in continuous form. Here averaging means in either the continuous or discrete domains, either integration or summation may be used.

$$X(\omega_m) = \int_{-\infty}^{\infty} x(t) e^{-j\omega_m t} dt \quad \text{---------- (5)}$$

The distinctive frequency features of sinusoidal functions make them especially attractive for exploring the characteristics of waveforms. This property naturally makes them suitable for investigating a waveform's frequency spectrum [110]. It is possible to employ other investigate functions, such as functions that focus on a certain waveform behavior or feature. Short-term Fourier transforms (STFT) may be used to translate or slide the probing function across the waveform, x(t), as is done in this case.

$$STFT(t,f) = \int_{-\infty}^{\infty} x(\tau)(w(t-\tau)\, e^{-2\pi f \tau}) d\tau \quad \text{---------- (6)}$$

A sliding window function, w(t-τ), is used to translate the window across x, and f, the frequency, serves as an indicator of a family member. In general, translated probing functions may be expressed as follows:

$$X(t, m) = \int_{-\infty}^{\infty} x(\tau) f(t-\tau)_m d\tau \quad \text{---------- (7)}$$

where $f(t)_m$ is a family of functions, and m is the number of the family.

A big enough family of functions $f(t)_m$ should always be able to address the whole waveform (x) in all its many features (t). It is possible to rebuild x(t) in this way, making the transformation bilateral. This extra layer of redundancy may be advantageous in certain situations, such as when it reduces noise or serves as a safety net, but it is not always essential. While the Fourier transform isn't really redundant, most transformations given by

equation (7) X(t,m) are, since they transfer one-dimensional (t) variables into two-dimensional variables (t, m).

The wavelet transform adds an important dimension to the fundamental idea provided by Equation (7). Many alternative probing functions may be employed in wavelet analysis, but the family always includes expanded or compressed variants, as well as translations [111]. Equation (8) defining Continuous wavelet transform (CWT) comes from this notion [112].

$$W(a,b) = \int_{-\infty}^{\infty} x(t)\frac{1}{\sqrt{|a|}}\psi * (\frac{t-b}{a})dt$$ ---------- (8)

The wavelet coefficients, W(a,b), define the relationship between both the signal and the wavelet at different scales and translations: the relationship between the signal and the wavelet at a particular scale and location, a, b.

A mother wavelet and its family members are created by dilatation and contraction [113]. The wavelet presented is the popular Morlet wavelet, called after a founder of wavelet research, and characterized by the equation:

$$\psi(t) = e^{-t^2}\cos(\pi\sqrt{\frac{2}{\ln(2)}}t)$$ ---------- (9)

Although the CWT coefficients may be used to recover the original waveform, this is seldom done due of the transform's redundancies. To get the original waveform back, the more efficient discrete wavelet transform is applied in this case [114]. The CWT has a major flaw: it is quite redundant. The CWT generates many more coefficients than are required to uniquely describe the signal, resulting in an up-sampling of the original waveform. However, if an analytic application such as the one described above requires a way to retrieve the original signal, this redundancy might be a significant expense. To retrieve all the coefficients, the computing effort may be too great. A bilateral transformation is used that provides the smallest number of coefficients necessary to properly reproduce the original signal.

5.12.1. Discrete Wavelet Transform (DWT):

Scale and translation variations are often limited to powers of 2 in the discrete wavelet transform (DWT) [115]. Filter banks make it simpler to learn and implement the DWT's

fundamental analytical expressions than it would be otherwise. The DWT is commonly referred equation (10) to as a recovery transform because of this:

$$x(t) = \sum_{k=-\infty}^{\infty} \sum_{l=-\infty}^{\infty} d(k,l) 2^{-\frac{k}{2}} \psi(2^{-k}t - l) \quad \text{---------- (10)}$$

Here d (k, l) sampling of W (a, b) at k and l. an equal to 2^k and b equal to 2^k l.

A Scaling function that makes it easier to compute the DWT, is a novel notion in the DWT. DWT implementation is more efficient if the highest resolution is calculated before the lower resolutions are applied. The scaling function is used to generate this smoother version [116]. However, a scaling function is frequently referred to as the smoother function [117]. Dilation or two-scale difference equations are used to define the scaling function, which is equation (11) [118]:

$$\Phi(t) = \sum_{n=-\infty}^{\infty} \sqrt{2} c(n) \Phi(2t - n) \quad \text{---------- (11)}$$

Here, c(n) is a sequence of scalars that specifies the scaling function. This is a challenging problem to answer since it incorporates two different time scales which are t and 2t.

Scaling functions are used to identify and describe each individual wavelet in a DWT:

$$\psi(t) = \sum_{n=-\infty}^{\infty} \sqrt{2} d(n) \Phi(2t - n) \quad \text{---------- (12)}$$

Here, d(n) represents series of scalar which is related to x(t) signal. These equations (12) are used to implement the DWT however, filter bank approaches are more often used.

EEG and EMG data were denoised using the DWT and a threshold approach [119]. MATLAB Wavelet toolbox was used to implement the DWT and threshold-based denoising [120]. Below Flow chart shows that denoising process algorithm.

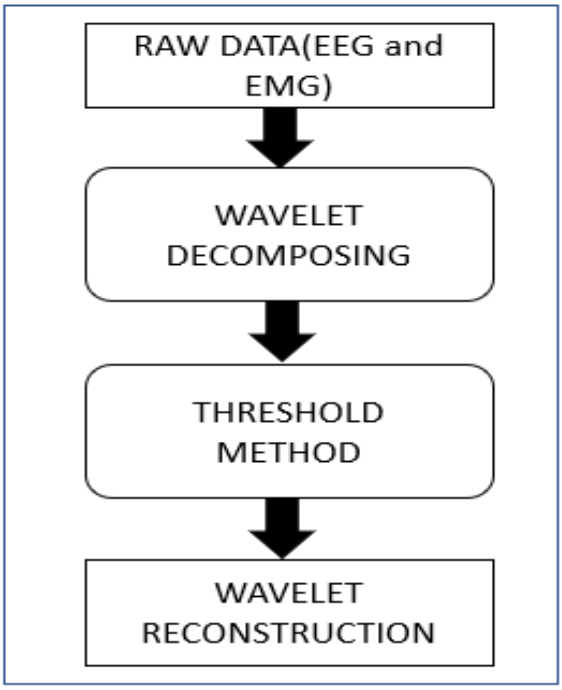

Fig.5.2 Flow chart for denoising process to raw data to filter data by the help of wavelet transform.

5.12.2. Wavelet decomposition:

Low and high pass filters are used to decompose a signal into its component waves, which are termed approximation and detail, respectively [121]. Multi resolution decomposition, which splits the signal into "details" at various scales and "approximation," is correlated with both filters' wavelet functions. In the discrete time domain, the DWT is calculated through lowpass and high pass filtering [122]. The denoised signal was forwarded after the residuals signal was eliminated using the Soft Minmax Thresholding Method. With un-scaled white noise structure, a threshold was manually determined for each level. Fig. (5.3) shows a raw EEG signal and its coefficients after decomposition with db6 at ten levels.

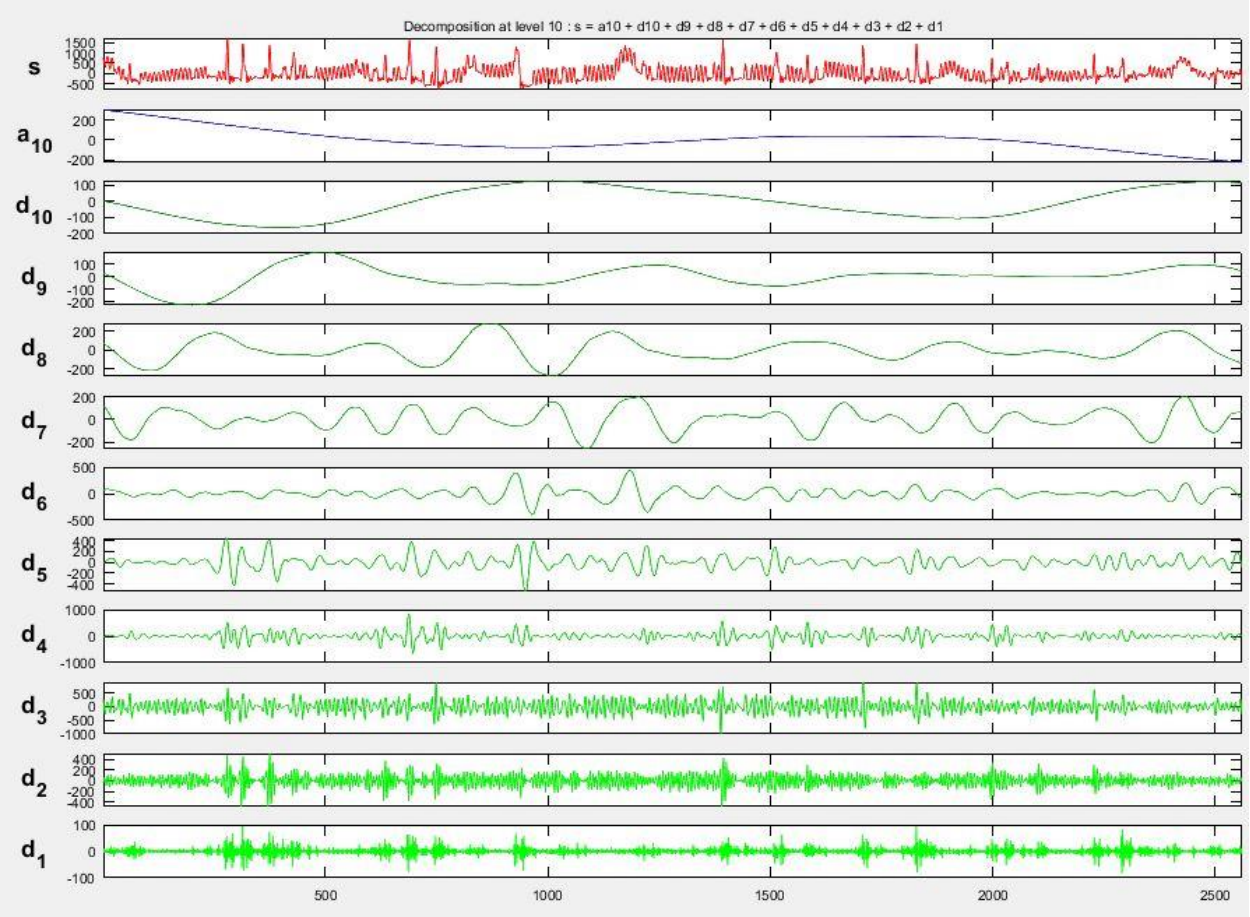

Fig.5.3 Decomposition at level 10 of EEG signal s: a10, d10, d9, d8, d7, d6, d5, d4, d3, d2, d1.

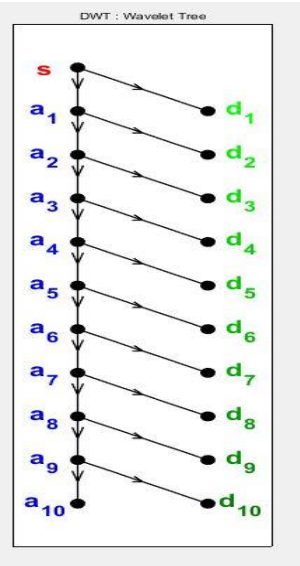

Fig. 5.4 Wavelet tree for db6 of level 10

5.12.3. Threshold method:

Let us assume that the equation below provides a model of the EMG or EEG signal

$f(t) = s(t)+n(t)$

Where, f(t) denoted as model of the EMG or EEG signal which contents noise; s(t) denoted as EMG or EEG signals and n(t) denoted as White Gaussian Noise N $(0,\sigma^2)$ respectively.

Let us assume that Ts is signal threshold and Tn is noise threshold.

Ts > 0 captures the energy of the initial signal s(t) to a level that is larger than a threshold. The magnitude of the noise signal transform values all lies below the noise threshold Tn, satisfying Tn>Ts. The noise in f(t) can then be reduced by applying a threshold to its transform. All values of its transform whose magnitude is less than Tn noise threshold are set to 0.

5.13. Power spectral density (PSD):

Power spectral density (PSD) depicts the frequency-domain power distribution of EEG and EMG signals [123]. Using Welch's periodogram, the PSD may be calculated. For analyzing the frequency domain components of a signal, power spectral density is used. The Welch method is a useful tool for finding the PSD of a signal. In this method the periodogram concept is used for calculating the PSD of a signal. Thus, PSD calculation help us to find band power which frequency band for both the signal EEG and EMG.

5.14. Analysis of fractal dimension using Higuchi fractal dimension (HFD):

Nonlinear dynamics are increasingly being used to analyses and extract features from signals that are random and unpredictable in nature. In the subject of physiological signal analysis, the study of signal complexity offers a wide range of applications. To analyses the change in fractal dimension about various weights, the estimation of fractal dimension from Higuchi's Fractal dimension [124] analysis is integrated here. As a nonlinear approach for analyzing biological data, HFD plays a significant role. HFD may be used to stationary, non-stationary, stochastic, deterministic, synthetic, and natural signals in addition to linear approaches.

Because the HFD outcome is determined by the K_{max} value rather than the duration of the signal, determining the best K_{max} is critical.

$X(1), X(2), X(3),\ldots, X(N).$

A given time series X(t) is transformed into a new time series X_k^m using the HFD technique.

Where, $$X_k^m; X(m), X(m+k), X(m+2k),\ldots, X\left(m+\left[\frac{N-m}{k}\right]\cdot k\right) \quad (m=1,2,\ldots,k),$$

Here [(N-m)/k] denotes Gauss's notation, m and k are integers, which indicates the in integers time and interval times respectively. Therefore, for a time interval, any k, we get k sets of new time series. The following equation (1) [125] gives the length of the curve formed by X_k^m.

$$L_m(k)=\left\{\left(\sum_{i=1}^{\left[\frac{N-m}{k}\right]}|X(m+ik)-X(m+(i-1)\cdot k)|\right)\frac{N-1}{\left[\frac{N-m}{k}\right]\cdot k}\right\}\Big/k. \quad \text{---------- (1)}$$

The normalized factor for curve length of subset time series is represented by the term

$[(N-1)/\left[\frac{N-m}{k}\right]k]$.

Now, the length of the curve for the time interval k is calculated as the average value of k sets of $L_m(k)$ given

$\langle L_m(k)\rangle$

If the graph is the curve of factor, then it will follow the relation given in equation (2)

$\langle L_m(k)\rangle \propto K^{-D}$ ---------- (2)

The fractal dimension derived by Higuchi's approach, often known as Higuchi's fractal dimension, is represented by the exponent D.

5.15. Correlation between EEG and EMG signals:

According to statistical theory, correlation is a phrase that describes how closely two variables are linked to one another. The correlation coefficient (r) that emerges because of this investigation. If *r* is a positive integer, its value ranges from -1 to 1. A negative relationship is represented by r = (-1), whereas a positive relationship is represented by r = (+1). The correlation between brain and muscle signals improves as *r* approaches 1. For correlation analysis. Below tables contents 8 subjects' correlation between brain signal and muscles signal.

CHAPTER 6

EXPERIMENTAL RESULTS

6.1 EEG and EMG denoising process:

MATLAB® has been used to import the raw data [126]. The sample rate is 4.5KHz, and the test time is 10 seconds for EMG signal. For EEG signal the sample rate 256Hz and test time 10 seconds. The wavelet function db6 was used for this experiment and proved to be successful in removing noise. The wavelet toolkit in MATLAB® was used to finish this work [127]. The denoised signal was advanced after the residuals signal was eliminated using a manual soft minmax thresholding procedure. Here the threshold for each level was manually determined. Now we can used this denoised data to measure another feature. Below fig. 3.5 shows that EMG signal before noise elimination and after eliminated of noise. Fig. 3.6 shows that EEG signal before elimination noise and after eliminated noise.

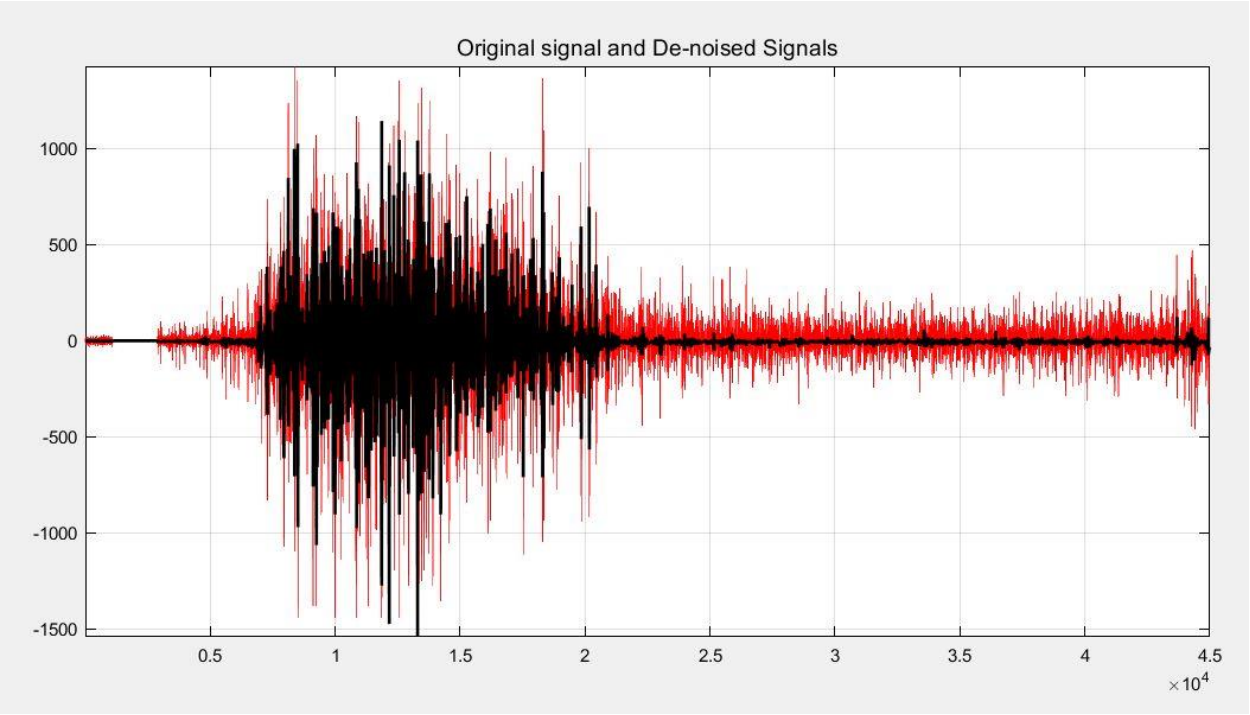

Fig. 6.5 In this figure red is denoted as EMG signal contain noise and black is denoted as denoise part of EMG signal.

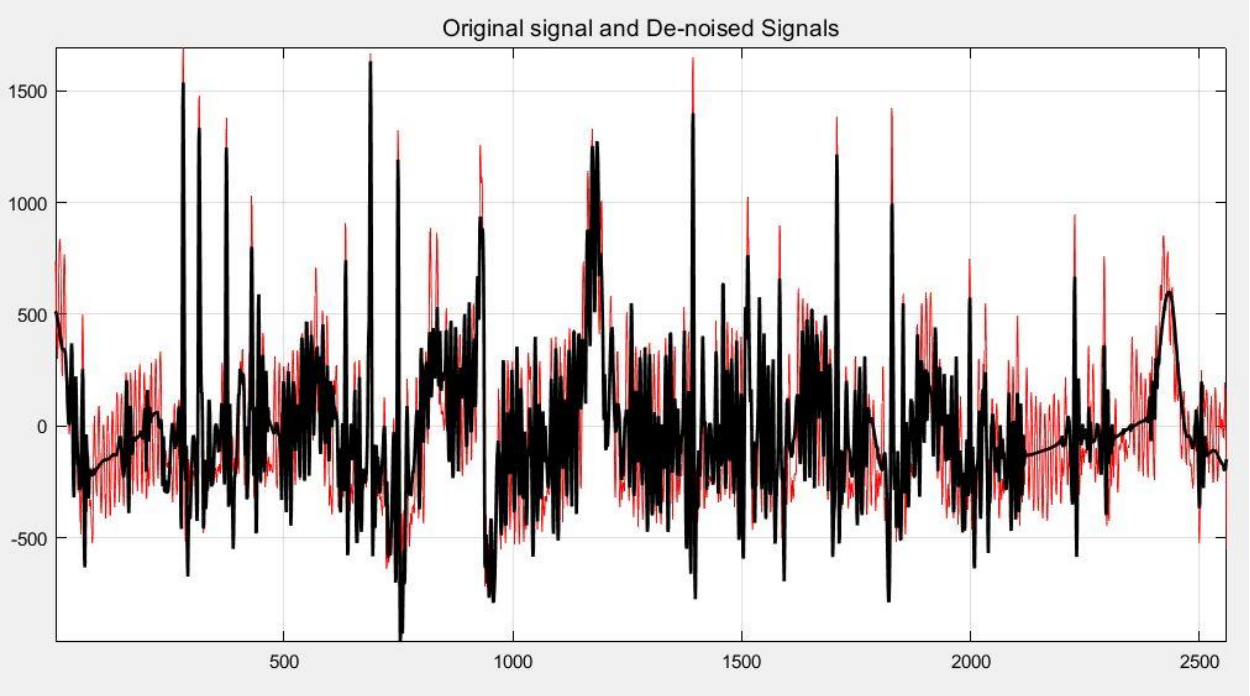

Fig.6.6 In this figure red part is noisy EEG signal and black part is denoise part of EEG signal.

6.2 Calculation Power Spectral Density (PSD):

6.2.1 Parallelly comparison of power spectral density (PSD) for before and after denoise EEG signals:

In previous chapter we have already discusses about PSD. In this chapter, the EEG and EMG signals of the one subject were plotted on a graph based on their weight.

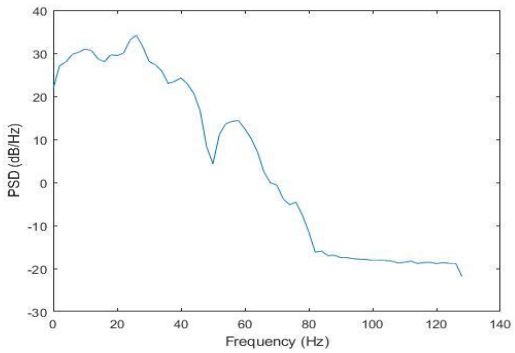	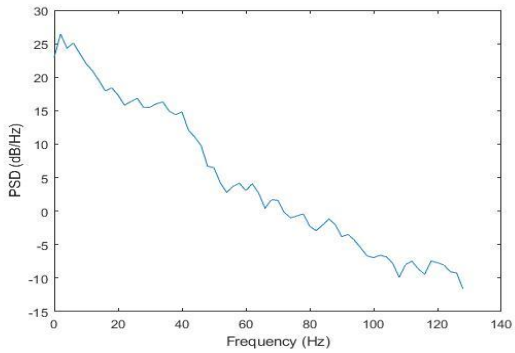
Before denoise PSD for C3-CZ at 0kg	After denoise PSD for C3-CZ at 0 kg
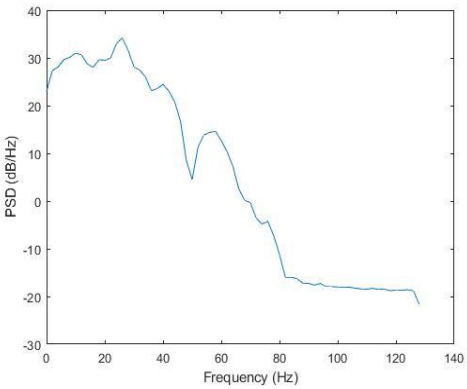	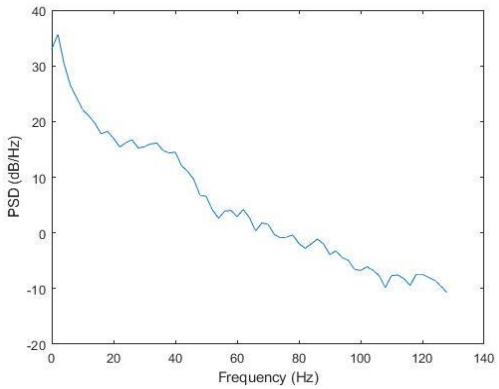
Before denoise PSD for C4-CZ at 0kg	After denoise PSD for C4-CZ at 0 kg
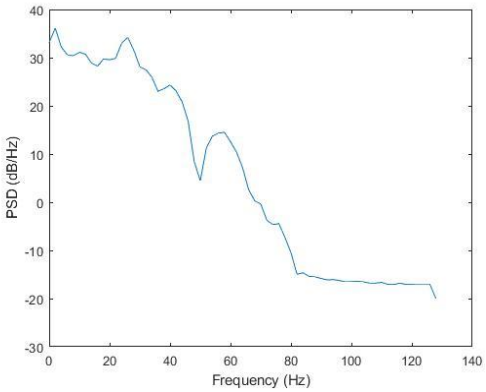	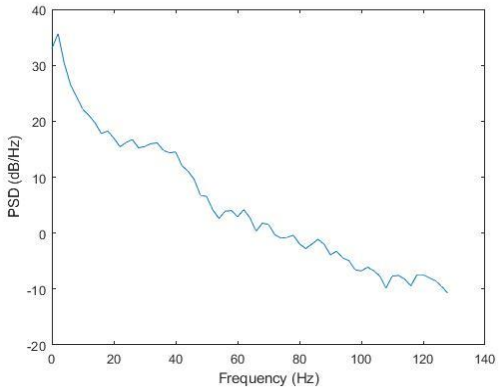
Before denoise PSD for CZ-REF at 0 kg	After denoise PSD for CZ-REF at 0 kg

Fig. 6.7 Before and after denoise of EEG signal PSD plot against 0kg weight lifting.

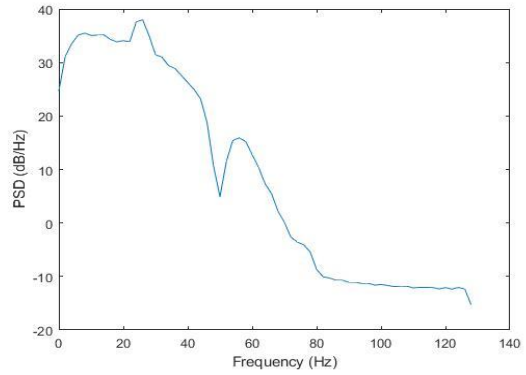	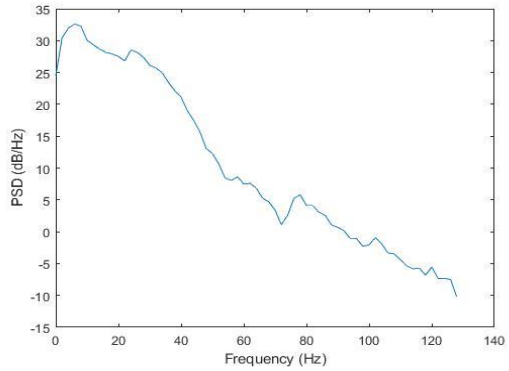
Before denoise PSD for C3-CZ at5 kg	After denoise PSD for C3-CZ at 5 kg
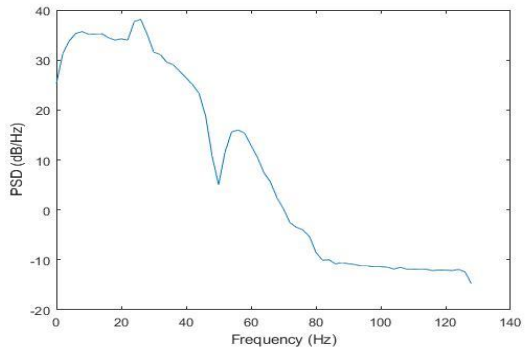	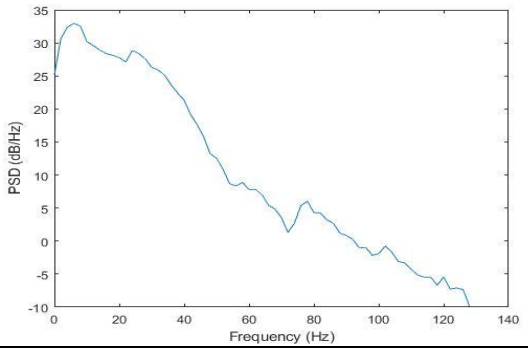
Before denoise PSD for C4-CZ at 5 kg	After denoise PSD for C4-CZ at 5 kg
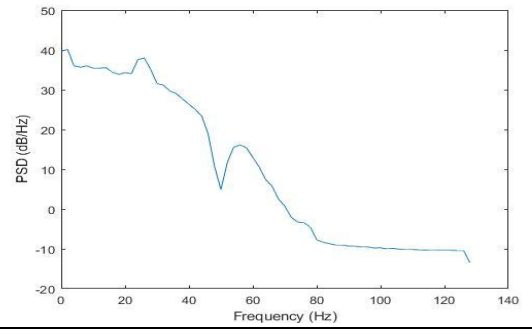	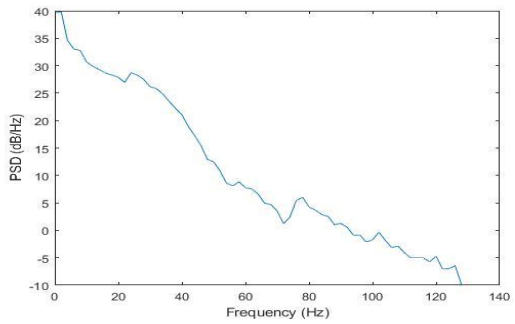
Before denoise PSD for CZ-REF at 5 kg	After denoise PSD for CZ-REF at 5 kg

Fig. 6.8 Before and after denoise of EEG signal PSD plot against 5kg weight lifting.

The following are some key conclusions that may be derived from above figures-

- Before denoise PSD plot clearly shows that some high frequency components are present and it is distributed. But after clearing noise PSD plot shows that higher frequency components are subpressed.
- Before denoise PSD value shows that at lower frequency which is in between 0 Hz to 20 Hz sharp region exists. But after eliminating noise PSD value shows a smooth curve.

6.2.2 Parallel comparison of power spectral density (PSD) for before and after denoise EMG signals:

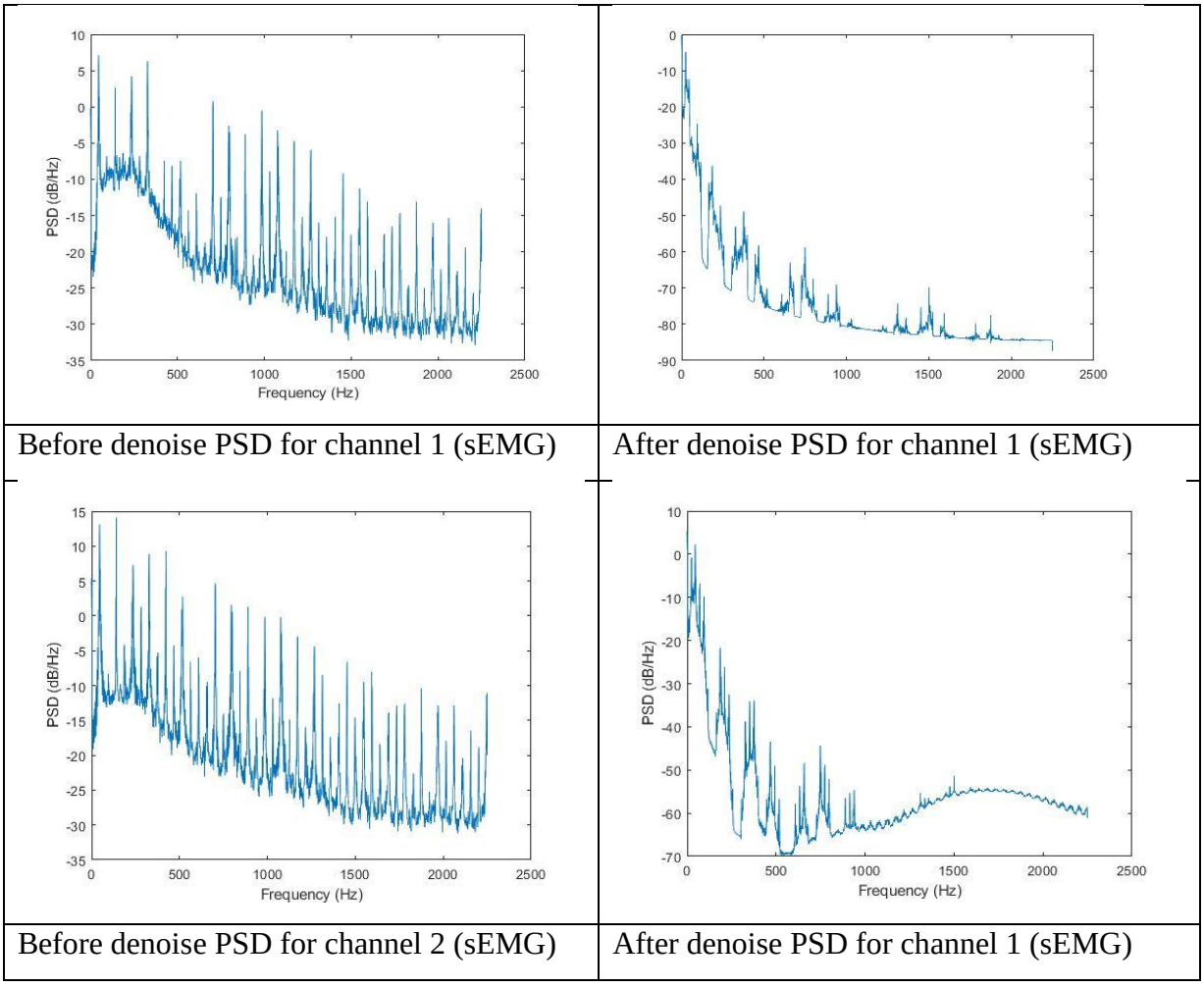

Before denoise PSD for channel 1 (sEMG)	After denoise PSD for channel 1 (sEMG)
Before denoise PSD for channel 2 (sEMG)	After denoise PSD for channel 1 (sEMG)

Fig.6.9 Before and after denoise of EMG signal PSD plot against 0 kg weight lifting.

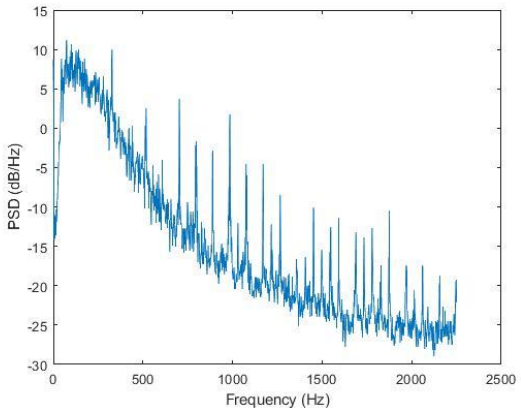	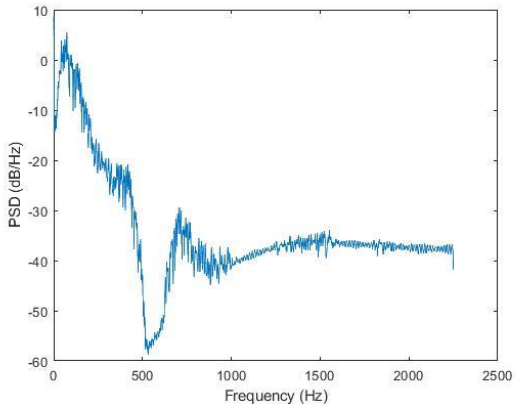
Before denoise PSD for channel 1 (sEMG)	After denoise PSD for channel 1 (sEMG)
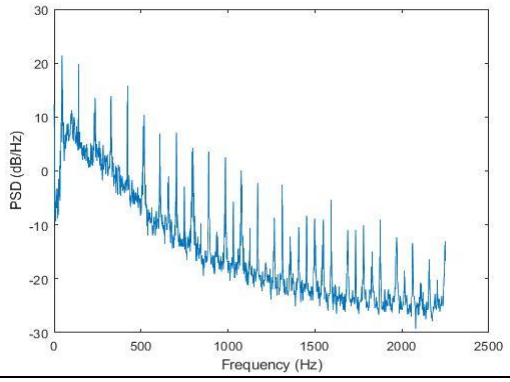	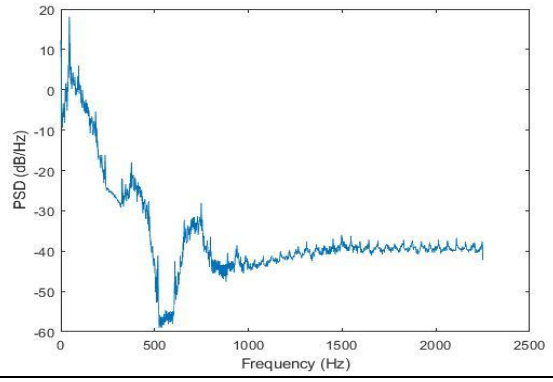
Before denoise PSD for channel 2 (sEMG)	After denoise PSD for channel 1 (sEMG)

Fig.6.10 Before and after denoise of EMG signal PSD plot against 5 kg weight lifting.

The following are some key conclusions that may be derived from above figures-

- Before denoise PSD for EMG channels clearly show that from 0 to 2000 Hz PSD value continuously decreased and contained unwanted picks.
- But after clearing noise in the region of 0 to 2000 Hz almosed all picks are eliminated.

6.3 Calculation of band power:

6.3.1 Calculating EMG band power due to increasing weights:

TABLE:6.3.1.1: Calculating EMG muscles band power due to increasing weight for Subject 1

WEIGHT	CHANNEL 1	CHANNEL 2
0	106.2553167	286.4153248
0.5	131.5143892	543.0214181
1	174.7648481	816.0083323
1.5	243.7172689	785.847509
2	484.2619345	1105.005996
2.5	490.1246616	1001.224116
3	672.9313573	1454.904666
3.5	695.2522952	1347.841746
5	1337.530882	2004.342025

Below figures are showing that graphical interpretation of EMG muscles band power variation due to increasing weight for subject 1.

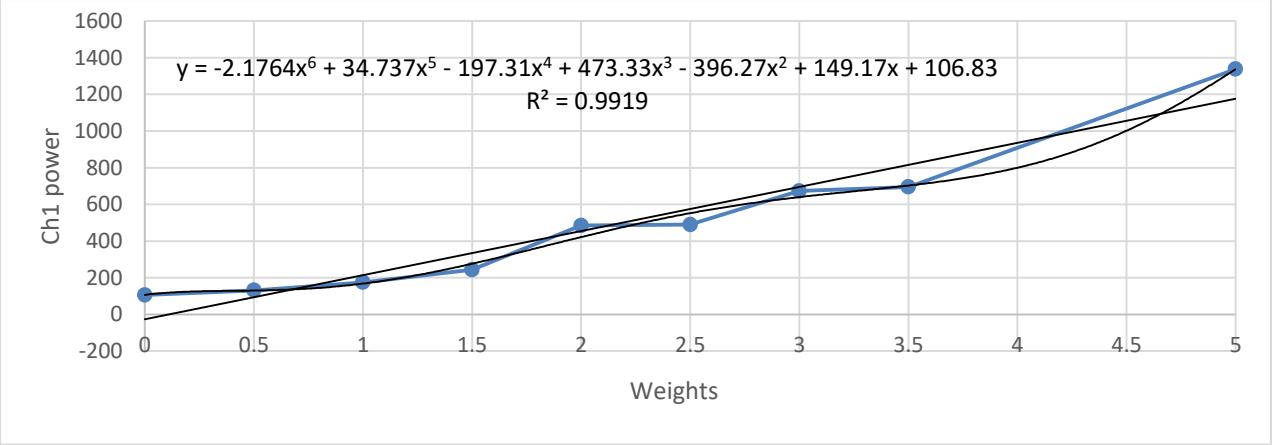

Fig.6.11 EMG muscles band power variation due to increasing load for channel 1

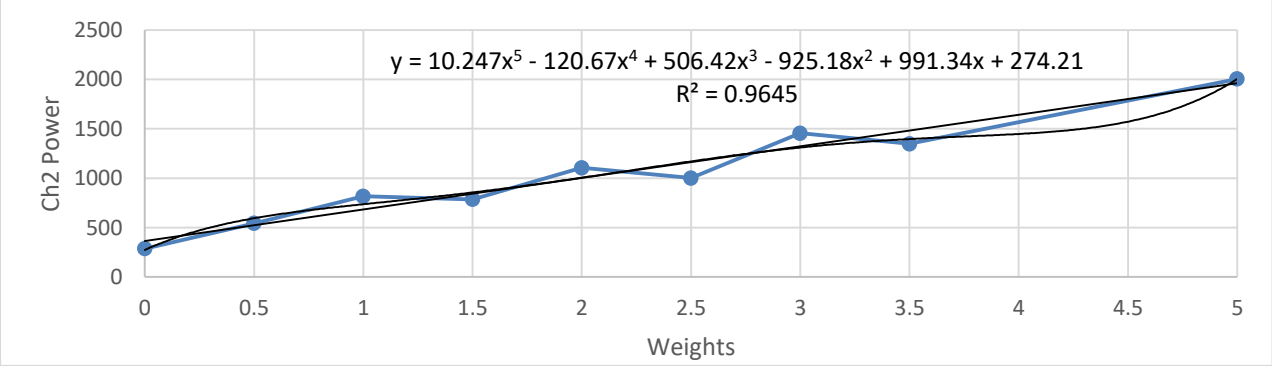

Fig.6.12 EMG muscles band power variation due to increasing load for channel 2.

TABLE:6.3.1.2: Calculating EMG muscles band power due to increasing weight for Subject 2

WEIGHT	CHANNEL 1	CHANNEL 2
0	1715.379026	317.8942222
0.5	2033.862397	297.0411903
1	2347.424901	664.1136669
1.5	2463.825351	639.2268184
2	2003.918214	1128.867614
2.5	3315.909557	971.4762597
3	3178.801767	1210.892567
3.5	4166.34883	1577.363602
5	18914.96276	1787.305328

Below figures are showing that graphical interpretation of EMG muscles band power variation due to increasing weight for subject 2.

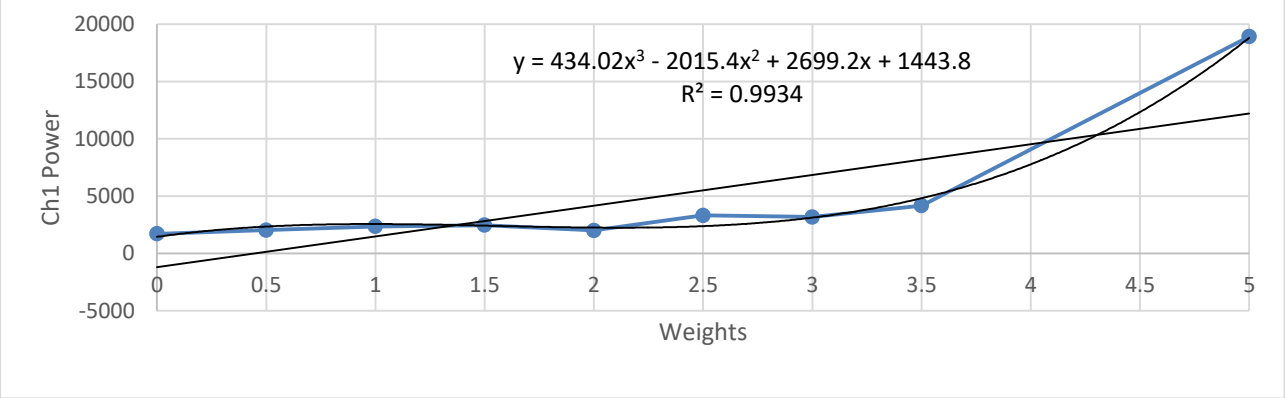

Fig.6.13 EMG muscles band power variation due to increasing load for channel 1.

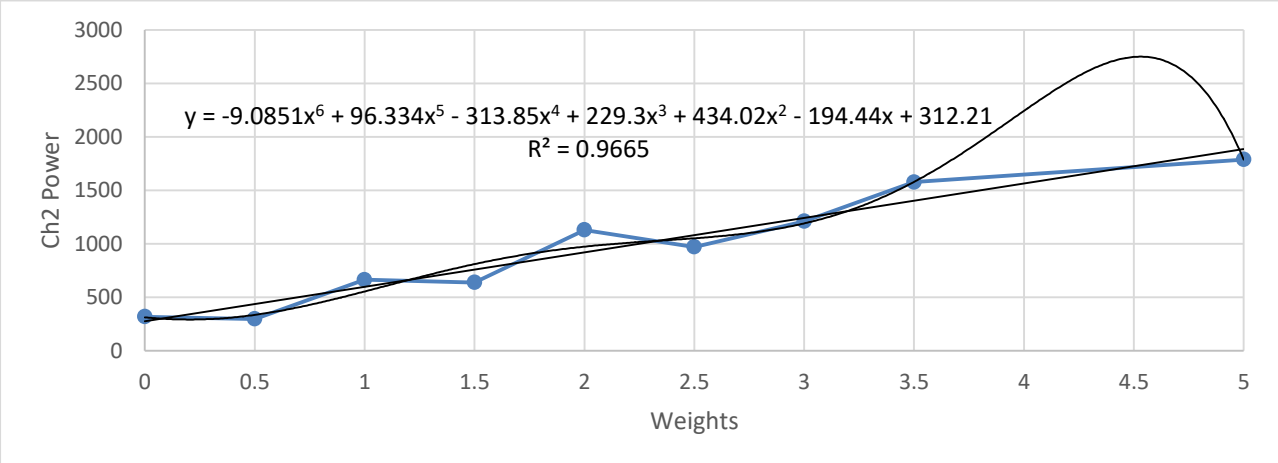

Fig.6.14 EMG muscles band power variation due to increasing load for channel 2.

TABLE:6.3.1.3: Calculating EMG muscles band power due to increasing weight for Subject 3

WEIGHT	CHANNEL 1	CHANNEL 2
0	17.21978348	118.7707557
0.5	20.77633787	167.6057207
1	24.11895835	283.0727467
1.5	30.12988746	434.1306445
2	35.32623878	796.0394592
2.5	39.38123615	1102.388287
3	34.31204122	1472.475047
3.5	34.15382371	2236.244712
5	82.72163088	6376.060029

Below figures are showing that graphical interpretation of EMG muscles band power variation due to increasing weight for subject 3.

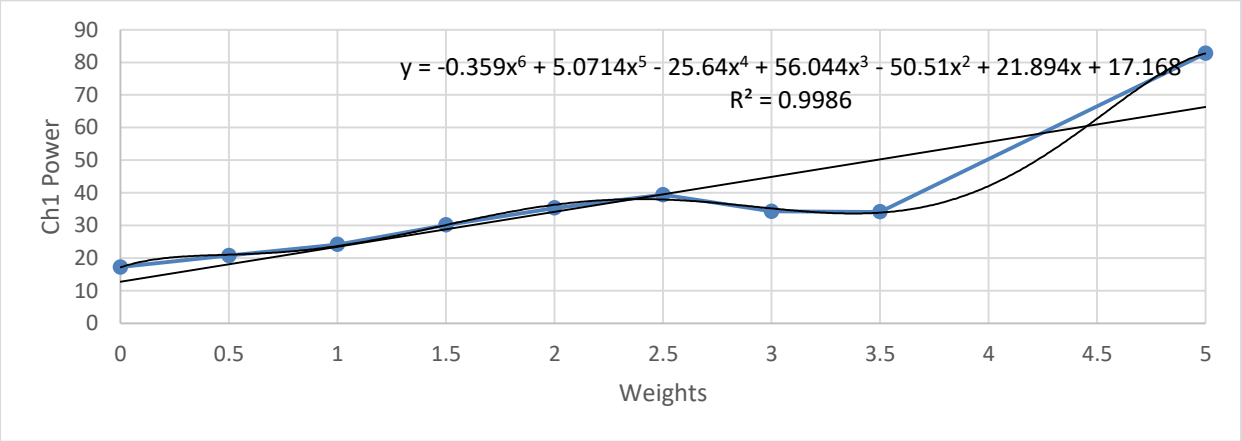

Fig.6.15 EMG muscles band power variation due to increasing load for channel 1.

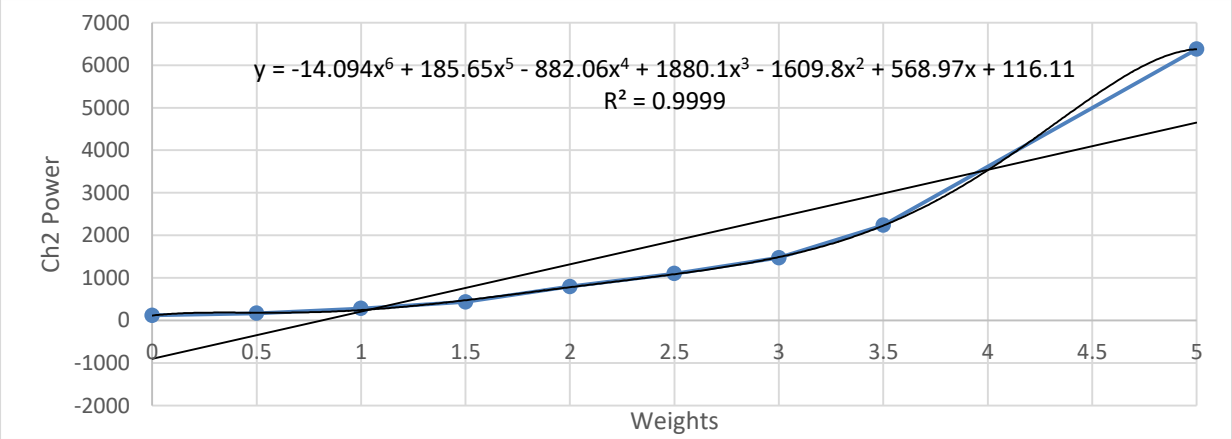

Fig.6.16 EMG muscles band power variation due to increasing load for channel 2.

TABLE:6.3.1.4: Calculating EMG muscles band power due to increasing weight for Subject 4

WEIGHT	CHANNEL 1	CHANNEL 2
0	751.3297643	693.2252807
0.5	725.7348181	3062.021159
1	1638.464322	1983.780139
1.5	2565.763602	1276.826942
2	2214.066531	3363.930249
2.5	2072.950867	5522.637703
3	3173.809553	5729.763792
3.5	3393.627654	5043.406485
5	6788.527491	5621.209661

Below figures are showing that graphical interpretation of EMG muscles band power variation due to increasing weight for subject 4.

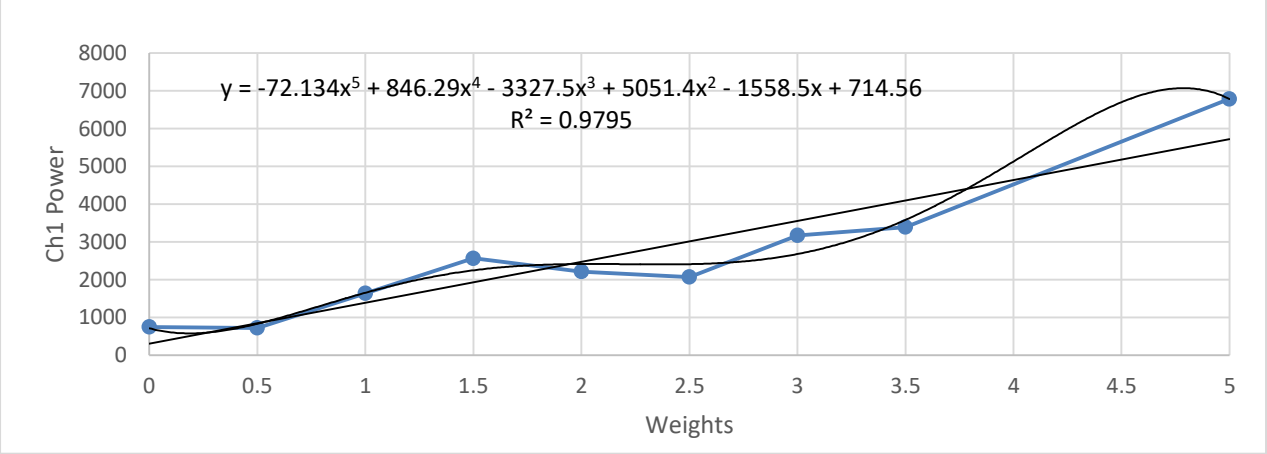

Fig.6.17 EMG muscles band power variation due to increasing load for channel 1.

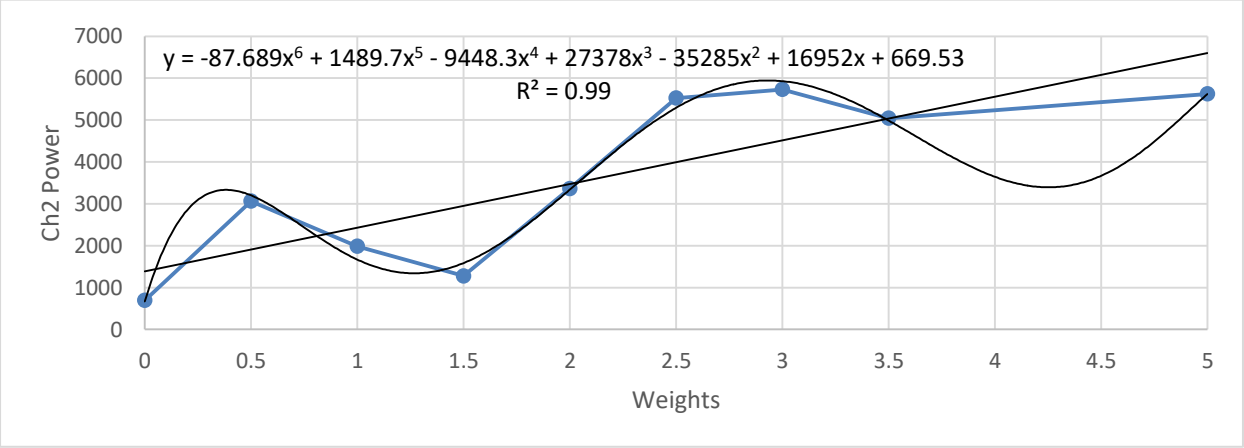

Fig.6.18 EMG muscles band power variation due to increasing load for channel 2.

AVERAGE EMG MUSCLES POWER:

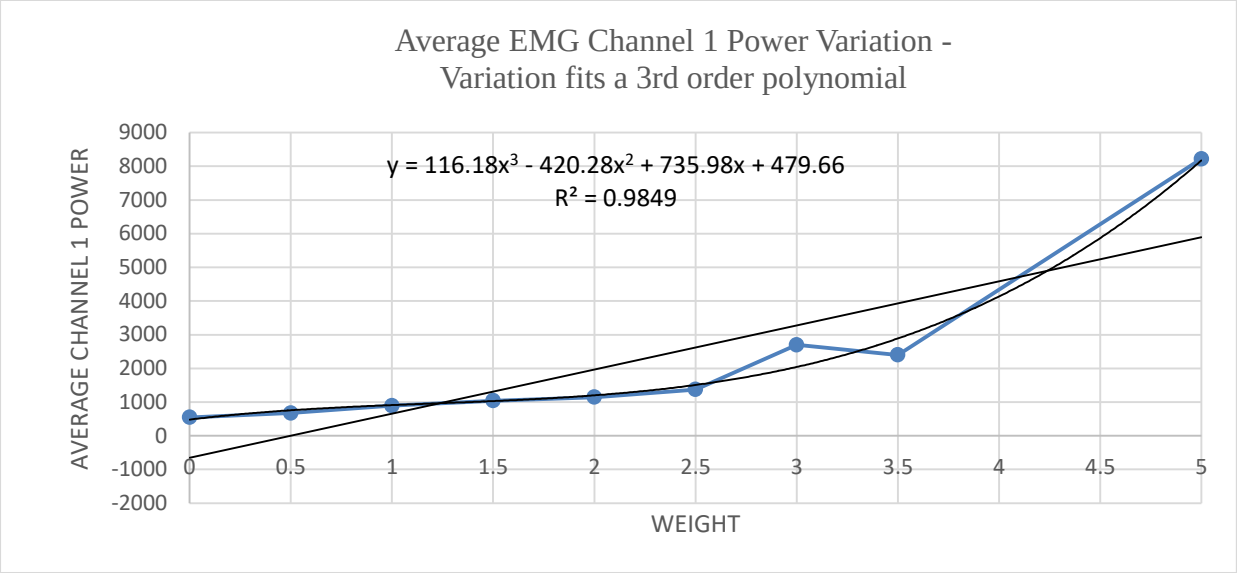

Fig. 6.19 Average EMG muscles band power variation due to increasing load for channel 1.

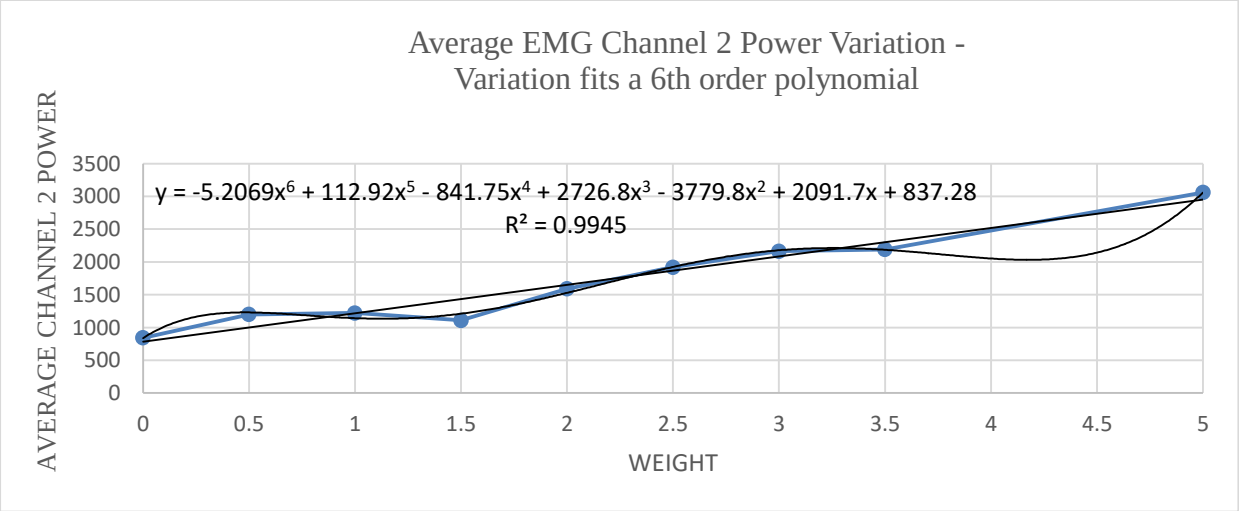

Fig. 6.20 Average EMG muscles band power variation due to increasing load for channel 2.

The findings from the above tables and charts are: -

- From the EMG power graph of channel 1, it can be seen that the power is **gradually increasing** from 0 kg to 5 kg. The R-Square value is 0.9849. This value fits the above power graph into a 3rd order polynomial equation.

- From the EMG power graph of channel 2, it can be seen that the power is **gradually increasing** from 0 kg to 5 kg. The R-Square value is 0.9945. This value fits the above power graph into a 6^{th} order polynomial equation.

6.3.2 RESULTS OF EEG ALPHA AND BETA BAND POWER AND EMG MUSCLES BAND POWER:

When it comes to calculating EEG band power and EMG muscles band power, we used MATLAB software. For finding the power in a certain frequency range, the sample rate, fs (sampling frequency) needs to be specified. Band-power employs a modified periodogram to calculate the average power in a frequency band. In addition, we have prepared a table and a graph for comparison with eight other subjects. Here, we have figured out the power of alpha and beta [128]. In addition, the power of the muscles EMG bands was also computed [129]. Both the calculations of power were done in relation to the lifting of various weights.

- **Alpha band power due to varying weight**

TABLE.6.3.2.5: Calculating EEG alpha band power due to increasing weight for Subject 1

ALPHA(8hz-13hz)			
WEIGHT	C3-CZ	C4-CZ	CZ-REF
0	6716.55	6828.44	6738.24
0.5	17282.09	17408.51	18293.89
1	16149.25	15857.89	17233.32
1.5	22955.30	22743.66	21937.44
2	32277.22	32025.71	33051.28
2.5	25075.65	25724.51	25801.58
3	10074.72	10454.15	11229.55
3.5	20883.52	21124.47	20583.42
5	25092.06	25852.93	25726.78

Below figures are showing that graphical interpretation of EEG alpha band power variation due to increasing weight for subject 1.

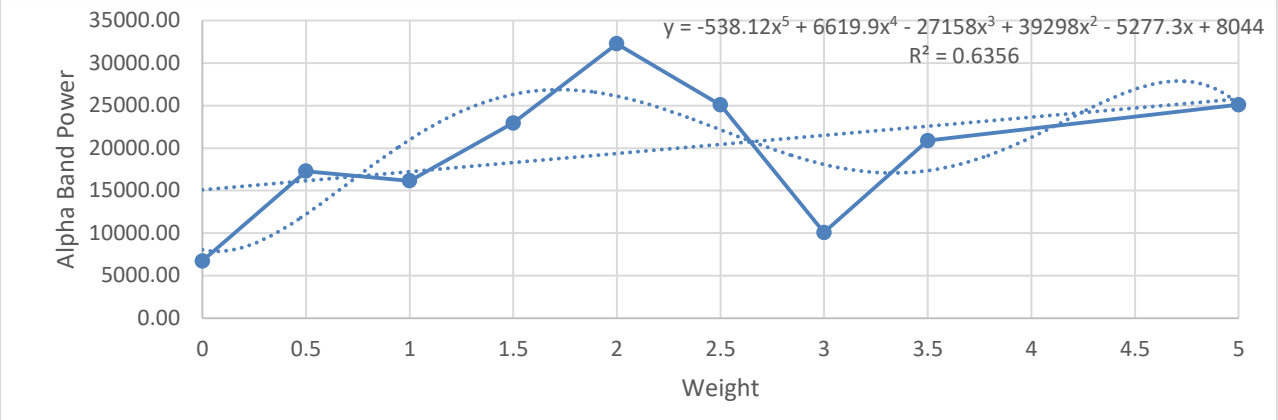

Fig.6.21 EEG alpha band power variation due to increasing load for lead C3-CZ

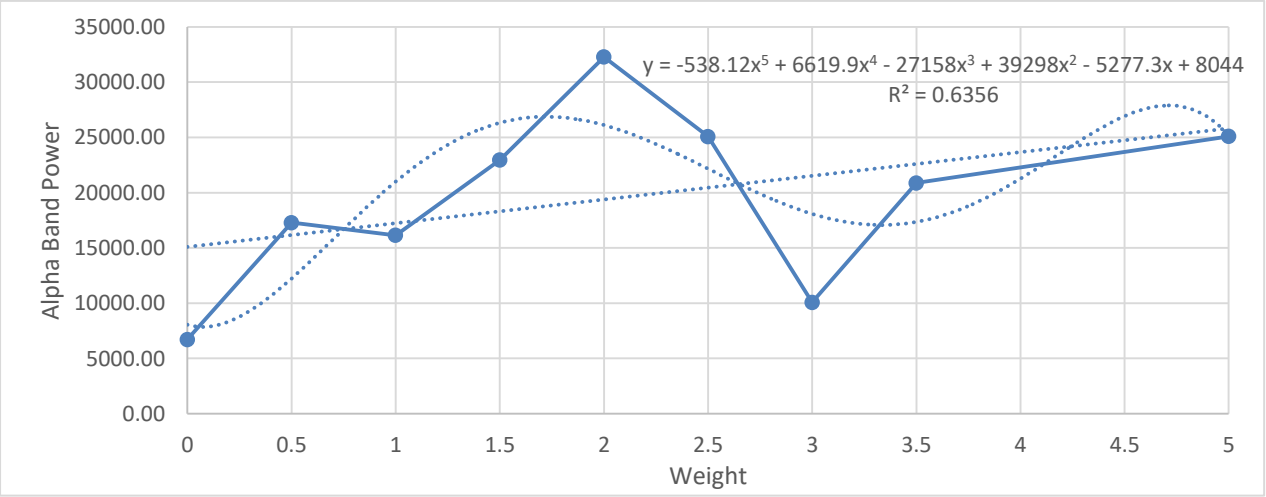

Fig.6.22 EEG alpha band power variation due to increasing load for lead C4-CZ

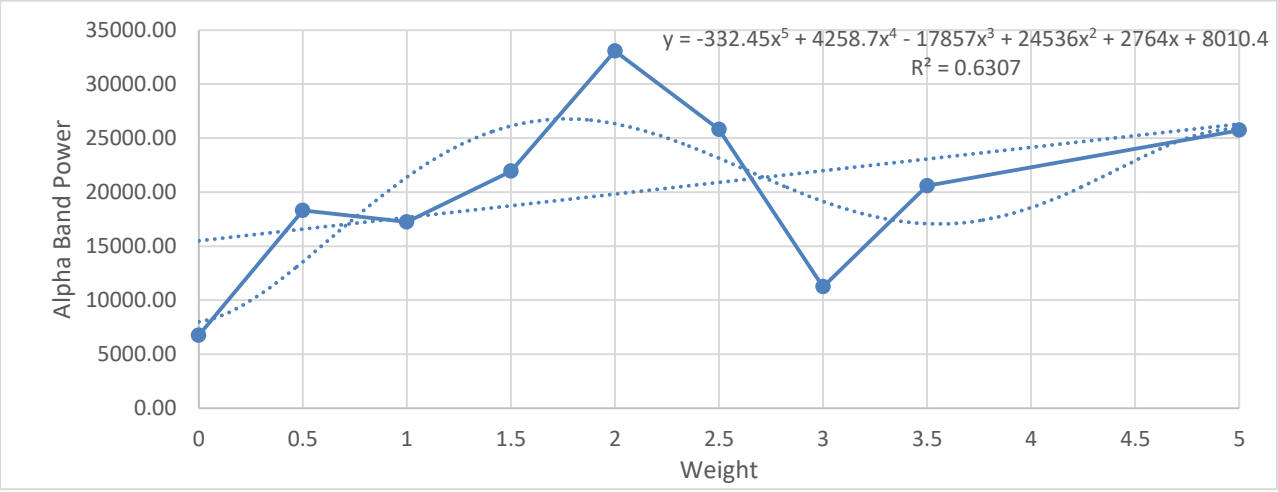

Fig.6.23 EEG alpha band power variation due to increasing load for lead CZ-REF

TABLE.6.3.2.6: Calculating EEG alpha band power due to increasing weight for Subject 2

ALPHA(8hz-13hz)			
WEIGHT	C3-CZ	C4-CZ	CZ-REF
0	36.61	46.00	189.45
0.5	216.42	429.22	318.78
1	148.99	113.89	371.23
1.5	112.15	159.33	347.62
2	28.06	78.85	177.06
2.5	56.10	185.41	230.85
3	197.23	172.23	464.69
3.5	86.94	73.59	289.90
5	81.66	60.86	291.05

Below figures are showing that graphical interpretation of EEG alpha band power variation due to increasing weight for subject 2.

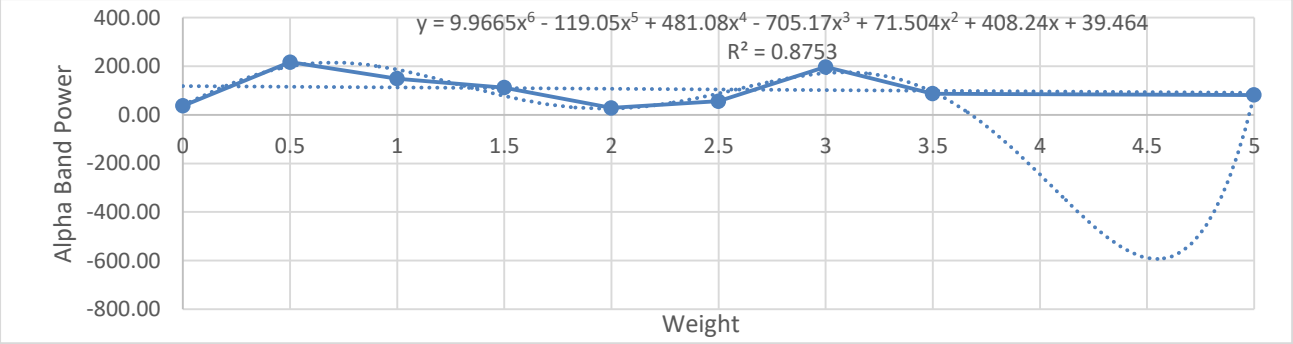

Fig.6.24 EEG alpha band power variation due to increasing load for lead C3-CZ

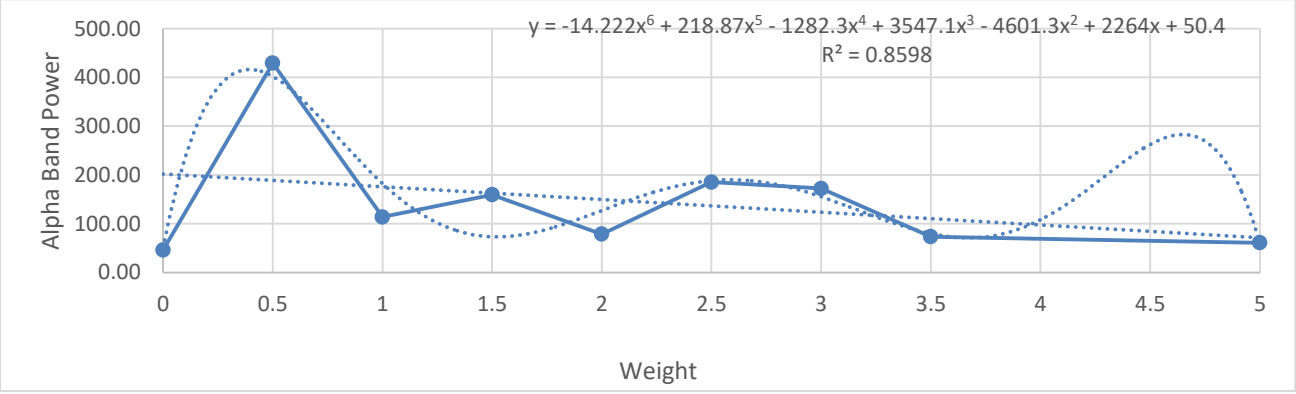

Fig.6.25 EEG alpha band power variation due to increasing load for lead C4-CZ

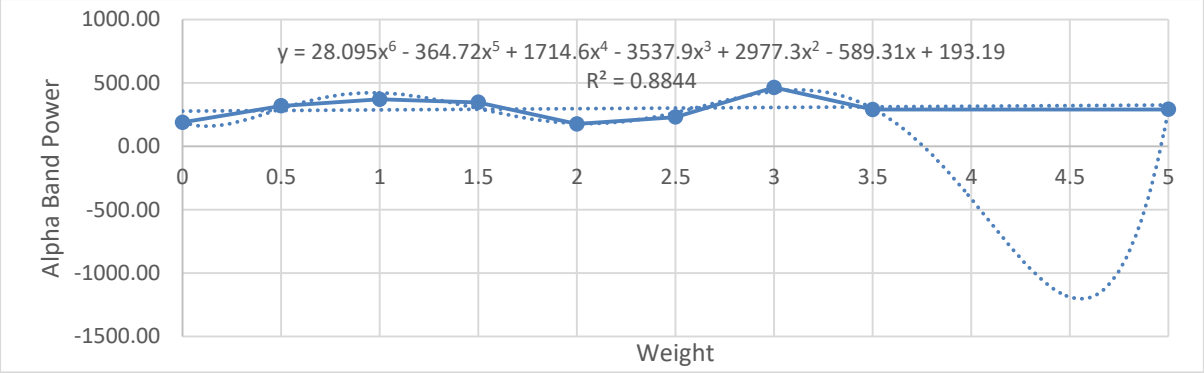

Fig.6.26 EEG alpha band power variation due to increasing load for lead CZ-REF

TABLE.6.3.2.7: Calculating EEG alpha band power due to increasing weight for Subject 3

ALPHA(8hz-13hz)			
WEIGHT	C3-CZ	C4-CZ	CZ-REF
0	184.23	168.27	315.67
0.5	272.91	227.38	421.16
1	157.50	113.67	442.40
1.5	365.46	170.95	532.04
2	271.81	190.02	653.76
2.5	189.86	157.65	422.07
3	190.87	195.62	384.82
3.5	338.04	138.24	501.67
5	258.57	233.25	576.95

Below figures are showing that graphical interpretation of EEG alpha band power variation due to increasing weight for subject 3.

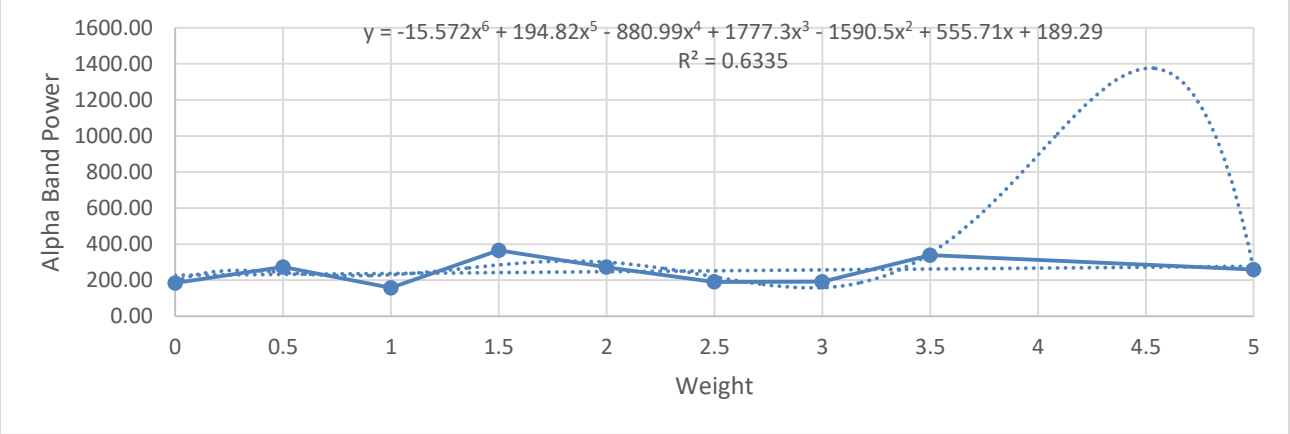

Fig.6.27 EEG alpha band power variation due to increasing load for lead C3-CZ

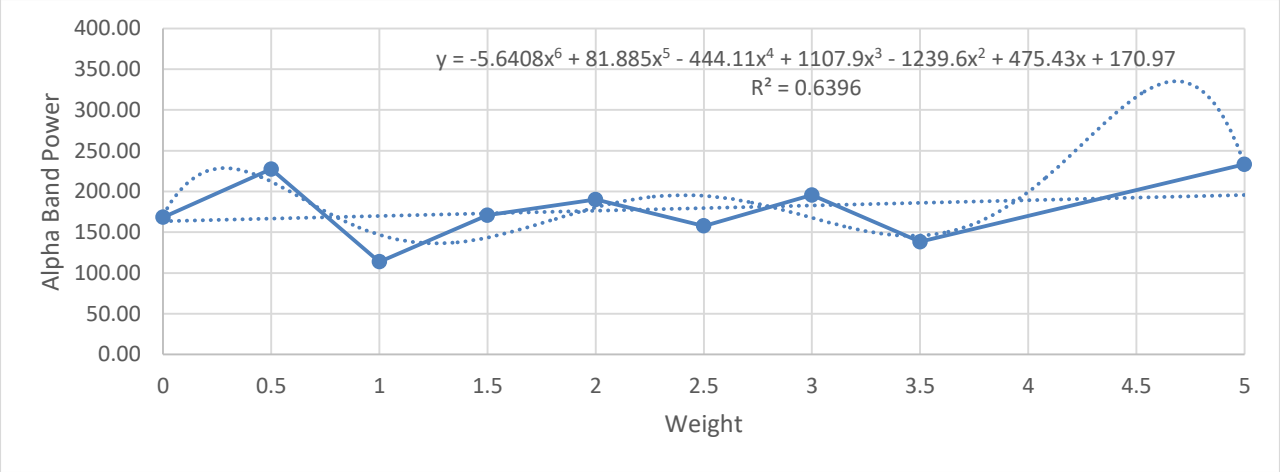

Fig.6.28 EEG alpha band power variation due to increasing load for lead C4-CZ

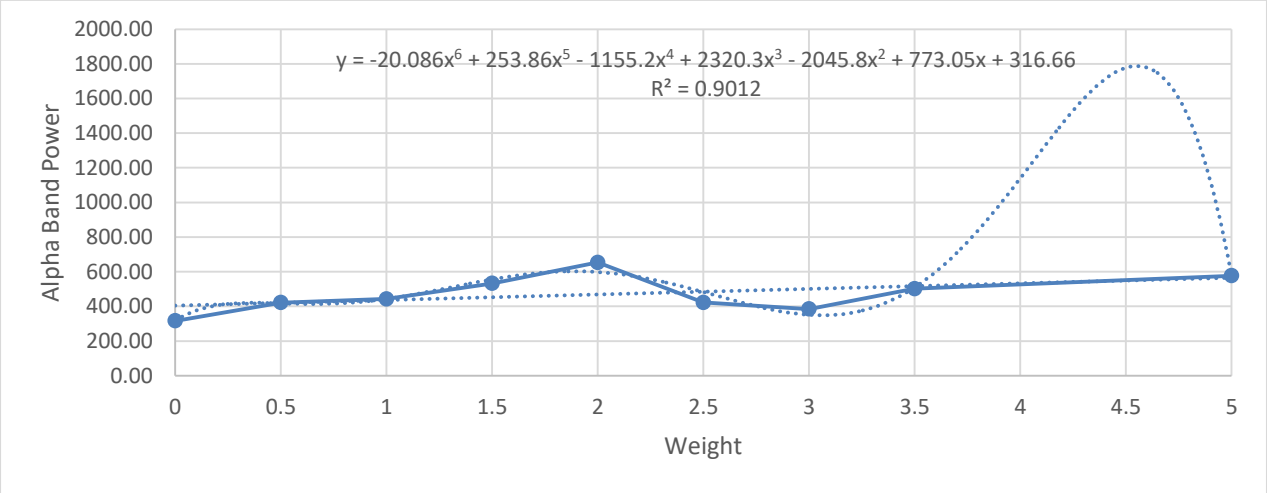

Fig.6.29 EEG alpha band power variation due to increasing load for lead CZ-REF

➢ AVERAGE ALPHA BAND POWER VARIATION:

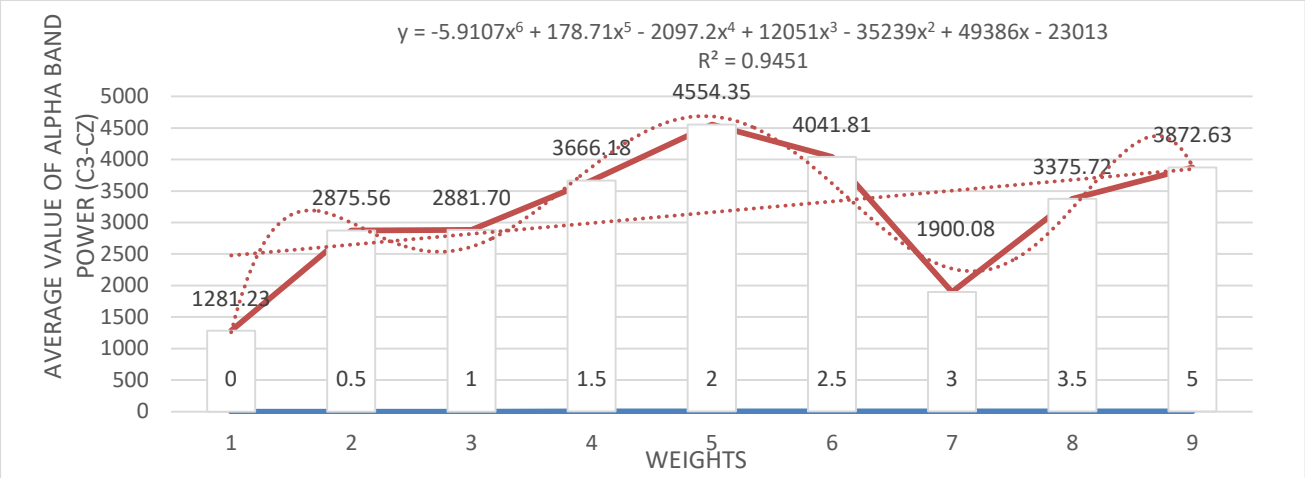

Fig.6.30 EEG average alpha band power variation due to varying load for lead C3-CZ.

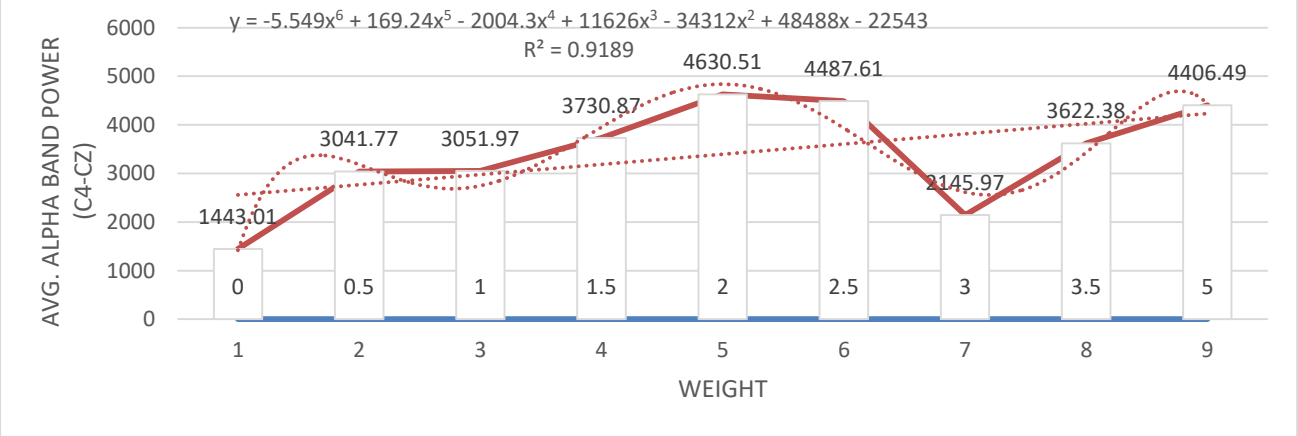

Fig.6.31 EEG average alpha band power variation due to varying load for lead C4-CZ

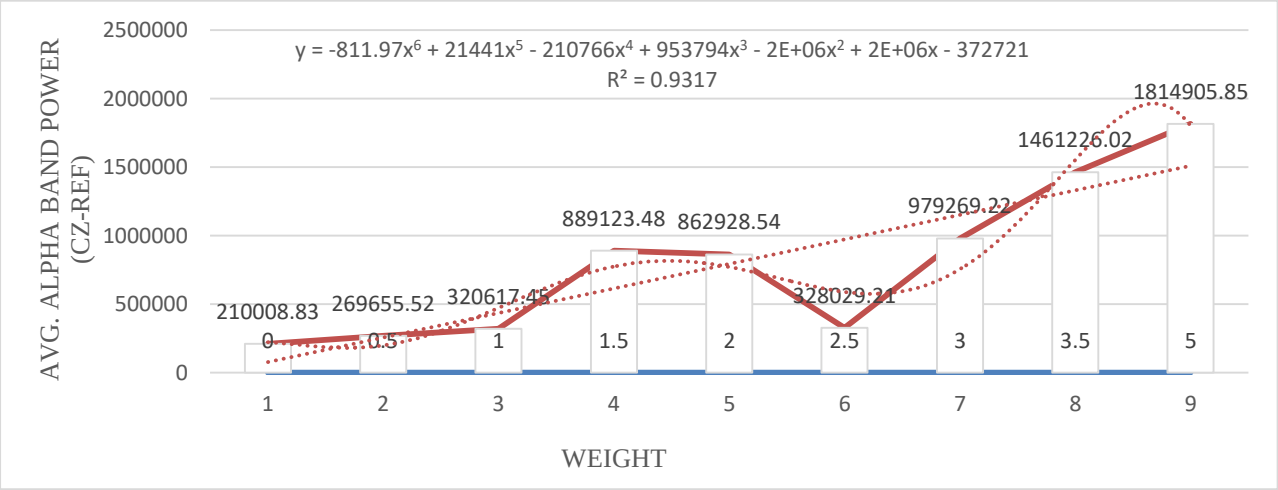

Fig.6.32 EEG average alpha band power variation due to varying load for lead CZ-REF

➢ Beta band power due to varying weight

TABLE.6.3.2.8: Calculating EEG beta band power due to increasing weight for Subject 1

BETA (13hz-30hz)			
WEIGHT	C3-CZ	C4-CZ	CZ-REF
0	3745.26	3698.55	3913.63
0.5	14967.13	15093.70	15165.82
1	10807.72	10728.91	11136.37
1.5	22904.82	22597.00	22202.80
2	20606.88	20509.61	21573.19
2.5	16632.60	17170.47	17396.39
3	10074.72	10454.15	11229.55
3.5	14791.89	15217.32	14835.85
5	19553.83	20177.00	20454.52

Below figures are showing that graphical interpretation of EEG beta band power variation due to increasing weight for subject 1.

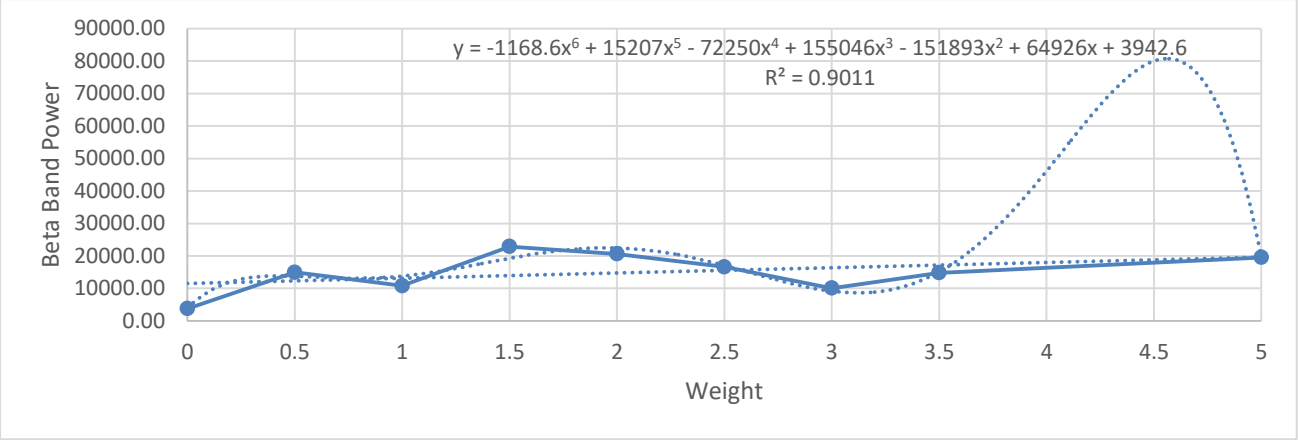

Fig.6.33 EEG beta band power variation due to increasing load for lead C3-CZ

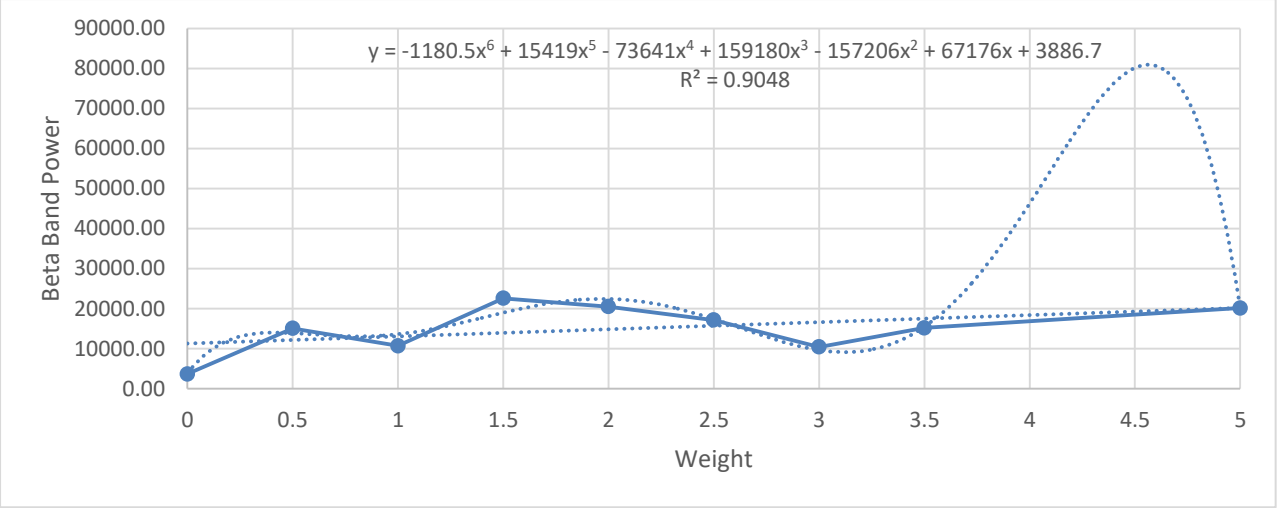

Fig.6.34 EEG beta band power variation due to increasing load for lead C4-CZ

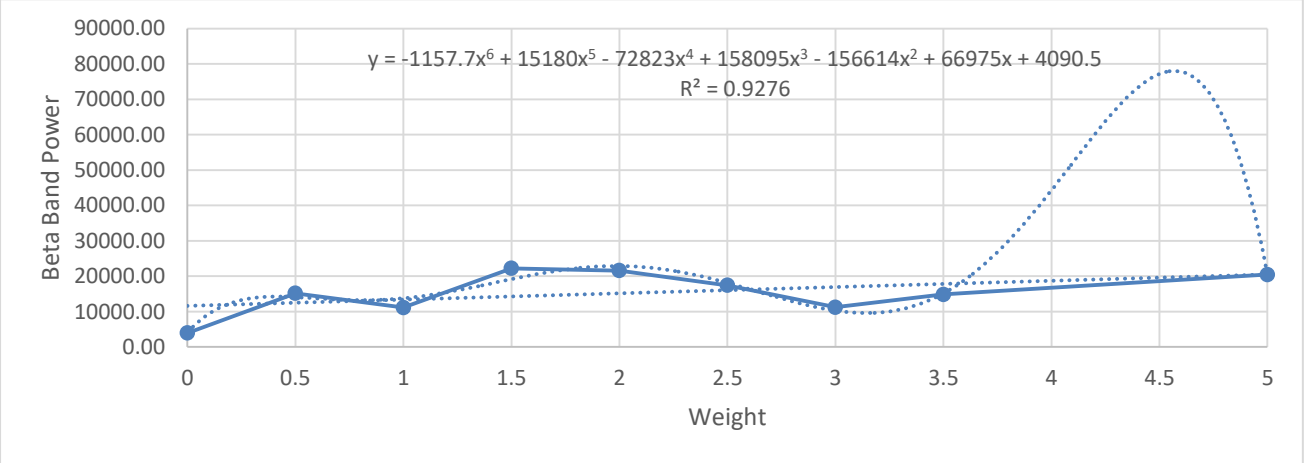

Fig.6.35 EEG beta band power variation due to increasing load for lead CZ-REF

TABLE.6.3.2.9: Calculating EEG beta band power due to increasing weight for Subject 2

BETA (13hz-30hz)			
WEIGHT	C3-CZ	C4-CZ	CZ-REF
0	12.38	24.34	48.02
0.5	31.55	32.35	80.14
1	38.66	41.05	123.28
1.5	18.00	28.31	93.95
2	16.98	35.37	56.76
2.5	16.88	21.68	61.36
3	197.23	172.23	464.69
3.5	16.65	32.13	84.46
5	16.12	37.21	96.66

Below figures are showing that graphical interpretation of EEG beta band power variation due to increasing weight for subject 2.

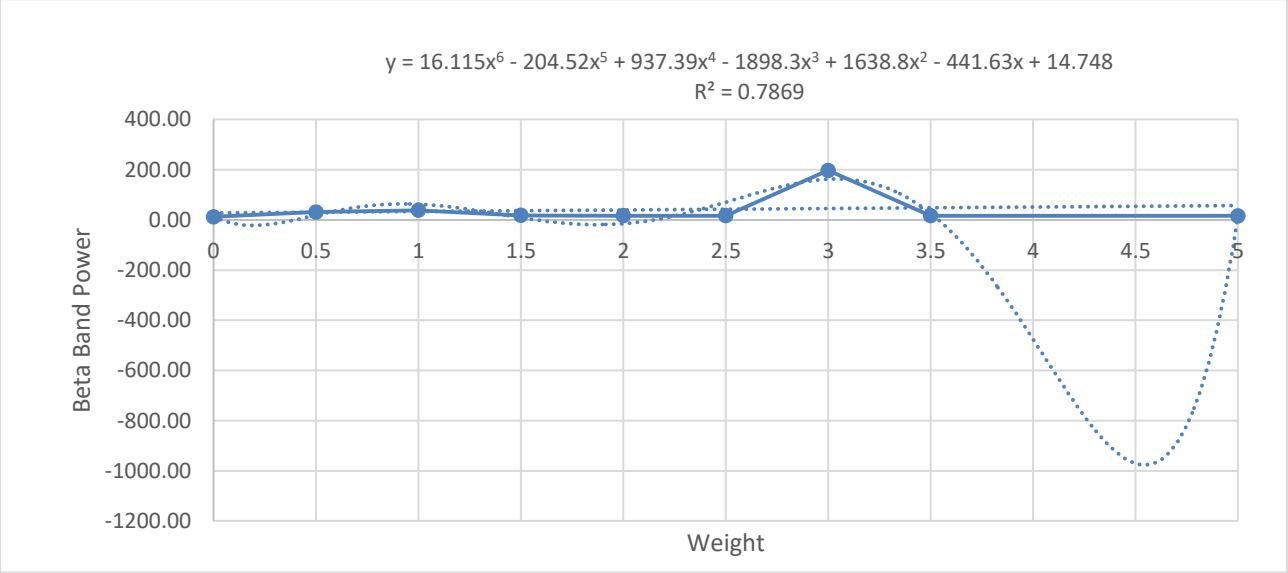

Fig.6.36 EEG beta band power variation due to increasing load for lead C3-CZ

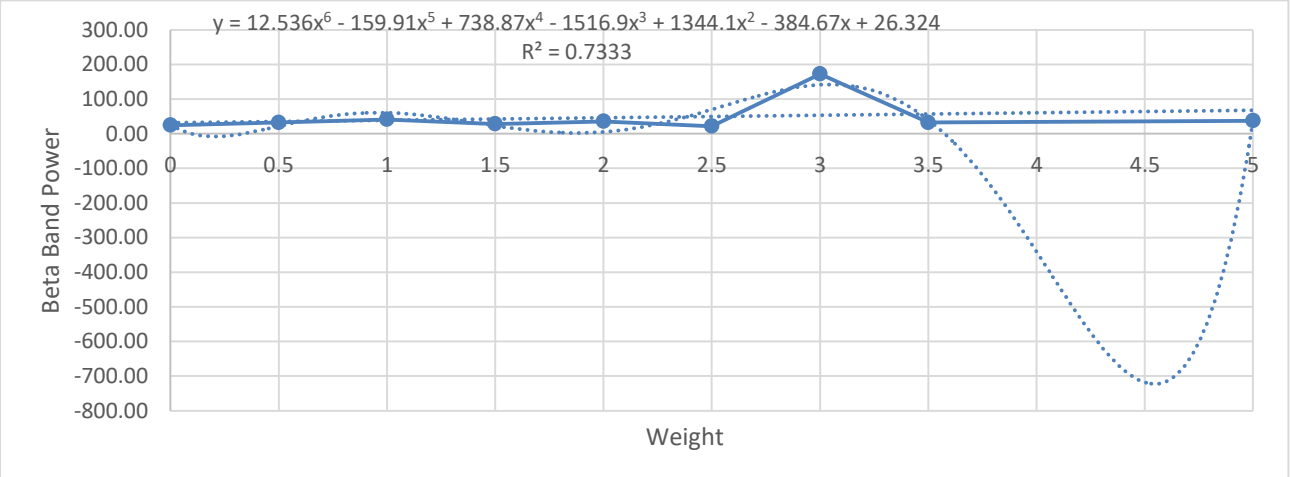

Fig.6.37 EEG beta band power variation due to increasing load for lead C4-CZ

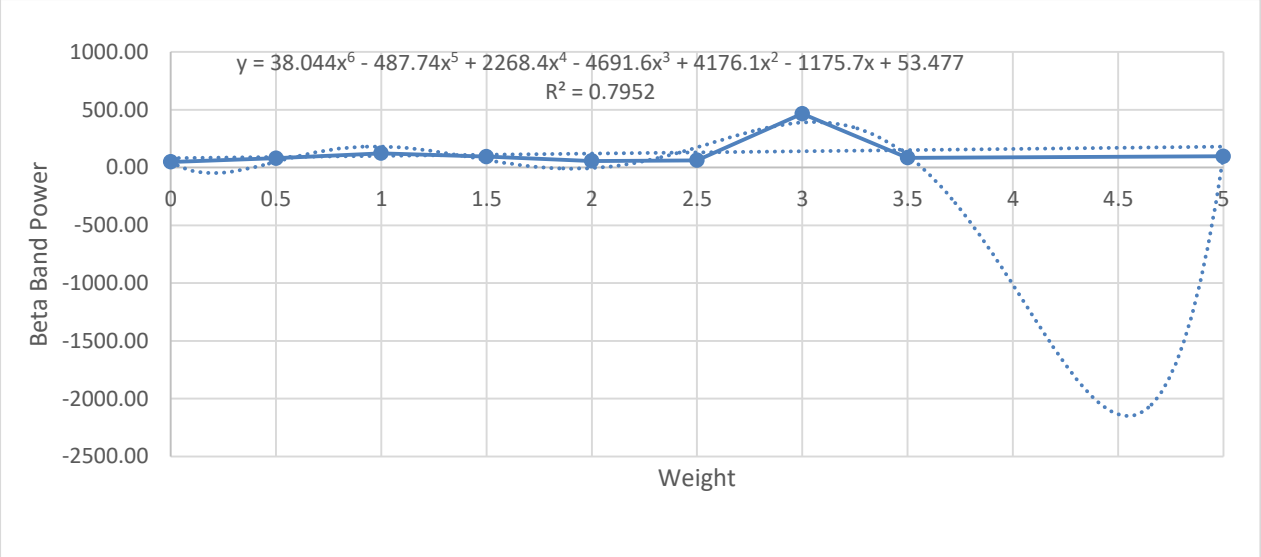

Fig.6.38 EEG beta band power variation due to increasing load for lead CZ-REF

➢ AVERAGE BETA BAND POWER VARIATION:

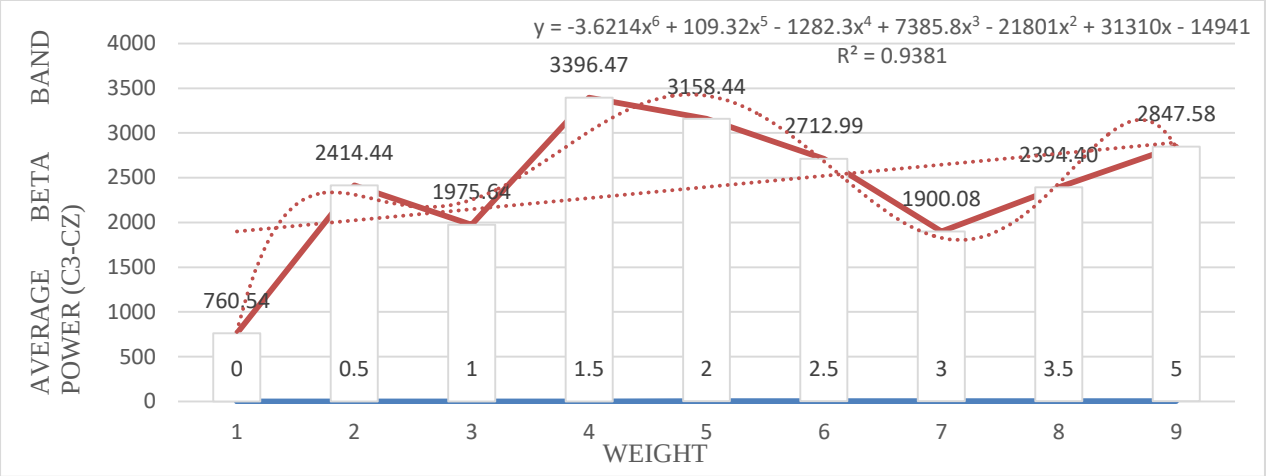

Fig.6.39 EEG average beta band power variation due to varying load for lead C3-CZ.

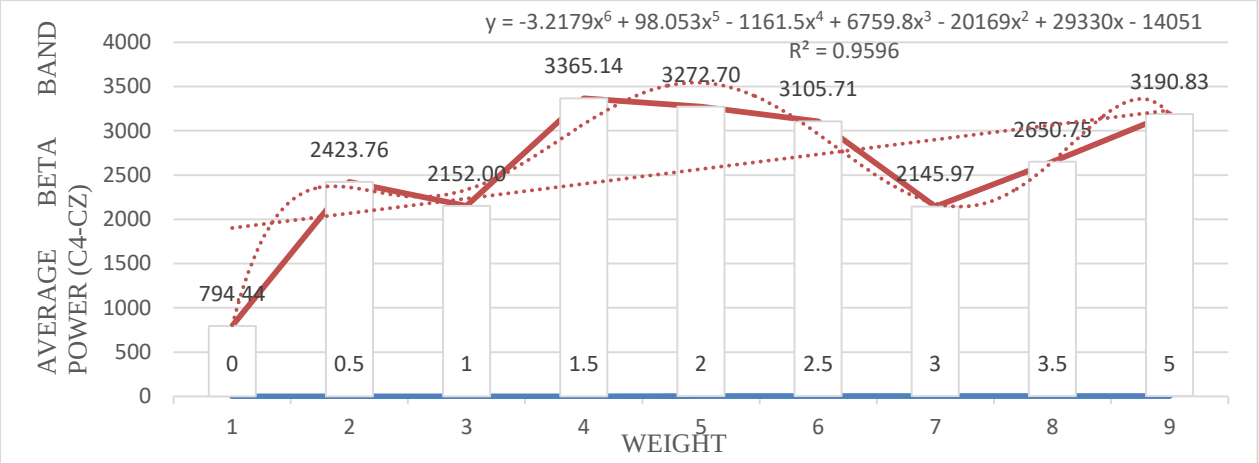

Fig.6.40 EEG average beta band power variation due to varying load for lead C4-CZ

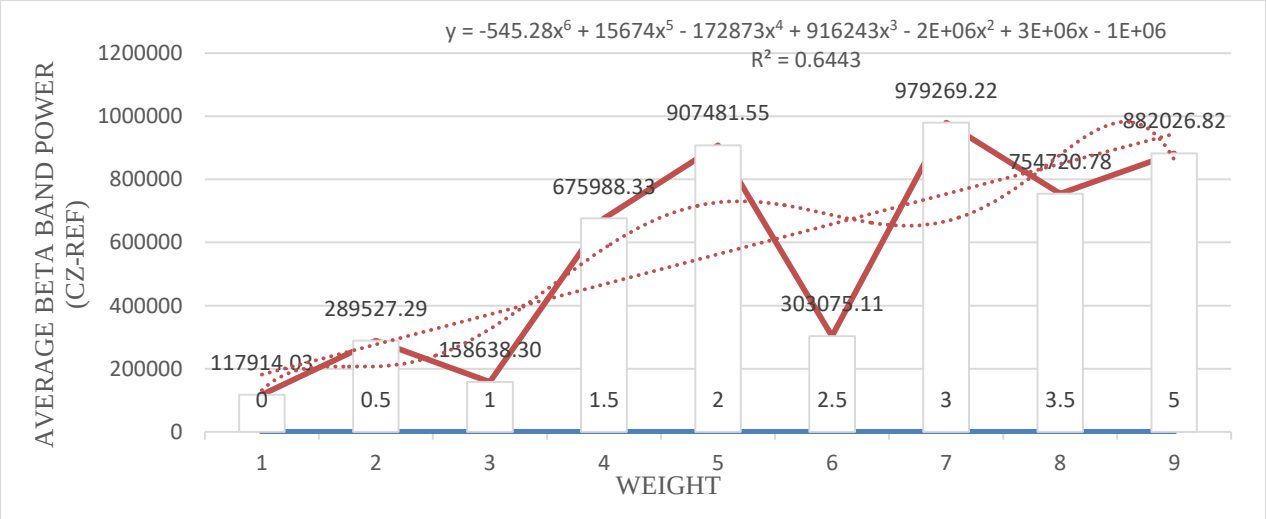

Fig.6.41 EEG average beta band power variation due to varying load for lead CZ-REF

The findings from the above tables and charts are: -

- From the EEG alpha band power graph of all leads, it can be seen that the power is increasing from 0 kg to 5 kg. There are fluctuations present in the graph for the weights of 0.5 kg, 1 kg, 1.5 kg, 2 kg, 2.5 kg, 3 kg, 3.5 kg. R-Square value obtained from the graph fits the above alpha band power graph into a 6^{th} order polynomial equation.

- From the EEG beta band power graph of all leads, it can be seen that the power is increasing from 0 kg to 5 kg. There are fluctuations present in the graph for the weights of 0.5 kg, 1 kg, 1.5 kg, 2 kg, 2.5 kg, 3 kg, 3.5 kg. R-Square value obtained from the graph fits the above beta band power graph into a 6^{th} order polynomial equation.

6.4 Calculating Fractal Dimension by the help of Higuchi's method:

For nonlinear dynamics we have used Higuchi fractal dimension for determining fractal dimension. In methodology section we have already discussed HFD algorithms. Now we want to see K_{max} value and respect to K_{max} value How to varying fractal dimension [130]. Below we have discussed all the tables as well as graphs for both EEG and EMG signals for all channels.

6.4.1 Selecting K_{max}:

Choosing the best Kmax has a direct impact on HFD outcomes. The right method for determining optimal Kmax values by monitoring the graph saturation point. The Kmax value is given by the corresponding point. For EMG signal Kmax was set to 100 and for EEG signal Kmax was set to 50 in this work.

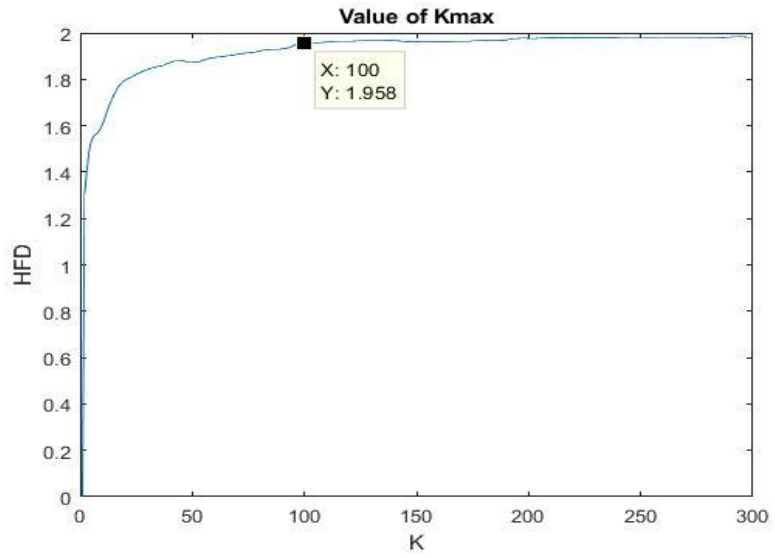

Fig.6.42 HFD vs K plot shows that Kmax value 100 for EMG signal.

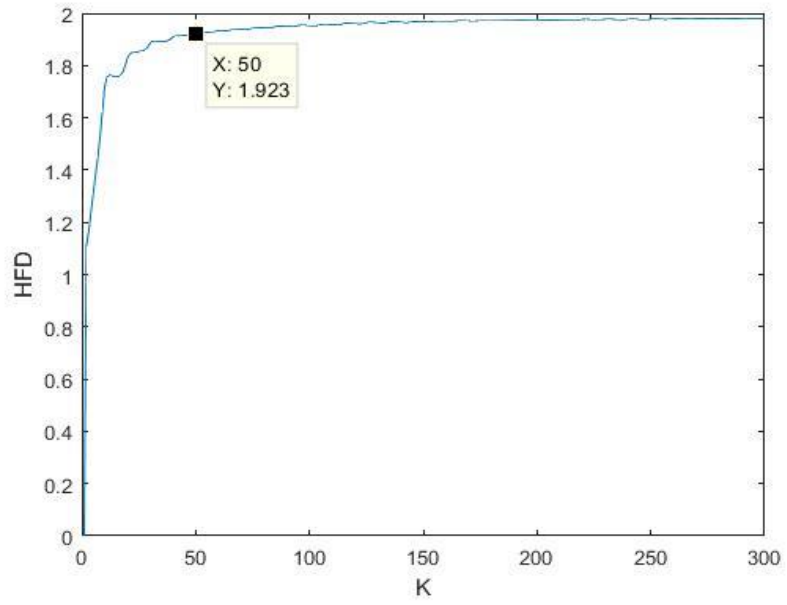

Fig.6.43 HFD vs K plot shows that Kmax value 50 for EEG signal.

By picking an appropriate value of Kmax, this approach allows for direct measurement of the fractal dimension. hfd(x,K_{max}), a MATLAB® function for calculating fractal dimension (FD), returns the FD value when x (EMG or EEG signal) and Kmax are supplied as inputs. As illustrated in Fig.6.42, Fig.6.43 the value of Kmax is determined as the point at which the FD value is not changing. Fractal analysis by the help of Higuchi's algorithm is given in the below tables and graphs for both signal EEG and EMG for eight subjects.

6.4.2 Calculating Fractal Dimension for EEG signal:

TABLE:6.4.2.10: Calculating EEG fractal dimension due to increasing weight for Subject 1

WEIGHT	C3-CZ	C4-CZ	CZ-REF
0	1.92309468	1.923186517	1.858721956
0.5	1.91169555	1.910662064	1.824779303
1	1.914170665	1.912610736	1.846954428
1.5	1.901333608	1.901319137	1.82433659
2	1.89896013	1.89857999	1.856321248
2.5	1.898150816	1.89750662	1.838692943
3	1.907212332	1.905530013	1.82917489
3.5	1.913260504	1.912923196	1.86655031
5	1.908072124	1.907374698	1.854518324

Below figures are showing that graphical interpretation of EEG fractal dimension variation due to increasing weight for subject 1.

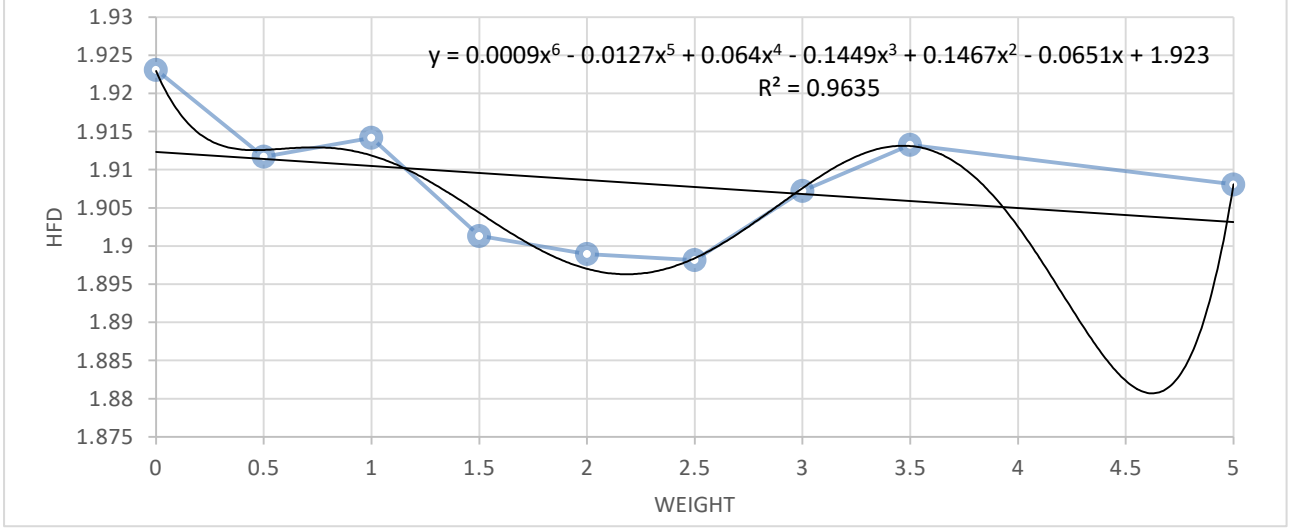

Fig.6.44 Fractal dimension variation due to increasing weight for EEG lead C3-CZ

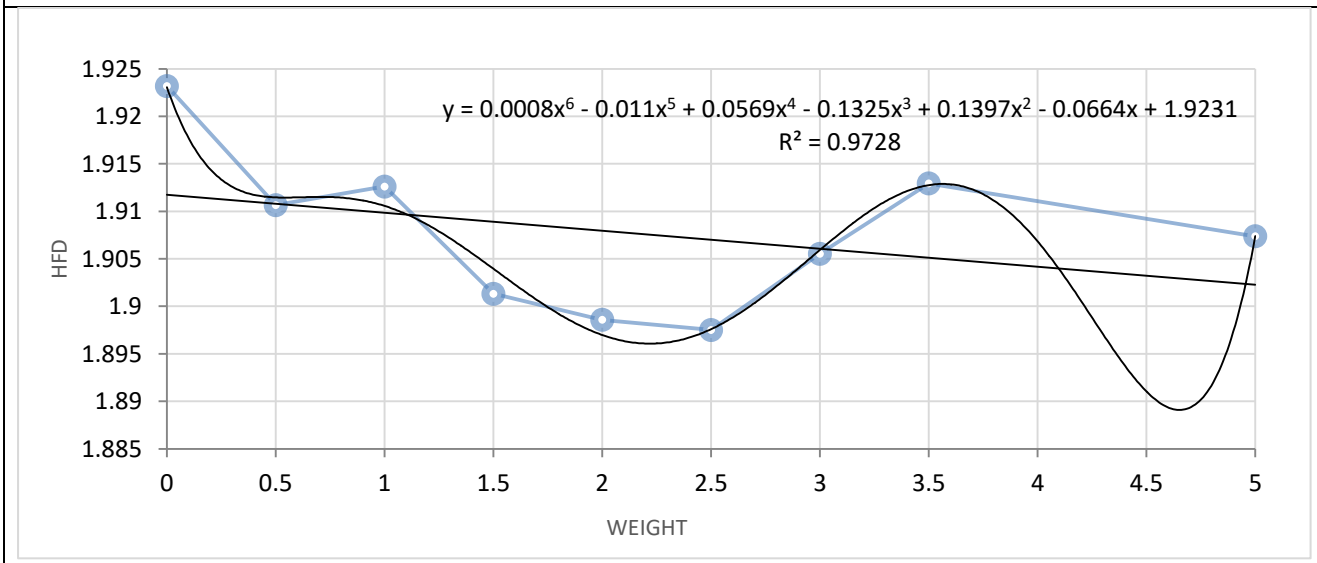

Fig.6.45 Fractal dimension variation due to increasing weight for EEG lead C4-CZ

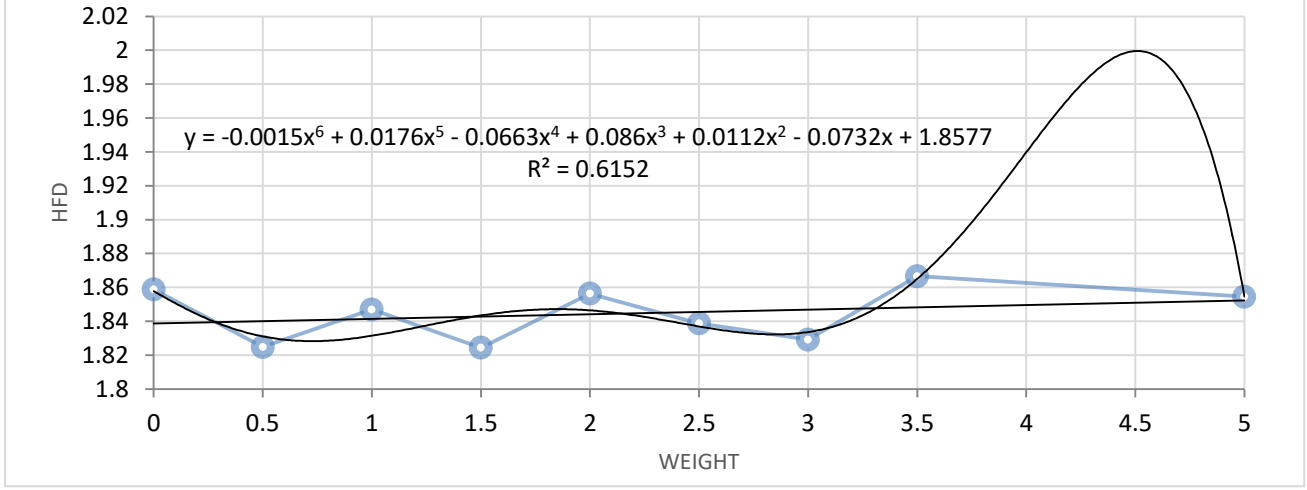

Fig.6.46 Fractal dimension variation due to increasing weight for EEG lead CZ-REF

TABLE:6.4.2.11: Calculating EEG fractal dimension due to increasing weight for Subject 2

WEIGHT	C3-CZ	C4-CZ	CZ-REF
0	1.759983	1.821871775	1.723601167
0.5	1.787811325	1.838936878	1.765415448
1	1.792066136	1.894983971	1.730210039
1.5	1.830531061	1.861234931	1.674718391
2	1.803737201	1.828151832	1.733350913
2.5	1.802190344	1.870740585	1.711476628
3	1.758826793	1.847056545	1.847056545
3.5	1.785740964	1.824845316	1.687324218
5	1.737820151	1.844292874	1.458237885

Below figures are showing that graphical interpretation of EEG fractal dimension variation due to increasing weight for subject 2.

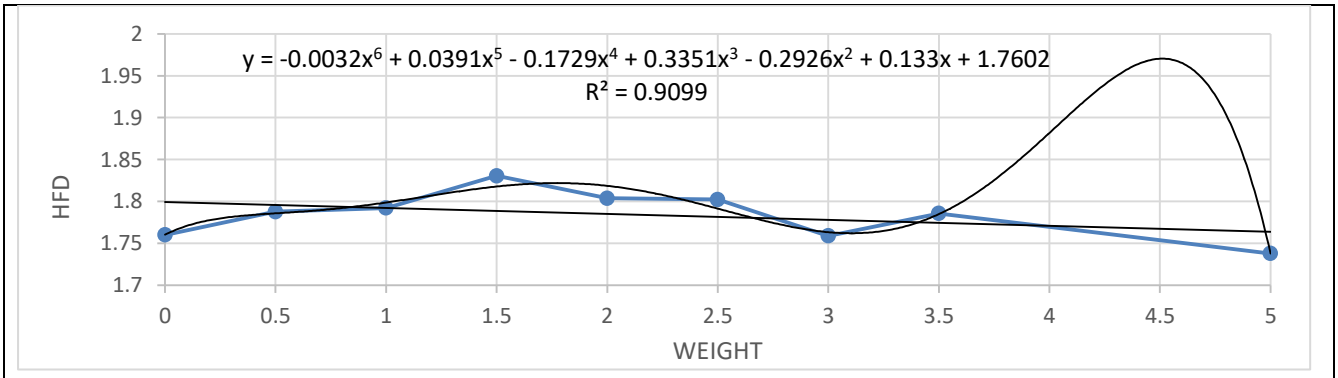

Fig.6.47 Fractal dimension variation due to increasing weight for EEG lead C3-CZ

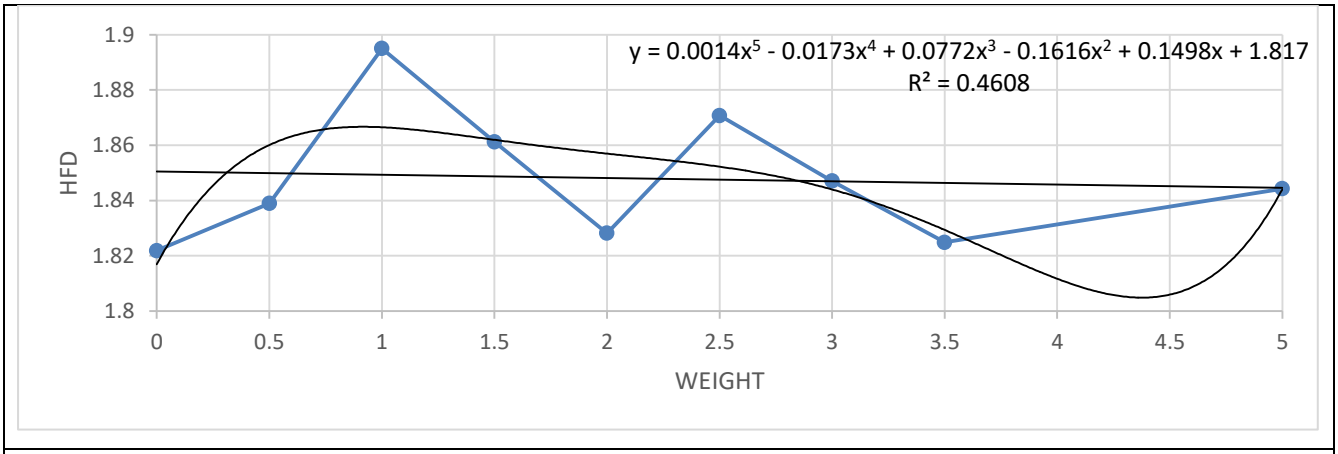

Fig.6.48 Fractal dimension variation due to increasing weight for EEG lead C4-CZ

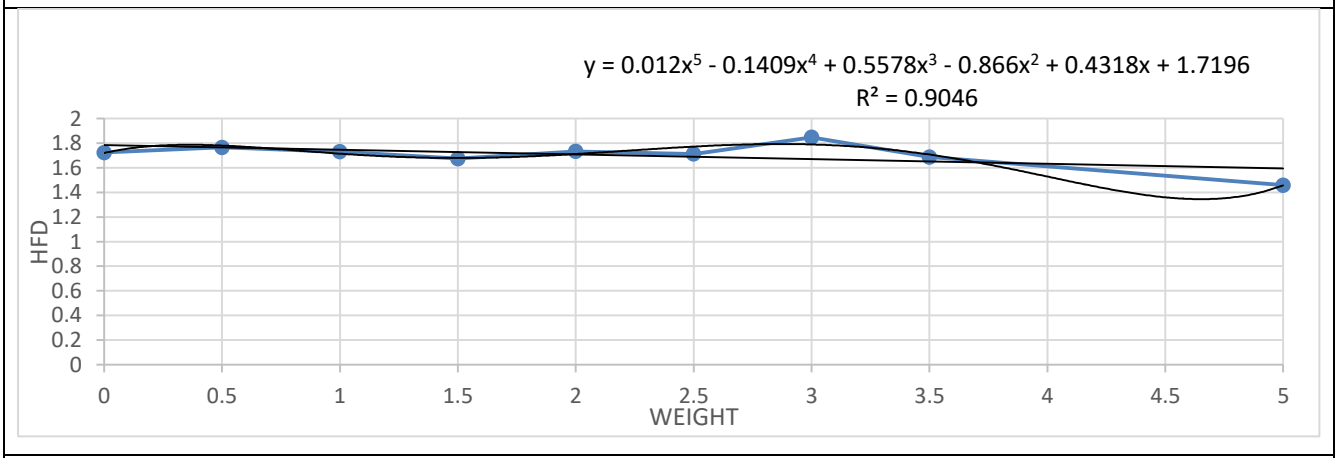

Fig.6.49 Fractal dimension variation due to increasing weight for EEG lead CZ-REF

TABLE:6.4.2.12: Calculating EEG fractal dimension due to increasing weight for Subject 3

WEIGHT	C3-CZ	C4-CZ	CZ-REF
0	1.806451903	1.831057157	1.642061965
0.5	1.814534929	1.811269499	1.668289803
1	1.814016284	1.800518775	1.722884338
1.5	1.779773718	1.786113783	1.759948386
2	1.791516734	1.801786927	1.772036338
2.5	1.83671097	1.850372381	1.791353042
3	1.776314433	1.789704825	1.763393229
3.5	1.806481871	1.814665798	1.77238635
5	1.827127408	1.775316821	1.774781011

Below figures are showing that graphical interpretation of EEG fractal dimension variation due to increasing weight for subject 3.

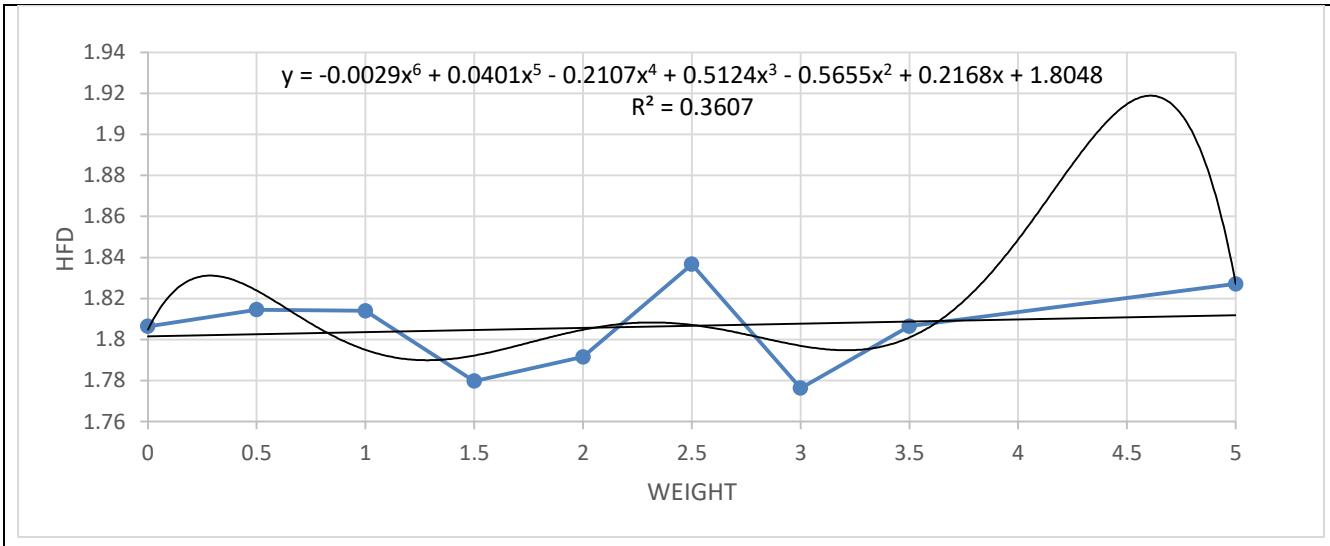

Fig.6.50 Fractal dimension variation due to increasing weight for EEG lead C3-CZ

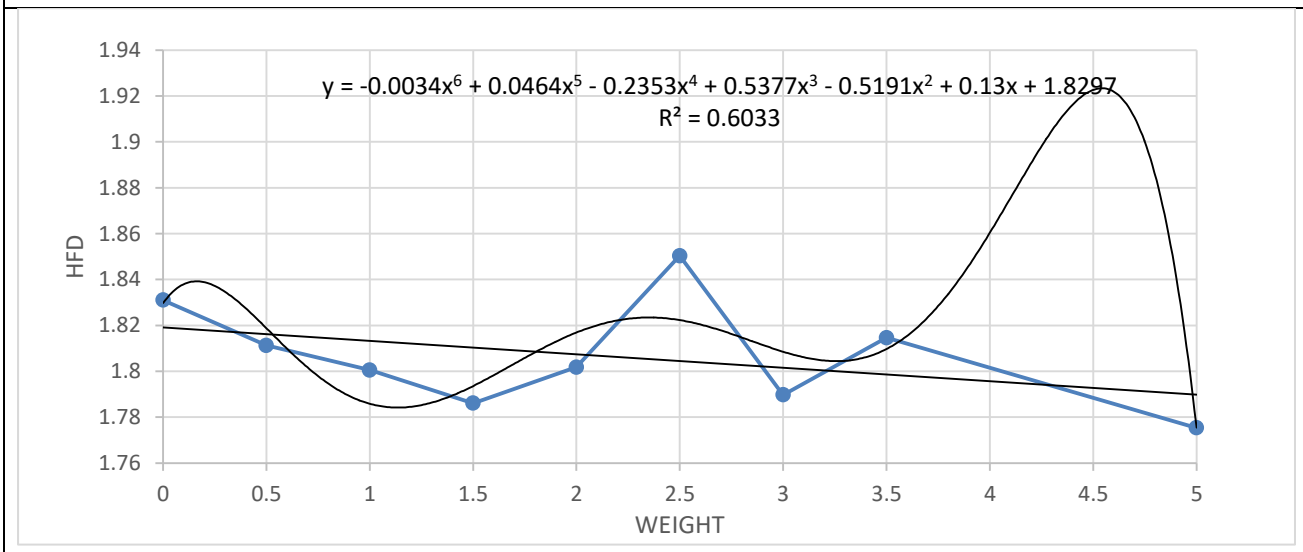

Fig.6.51 Fractal dimension variation due to increasing weight for EEG lead C4-CZ

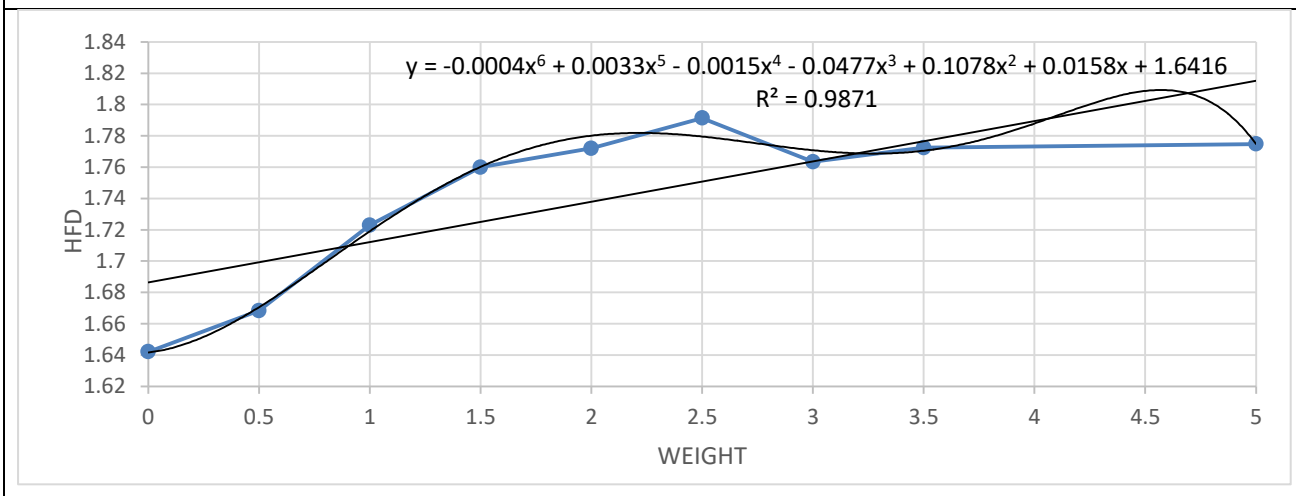

Fig.6.52 Fractal dimension variation due to increasing weight for EEG lead CZ-REF

TABLE:6.4.2.13: Calculating EEG fractal dimension due to increasing weight for Subject 4

WEIGHT	C3-CZ	C4-CZ	CZ-REF
0	1.875025422	1.776764289	1.661924677
0.5	1.867975073	1.769724543	1.592297578
1	1.84401862	1.732621261	1.451993438
1.5	1.856625449	1.745884244	1.620235002
2	1.863343028	1.748027112	1.582353839
2.5	1.883446925	1.767179837	1.587923156
3	1.86025626	1.785466256	1.559793795
3.5	1.836781635	1.747437446	1.482151443
5	1.857600237	1.77138424	1.552669977

Below figures are showing that graphical interpretation of EEG fractal dimension variation due to increasing weight for subject 4.

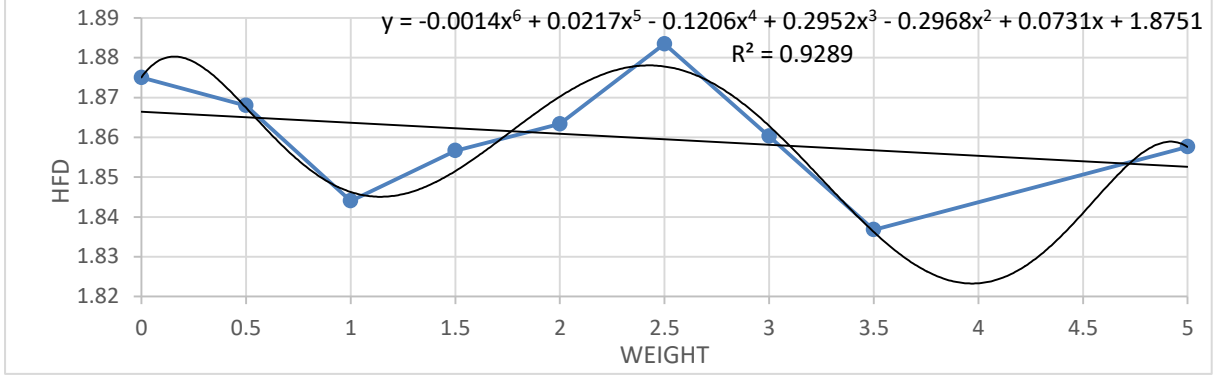

Fig.6.53 Fractal dimension variation due to increasing weight for EEG lead C3-CZ

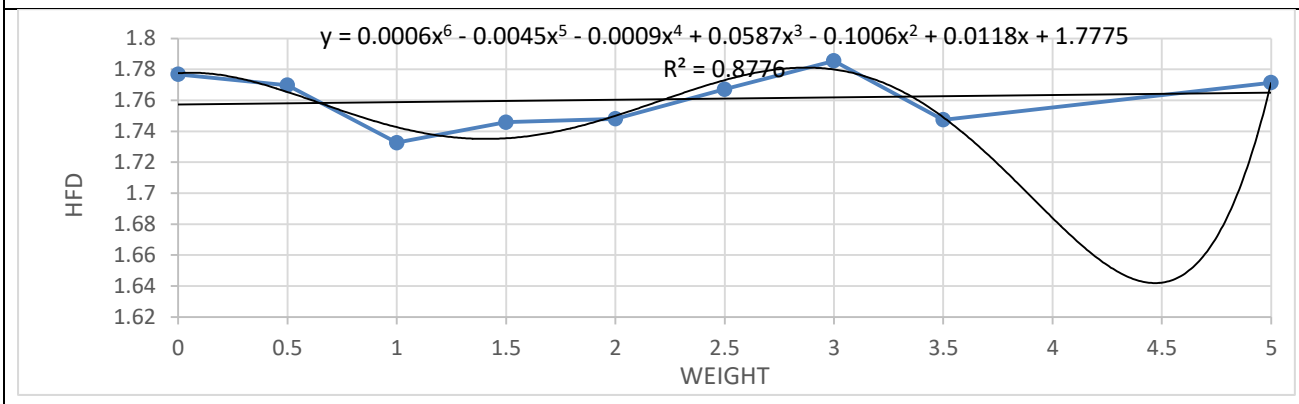

Fig.6.54 Fractal dimension variation due to increasing weight for EEG lead C4-CZ

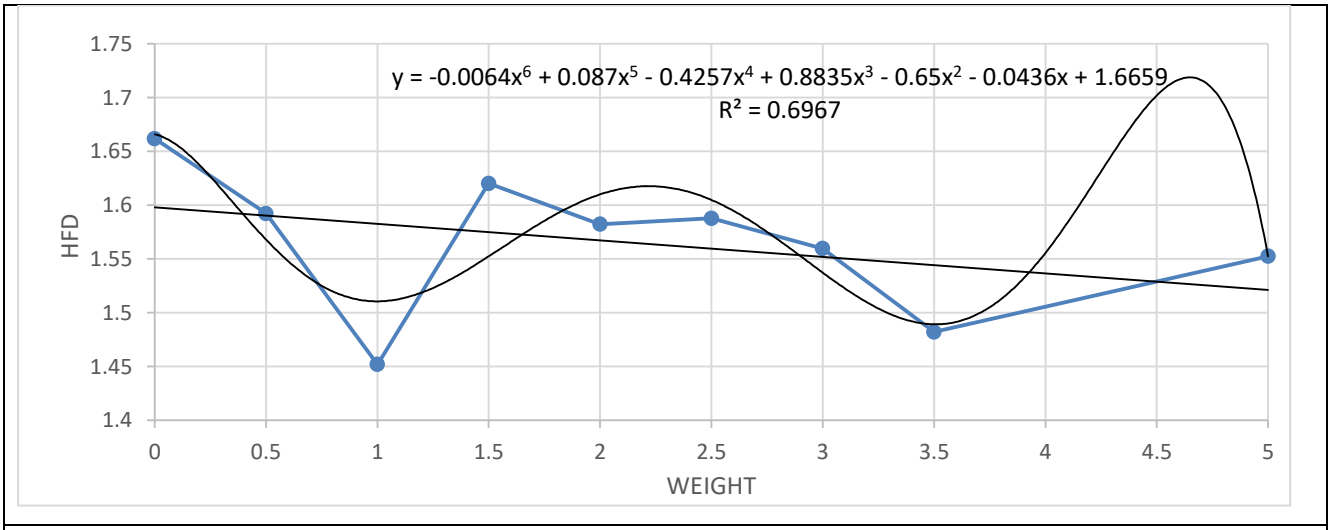

Fig.6.55 Fractal dimension variation due to increasing weight for EEG lead CZ-REF

TABLE:6.4.2.14 Calculating EEG fractal dimension due to increasing weight for Subject 5

WEIGHT	C3-CZ	C4-CZ	CZ-REF
0	1.834026392	1.871439788	1.313311647
0.5	1.825370537	1.85524414	1.402195397
1	1.827691926	1.823303556	1.327708519
1.5	1.8520776	1.850986034	1.321908206
2	1.825703666	1.877651656	1.457389765
2.5	1.84878014	1.863299303	1.773159451
3	1.795647323	1.864217343	1.692084539
3.5	1.807483426	1.867583248	1.790226575
5	1.831132554	1.856473793	1.768755375

Below figures are showing that graphical interpretation of EEG fractal dimension variation due to increasing weight for subject 5.

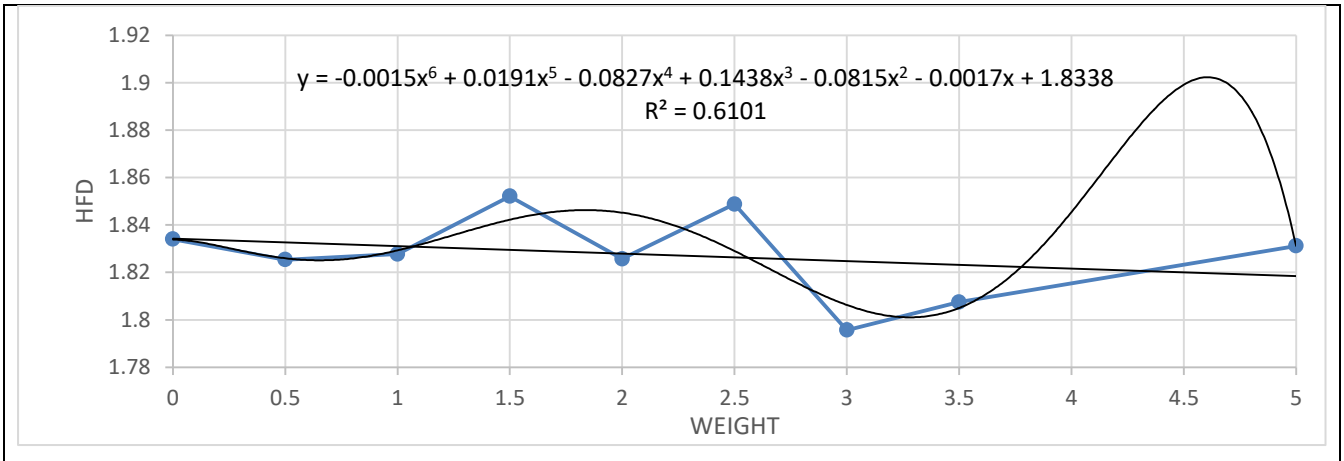

Fig.6.56 Fractal dimension variation due to increasing weight for EEG lead C3-CZ

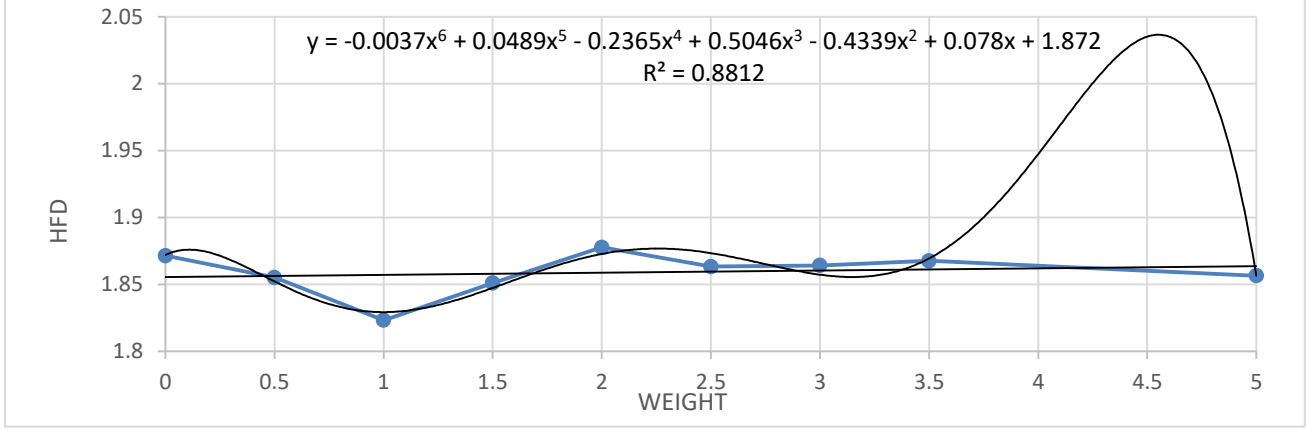

Fig.6.57 Fractal dimension variation due to increasing weight for EEG lead C4-CZ

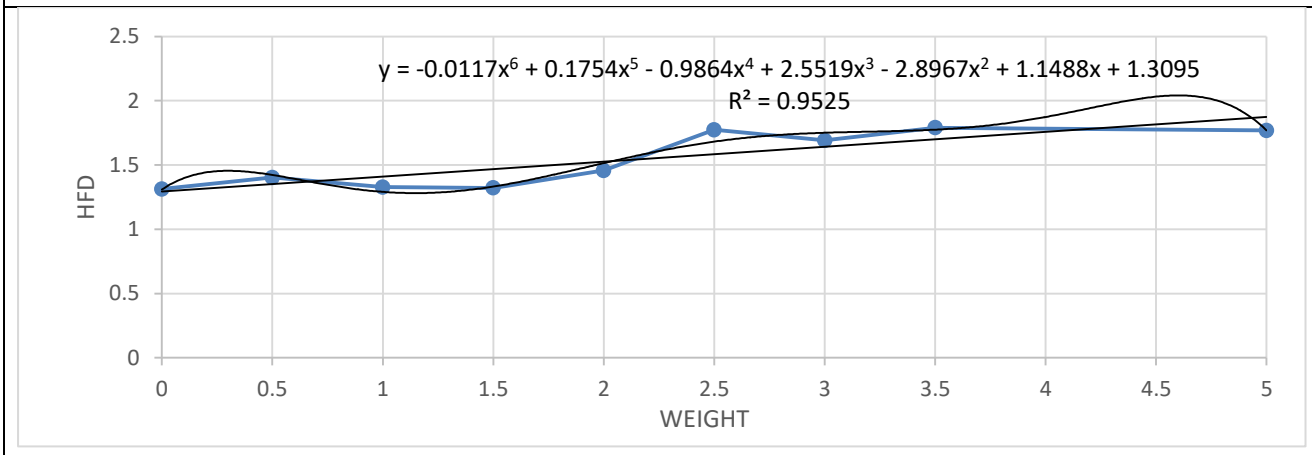

Fig.6.58 Fractal dimension variation due to increasing weight for EEG lead CZ-REF

- **AVERAGE FRACTAL DIMENSION VARIATION FOR EEG DIFFERENT LEADS:**

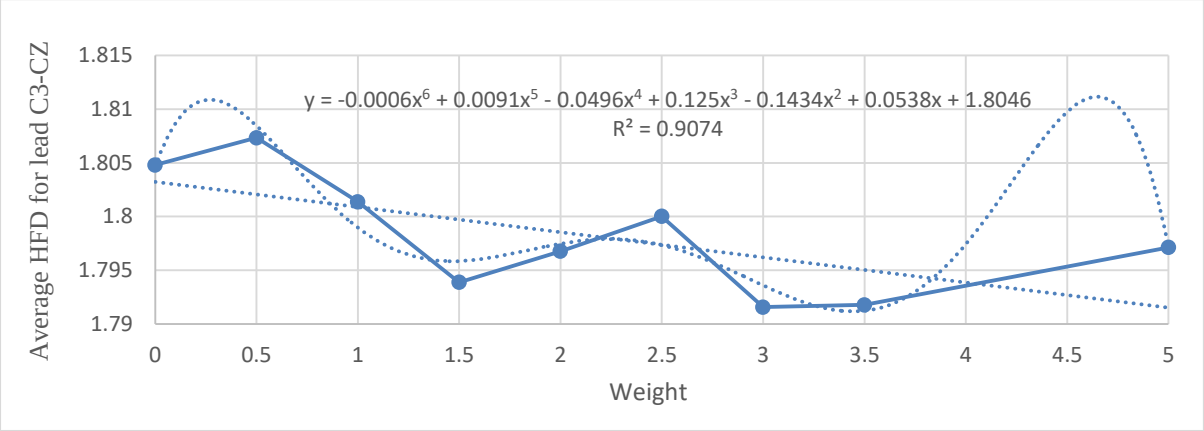

Fig.6.59 Variation of average fractal dimension for lead C3-CZ due to change in load condition.

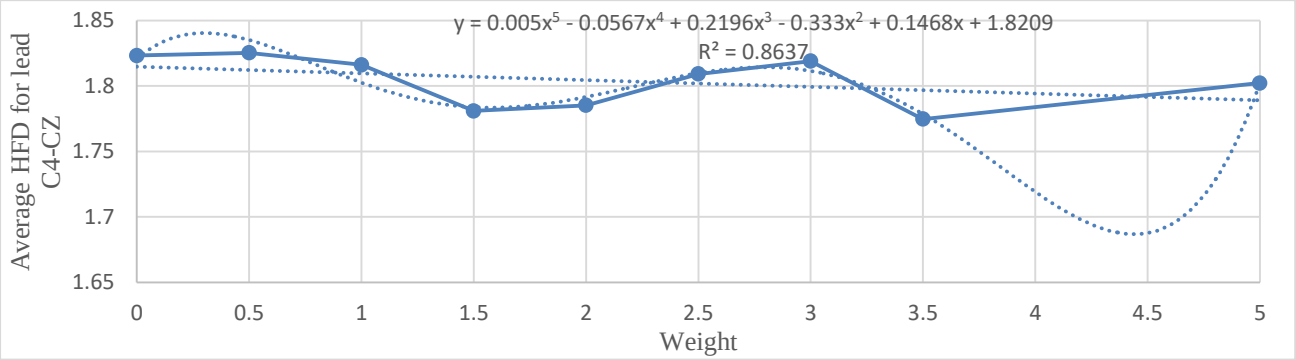

Fig.6.60 Variation of average fractal dimension for lead C4-CZ due to change in load condition.

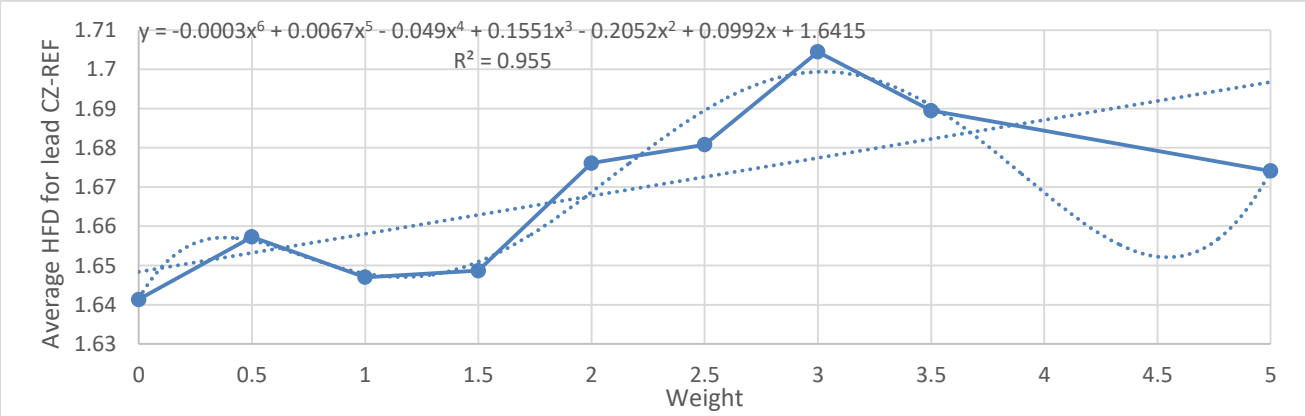

Fig.6.61 Variation of average fractal dimension for lead CZ-REF due to change in load condition.

The findings from the above fractal analysis graph of EEG signal for all the subjects are: -

- For the transverse bipolar montage, the **fractal dimension decreased**. For this montage the R-Square value fits the graph into a 6^{th} order polynomial.
- For the referential montage the **fractal dimension increased**. For this montage the R-Square value fits the graph into a 6^{th} order polynomial.

6.4.3 Calculating Fractal Dimension for EMG signal:

TABLE:6.4.3.15: Calculate the fractal dimension of EMG signal due to increasing weight for Subject 1.

WEIGHT	HFD (CHANNEL 1)	HFD (CHANNEL 2)
0	1.956641591	1.958486833
0.5	1.957671016	1.943207508
1	1.945304724	1.933923732
1.5	1.936456611	1.933736885
2	1.925897599	1.932284125
2.5	1.923757053	1.934520951
3	1.91630557	1.922237339
3.5	1.918394416	1.927459639
5	1.903197473	1.910348612

Below figures are showing that graphical interpretation of EMG fractal dimension variation due to increasing weight for subject 1.

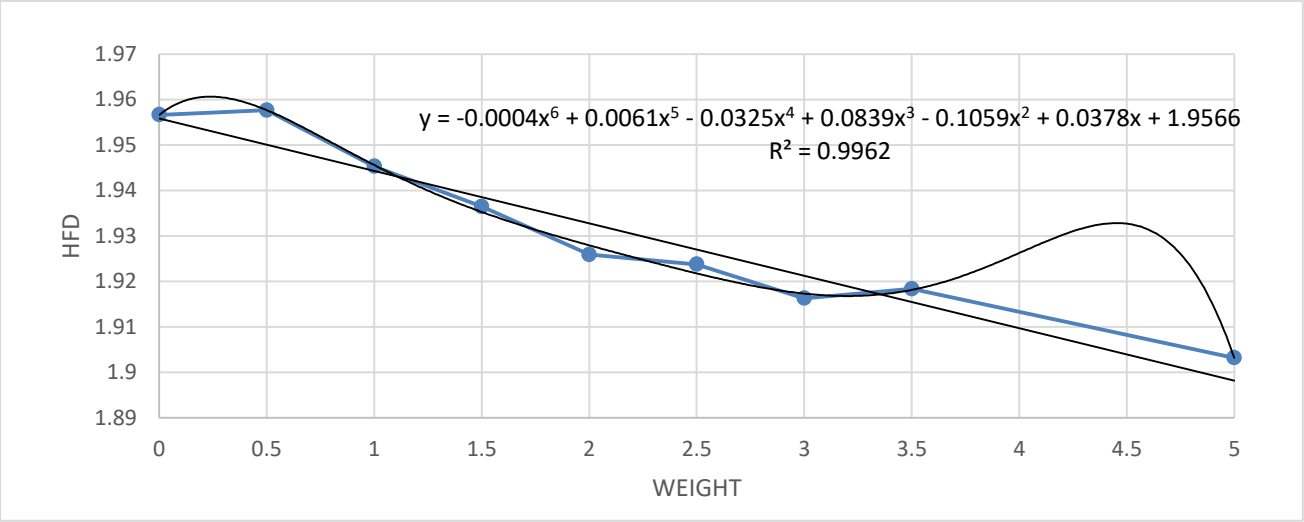

Fig.6.62 Fractal dimension variation due to increasing weight for EMG channel 1.

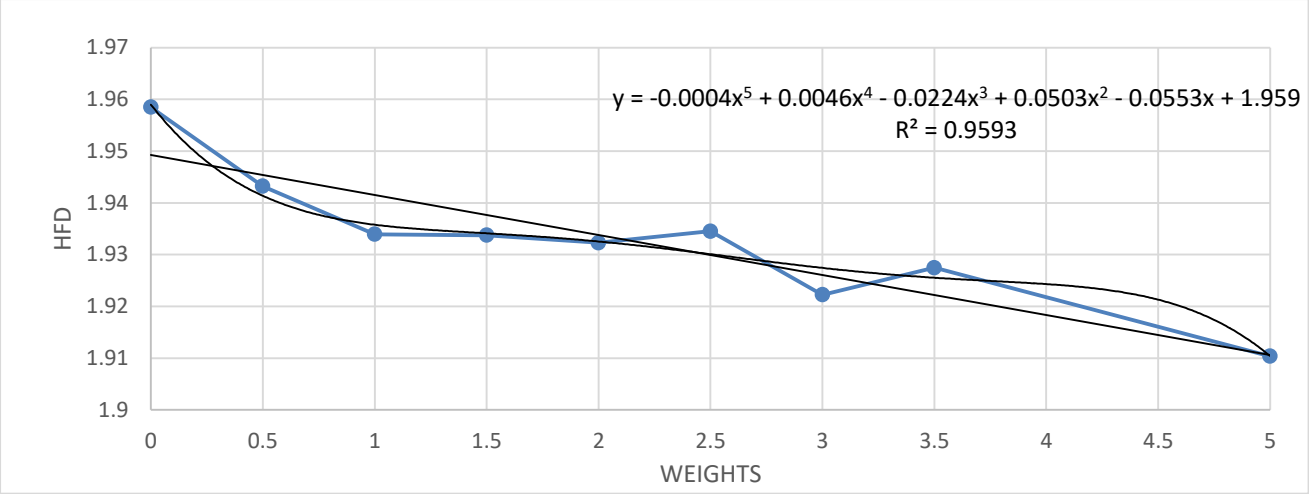

Fig.6.63 Fractal dimension variation due to increasing weight for EMG channel 2.

TABLE:6.4.3.16: Calculate the fractal dimension of EMG signal due to increasing weight for Subject 2.

WEIGHT	HFD (CHANNEL 1)	HFD (CHANNEL 2)
0	1.932064492	1.963592149
0.5	1.924597293	1.958201936
1	1.916505099	1.947185256
1.5	1.917386181	1.952272163
2	1.904508076	1.950091758
2.5	1.907294404	1.942549393
3	1.898765633	1.942155489
3.5	1.906323047	1.937943912
5	1.906042419	1.922621408

Below figures are showing that graphical interpretation of EMG fractal dimension variation due to increasing weight for subject 2.

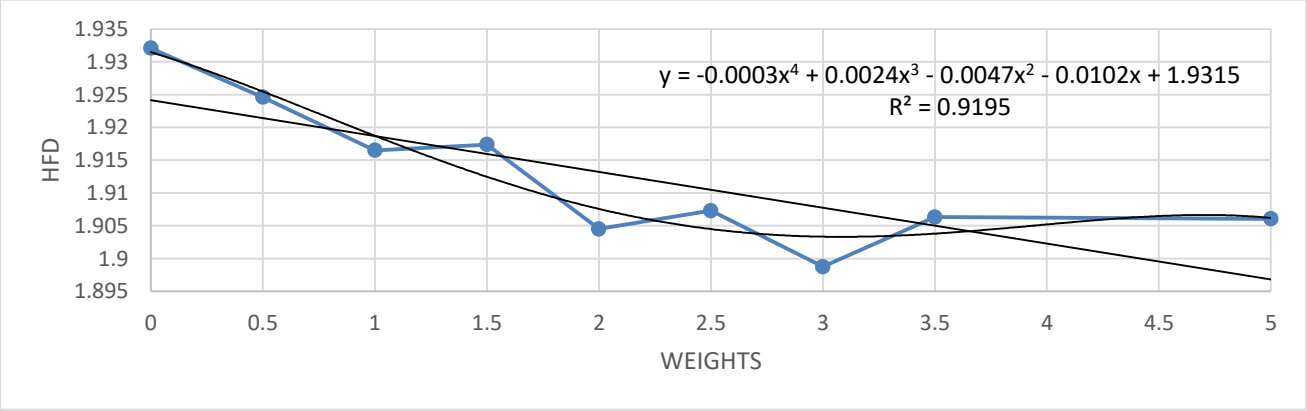

Fig.6.64 Fractal dimension variation due to increasing weight for EMG channel 1.

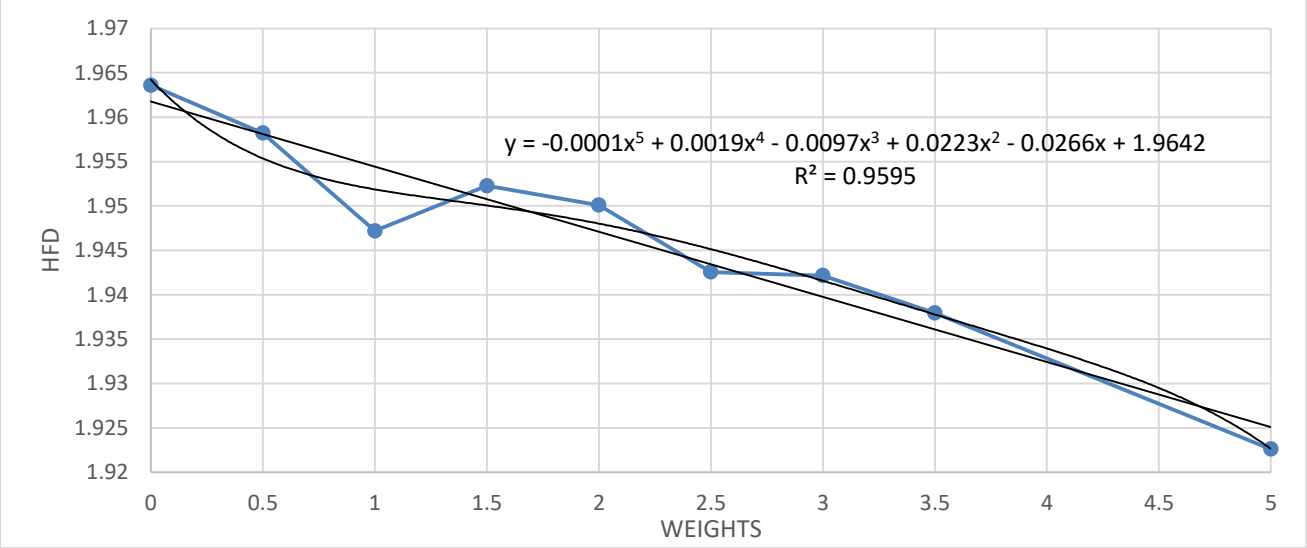

Fig.6.65 Fractal dimension variation due to increasing weight for EMG channel 2.

TABLE:6.4.3.17: Calculate the fractal dimension of EMG signal due to increasing weight for Subject 3.

WEIGHT	HFD (CHANNEL 1)	HFD (CHANNEL 2)
0	1.985436237	1.926247153
0.5	1.98674489	1.918534508
1	1.974396718	1.927622935
1.5	1.97206224	1.924342102
2	1.971828675	1.919568227
2.5	1.957366075	1.917045082
3	1.793217818	1.922358622
3.5	1.955495771	1.919170198
5	1.941313163	1.903248973

Below figures are showing that graphical interpretation of EMG fractal dimension variation due to increasing weight for subject 3.

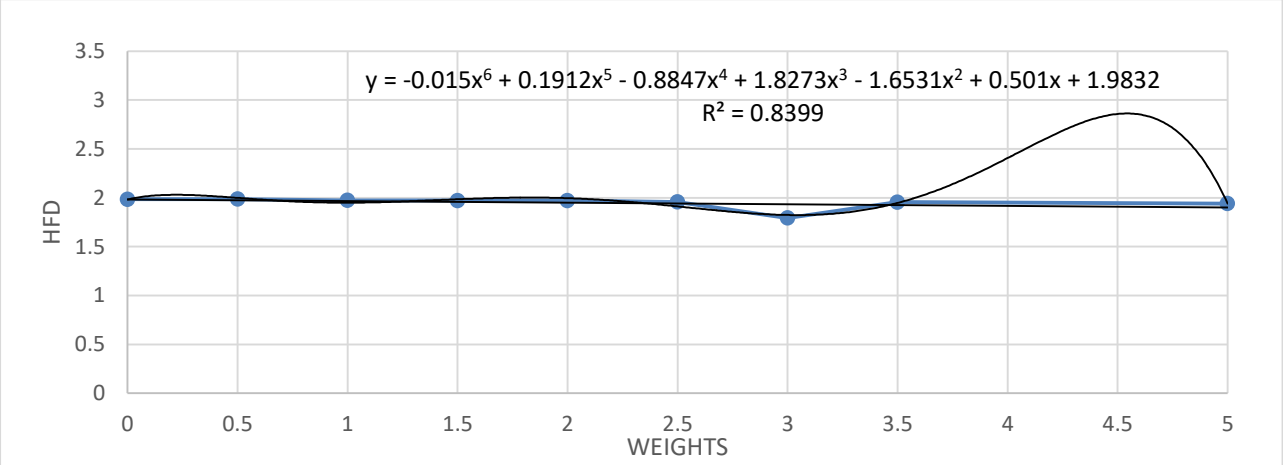

Fig.6.66 Fractal dimension variation due to increasing weight for EMG channel 1

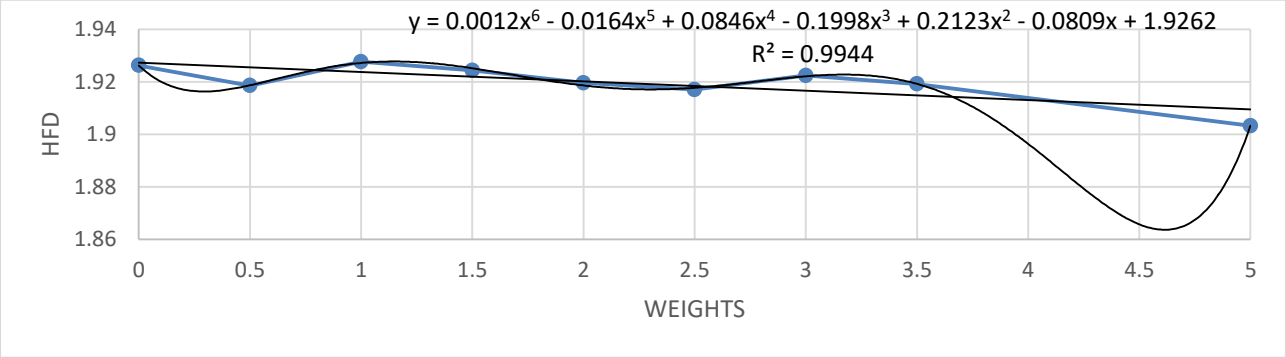

Fig.6.67 Fractal dimension variation due to increasing weight for EMG channel 2

TABLE:6.4.3.18: Calculate the fractal dimension of EMG signal due to increasing weight for Subject 4.

WEIGHT	HFD (CHANNEL 1)	HFD (CHANNEL 2)
0	1.886329559	1.936448784
0.5	1.901270747	1.934663879
1	1.888867858	1.912659862
1.5	1.902150641	1.912681334
2	1.8983859	1.904649712
2.5	1.890531334	1.90756674
3	1.895627511	1.904324638
3.5	1.902341869	1.901182177
5	1.89726411	1.904433591

Below figures are showing that graphical interpretation of EMG fractal dimension variation due to increasing weight for subject 4.

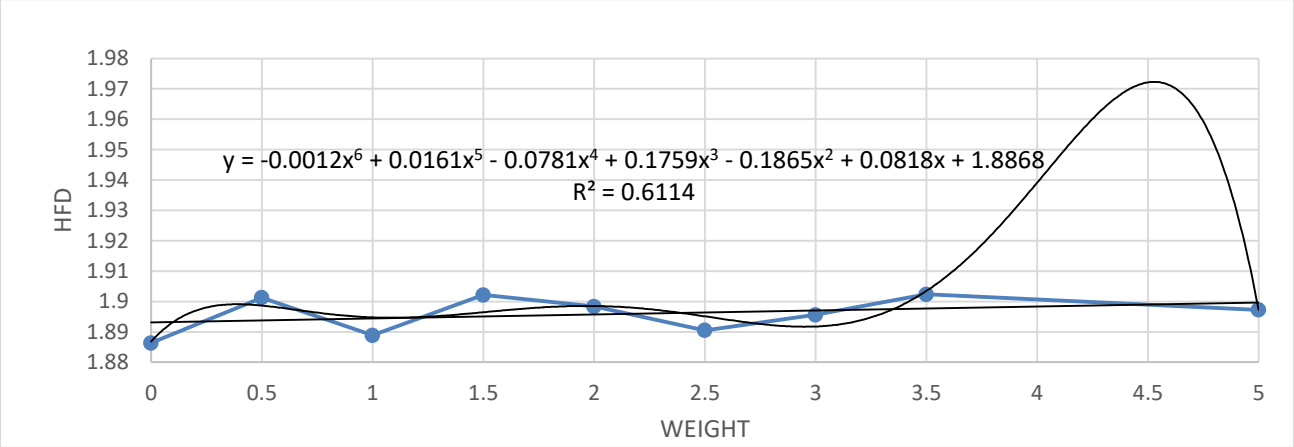

Fig.6.68 Fractal dimension variation due to increasing weight for EMG channel 1.

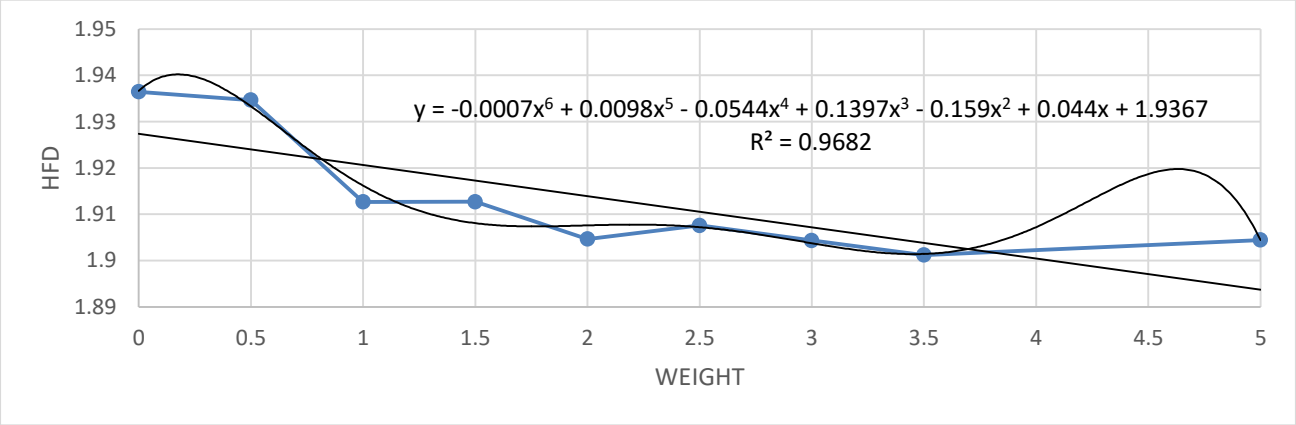

Fig.6.69 Fractal dimension variation due to increasing weight for EMG channel 2

TABLE:6.4.3.19: Calculate the fractal dimension of EMG signal due to increasing weight for Subject 5.

WEIGHT	HFD (CHANNEL 1)	HFD (CHANNEL 2)
0	1.889084792	1.937224969
0.5	1.873328116	1.930857441
1	1.872160038	1.921678996
1.5	1.872883548	1.929914316
2	1.868278366	1.926321705
2.5	1.871063565	1.92666417
3	1.866189665	1.923192765
3.5	1.864091997	1.918427571
5	1.85717918	1.911986451

Below figures are showing that graphical interpretation of EMG fractal dimension variation due to increasing weight for subject 5.

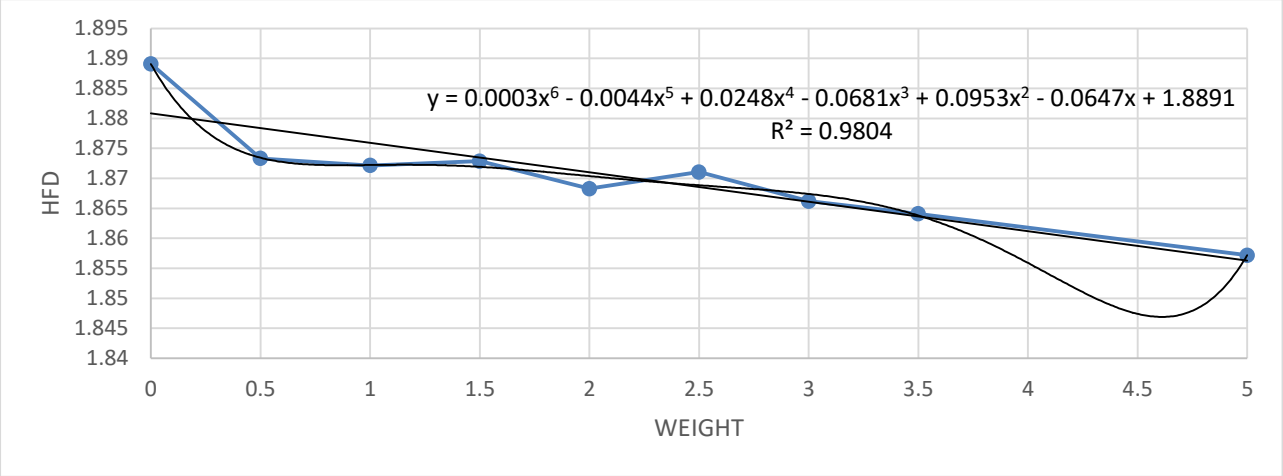

Fig.6.70 Fractal dimension variation due to increasing weight for EMG channel 1.

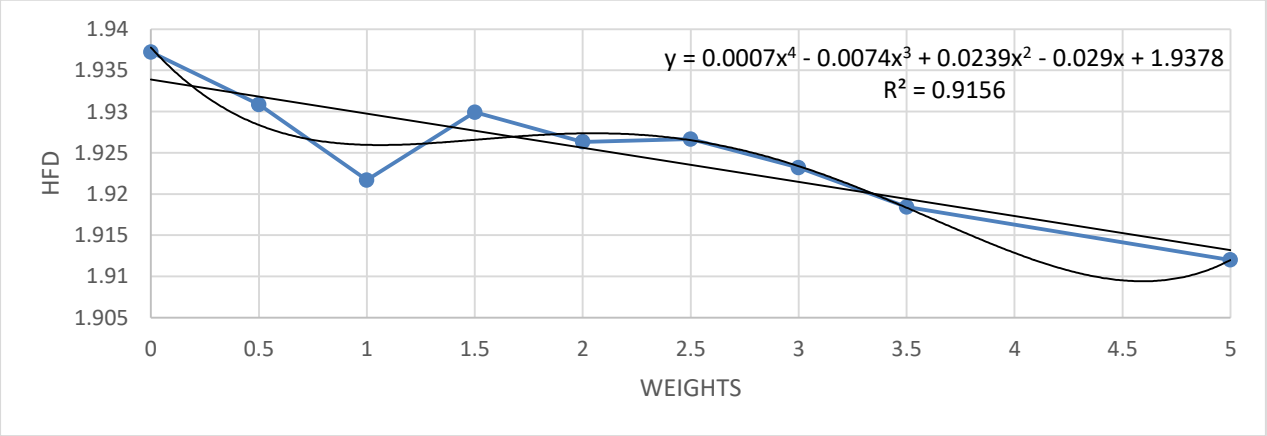

Fig.6.71 Fractal dimension variation due to increasing weight for EMG channel 2.

TABLE:6.4.3.20: Calculate the fractal dimension of EMG signal due to increasing weight for Subject 6.

WEIGHT	HFD (CHANNEL 1)	HFD (CHANNEL 2)
0	1.95688162	1.942806696
0.5	1.957634183	1.932370156
1	1.948351263	1.929144118
1.5	1.945345839	1.916928865
2	1.93818005	1.907398653
2.5	1.933530598	1.900759477
3	1.927931478	1.897202764
3.5	1.927722615	1.893419375
5	1.943524597	1.877618801

Below figures are showing that graphical interpretation of EMG fractal dimension variation due to increasing weight for subject 6.

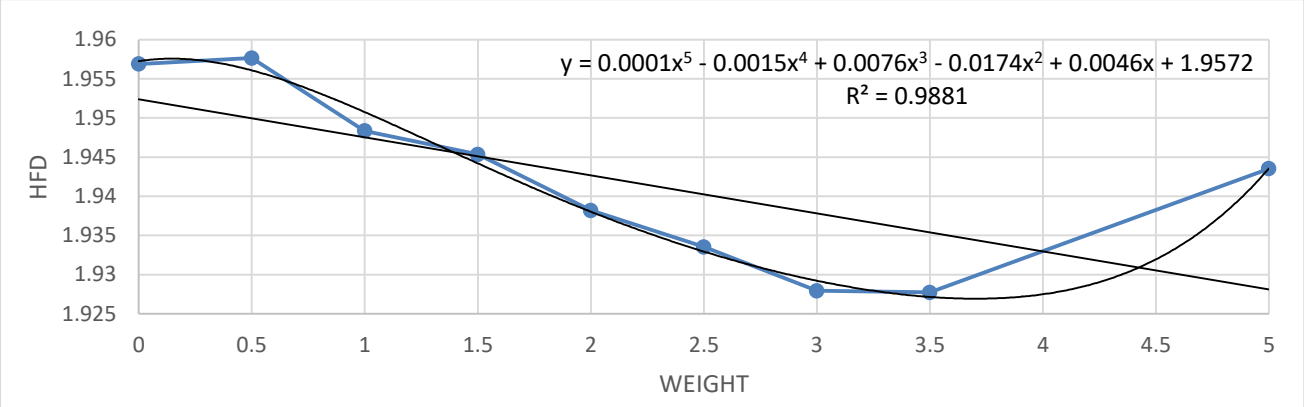

Fig.6.72 Fractal dimension variation due to increasing weight for EMG channel 1.

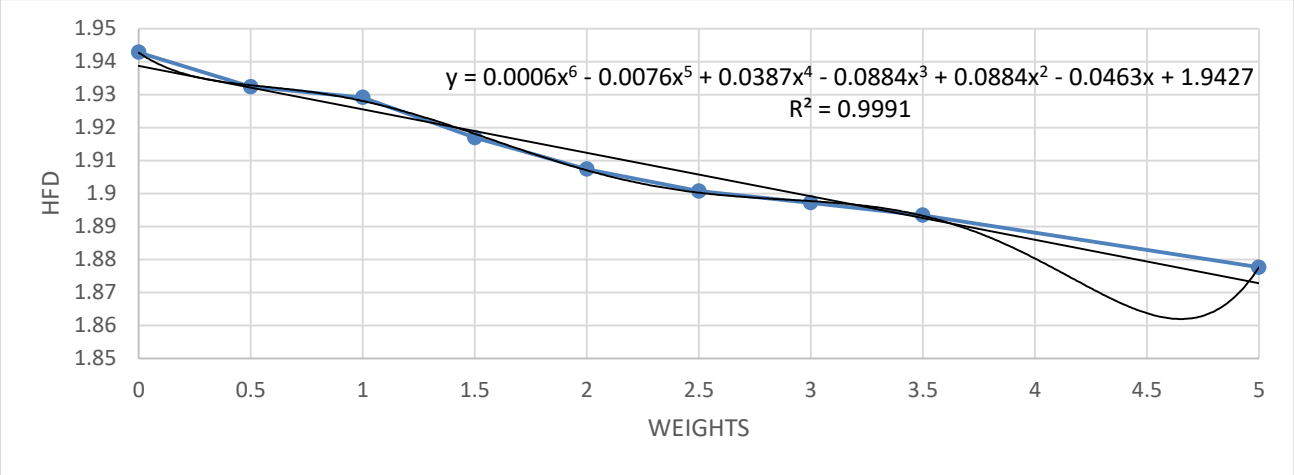

Fig.6.73 Fractal dimension variation due to increasing weight for EMG channel 2.

TABLE:6.4.3.21: Calculate the fractal dimension of EMG signal due to increasing weight for Subject 7.

WEIGHT	HFD (CHANNEL 1)	HFD (CHANNEL 2)
0	1.924410129	1.959354796
0.5	1.93860575	1.965631799
1	1.911679924	1.966530844
1.5	1.914752259	1.964733444
2	1.906328273	1.966819884
2.5	1.908013089	1.964350011
3	1.905182339	1.964531744
3.5	1.904830536	1.960190185
5	1.886681449	1.9259808

Below figures are showing that graphical interpretation of EMG fractal dimension variation due to increasing weight for subject 7.

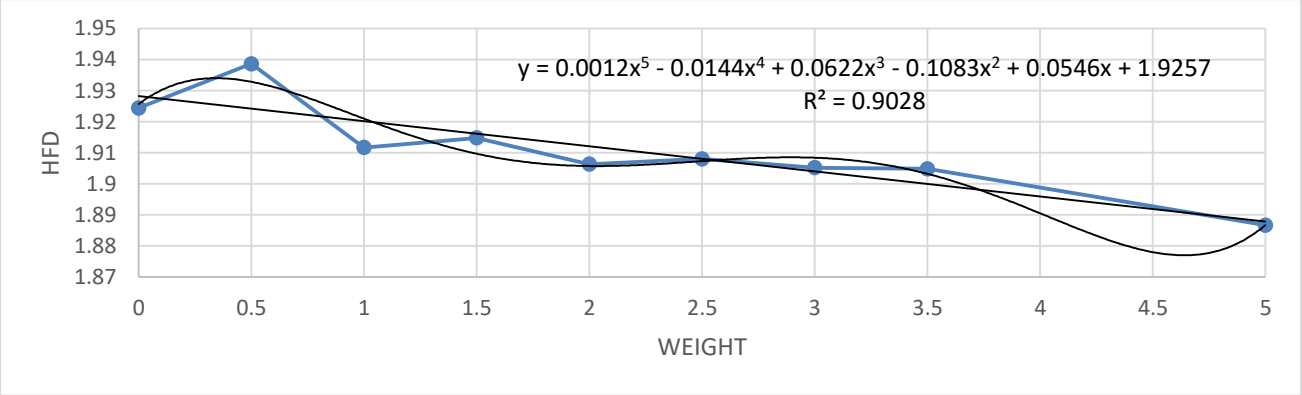

Fig.6.74 Fractal dimension variation due to increasing weight for EMG channel 1.

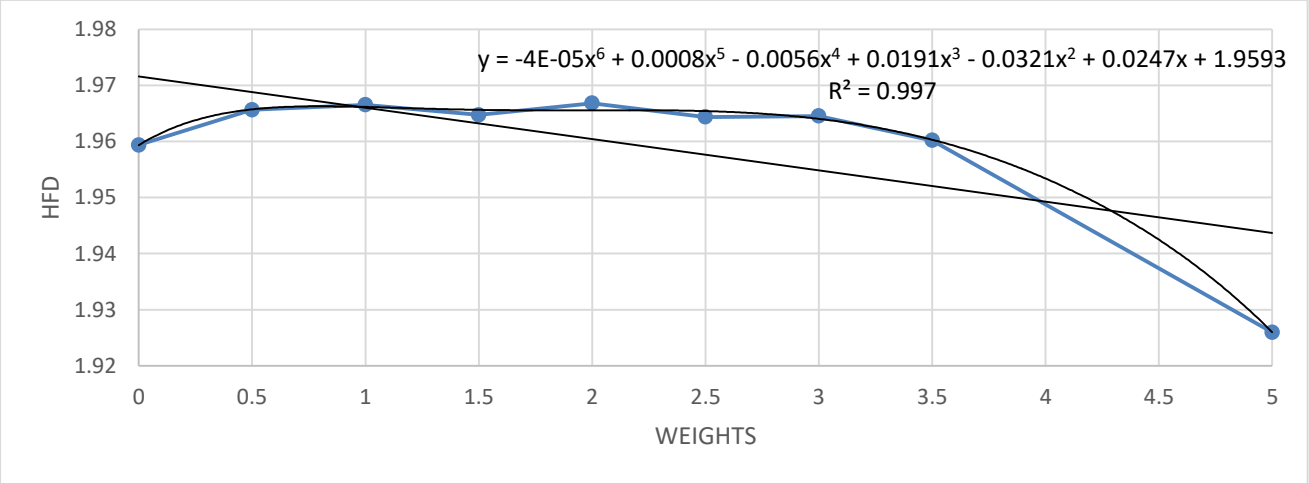

Fig.6.75 Fractal dimension variation due to increasing weight for EMG channel 2.

TABLE:6.4.3.22: Calculate the fractal dimension of EMG signal due to increasing weight for Subject 8.

WEIGHT	HFD (CHANNEL 1)	HFD (CHANNEL 2)
0	1.908825199	1.90857979
0.5	1.903109009	1.91995263
1	1.881466091	1.913002078
1.5	1.883579276	1.910840924
2	1.88597235	1.914857945
2.5	1.88597235	1.914857945
3	1.881328621	1.914087124
3.5	1.865454754	1.896206703
5	1.865108231	1.904726257

Below figures are showing that graphical interpretation of EMG fractal dimension variation due to increasing weight for subject 8.

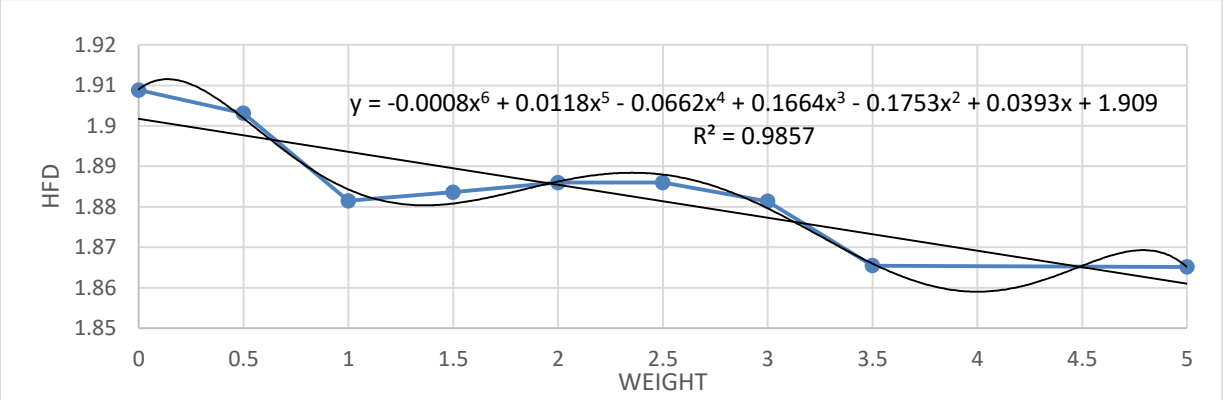

Fig.6.76 Fractal dimension variation due to increasing weight for EMG channel 1.

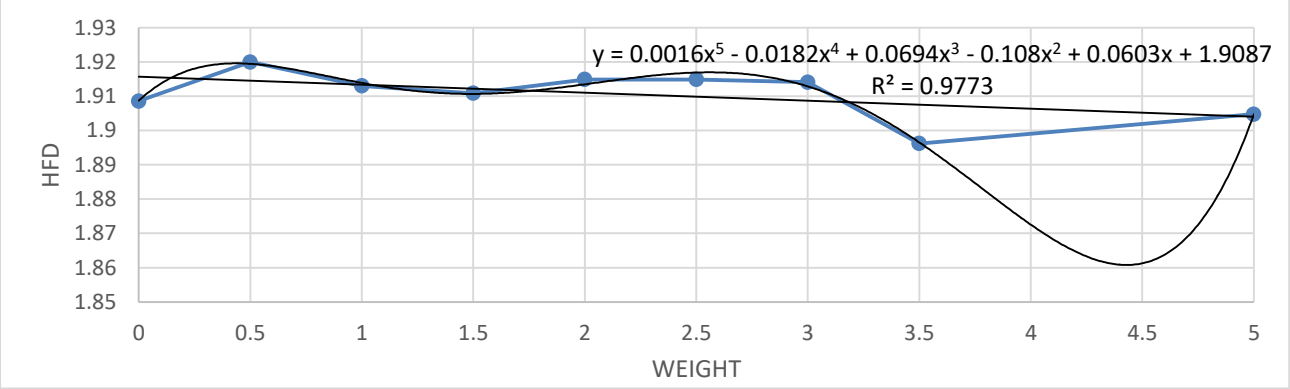

Fig.6.77 Fractal dimension variation due to increasing weight for EMG channel 2.

- **AVERAGE EMG FRACTAL DIMENSION:**

TABLE:6.4.3.23: Calculate the average fractal dimension of EMG signal due to increasing weight.

WEIGHT	AVG. HFD (CHANNEL1)	AVG. HFD (CHANNEL 2)
0	1.93	1.9416
0.5	1.9304	1.9379
1	1.9173	1.9315
1.5	1.9181	1.9307
2	1.9124	1.9277
2.5	1.9097	1.926
3	1.8856	1.9238
3.5	1.9056	1.9192
5	1.9	1.9076

Below figures are showing that graphical interpretation of EMG average fractal dimension variation due to increasing weight for all subjects together.

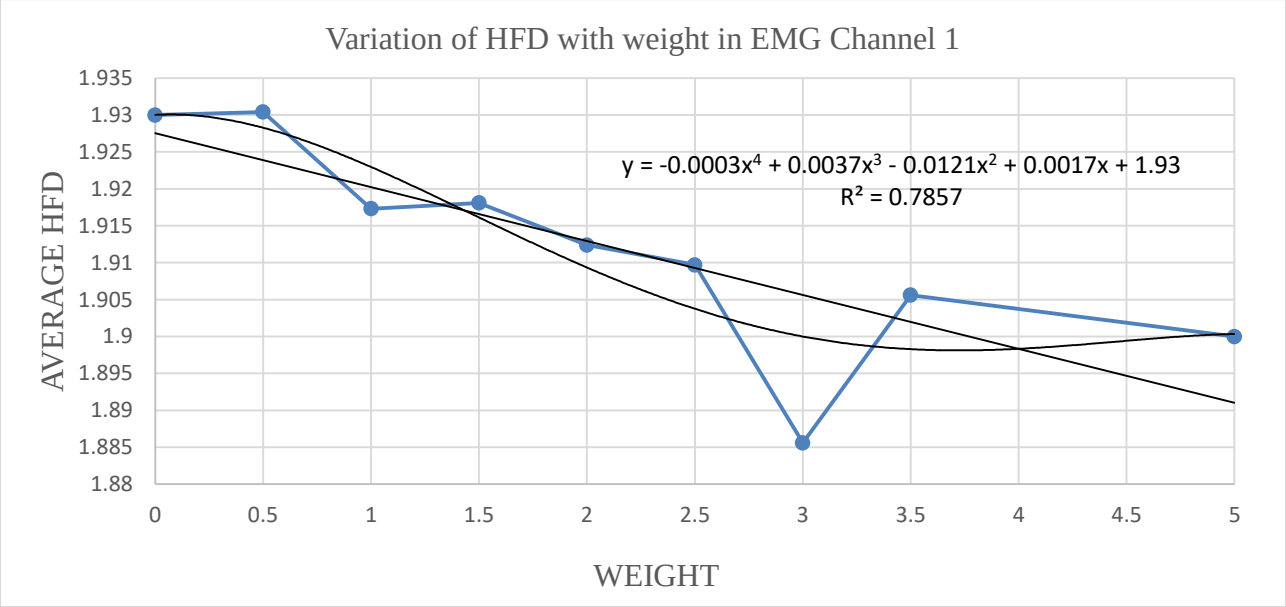

Fig.6.78 Average Fractal dimension variation due to increasing weight for EMG channel 1

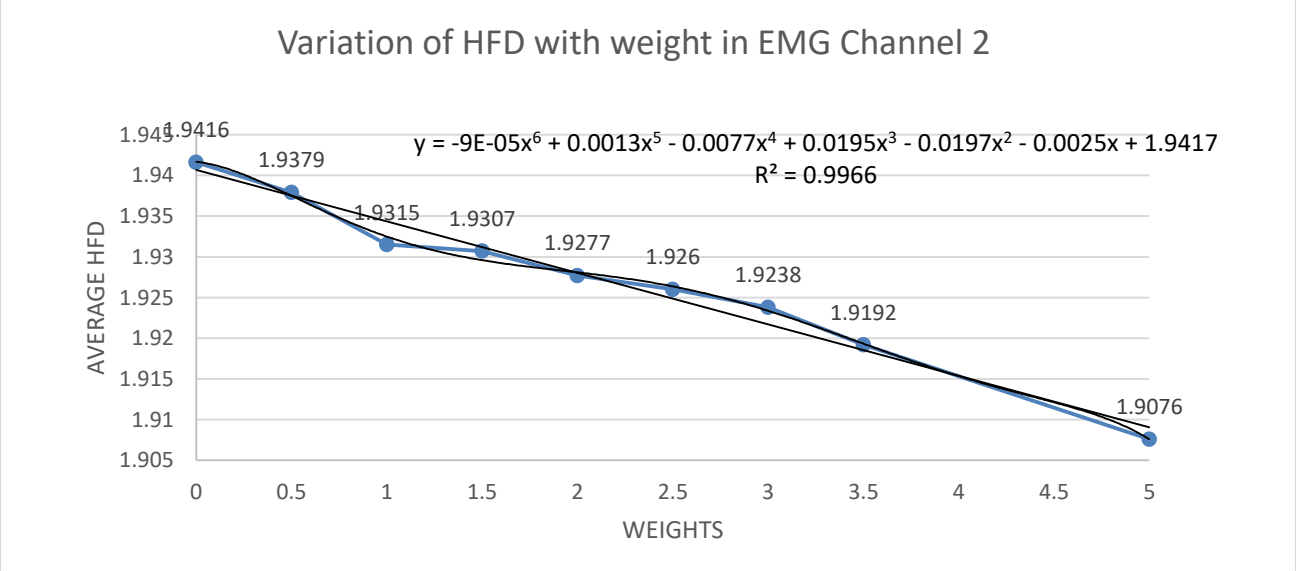

Fig.6.79 Average Fractal dimension variation due to increasing weight for EMG channel 2.

The findings from the above fractal analysis graph of EMG signal for all the subjects are: -

- For channel 1 the fractal dimension decreased. In this R-Square value is 0.7857 which fits the graph into a 4^{th} order polynomial.
- For channel 2 the fractal dimension decreased. In this R-Square value is 0.9966 which fits the graph into a 6^{th} order polynomial.

6.5 CORRELATION BETWEEN EVERY PAIR OF LEAD:

TABLE:6.5.24: Correlation between every pair of lead – subject 1

CORRELATION BETWEEN EVERY PAIRS OF LEAD – SUBJECT 1										
	C3-CZ & C4-CZ	**C3-CZ & CZ-REF**	**C3-CZ & CH1**	**C3-CZ & CH2**	**C4-CZ & CZ-REF**	**C4-CZ & CH1**	**C4-CZ & CH2**	**CZ-REF & CH1**	**CZ-REF & CH2**	**CH1 & CH2**
0	0.9949	-0.8511	-0.0015	0.0100	-0.8459	-0.0010	0.0058	0.0244	-0.0213	-0.5677
0.5	0.9923	-0.7738	-0.0111	-0.0507	-0.7536	-0.0176	-0.0401	-0.0241	0.0690	-0.5493
1	0.9945	-0.8798	-0.0294	-0.0074	-0.8422	-0.0302	-0.0067	0.0254	0.0103	-0.5309
1.5	0.9967	-0.8243	0.0178	-0.0146	-0.8082	0.0161	-0.0131	-0.0036	-0.0105	-0.6120
2	0.9973	-0.8623	-0.0029	-0.0809	-0.8484	-0.0015	-0.0821	0.0039	0.0731	-0.5654
2.5	0.9975	-0.8285	-0.0157	0.0113	-0.8159	-0.0162	0.0067	0.0340	0.0077	-0.4978
3	0.9922	-0.7279	-0.0513	-0.1084	-0.7318	-0.0604	-0.1124	0.0692	0.1181	-0.2443
3.5	0.9945	-0.8518	-0.0523	-0.0511	-0.8337	-0.0516	-0.0499	0.0440	0.0474	-0.3957
5	0.9960	-0.8471	0.0103	-0.0392	-0.8198	0.0136	-0.0377	0.0108	0.0242	-0.3567

TABLE:6.5.25: Correlation between every pair of lead – subject 2

CORRELATION BETWEEN EVERY PAIRS OF LEAD – SUBJECT 2										
	C3-CZ & C4-CZ	**C3-CZ & CZ-REF**	**C3-CZ & CH1**	**C3-CZ & CH2**	**C4-CZ & CZ-REF**	**C4-CZ & CH1**	**C4-CZ & CH2**	**CZ-REF & CH1**	**CZ-REF & CH2**	**CH1 & CH2**
0	-0.2787	-0.0855	-0.0172	-0.0759	0.2847	-0.0547	-0.0103	-0.0013	0.0589	-0.4153
0.5	-0.3102	-0.1325	0.0273	-0.0656	0.0910	-0.0256	-0.0148	0.0499	-0.0516	-0.4225
1	-0.5058	-0.2065	-0.0096	0.0461	0.2201	0.0008	0.0275	-0.0064	0.0992	-0.3438
1.5	-0.3854	0.0398	-0.0226	-0.0374	0.0412	0.0341	0.0511	0.0147	-0.0315	-0.2136
2	0.2661	0.1998	-0.0134	-0.0820	-0.1070	0.1182	-0.0551	-0.1321	0.0712	-0.2725
2.5	-0.4503	0.3145	-0.0040	-0.0557	-0.0109	0.0212	0.0054	-0.0024	-0.0513	-0.2401
3	-0.2909	0.1234	0.0380	0.0054	-0.2139	-0.1066	-0.0691	0.09461	0.0795	-0.2066
3.5	-0.2595	0.2738	-0.0018	0.0327	-0.0545	0.0427	0.0235	-0.0284	-0.0054	-0.3046
5	0.2401	-0.1078	-0.0319	-0.0426	0.0958	-0.0366	0.0530	-0.0347	-0.0171	-0.4150

TABLE:6.5.26: Correlation between every pair of lead – subject 3

CORRELATION BETWEEN EVERY PAIRS OF LEAD – SUBJECT 3										
	C3-CZ & C4-CZ	**C3-CZ & CZ-REF**	**C3-CZ & CH1**	**C3-CZ & CH2**	**C4-CZ & CZ-REF**	**C4-CZ & CH1**	**C4-CZ & CH2**	**CZ-REF & CH1**	**CZ-REF & CH2**	**CH1 & CH2**
0	0.1393	-0.1830	-0.0160	-0.0532	0.2293	0.0122	-0.0433	-0.0208	0.0480	-0.3710
0.5	-0.3693	-0.1034	0.0616	-0.0188	-0.1553	-0.0906	0.0067	0.0585	-0.0186	-0.3173
1	-0.0613	-0.0621	0.0137	0.1458	-0.1100	-0.1258	0.0431	-0.0196	0.1170	-0.2643
1.5	-0.2015	-0.2664	-0.0010	0.0845	-0.1391	-0.0259	0.1182	0.0866	-0.0938	-0.2859
2	-0.1802	-0.1193	0.0189	-0.0767	0.0110	0.0559	-0.0528	0.0354	0.0458	-0.2666
2.5	-0.1367	-0.0532	0.0138	0.0379	0.2234	0.0358	-0.0496	-0.0620	-0.0478	0.0964
3	0.1609	-0.3625	-0.0273	-0.0018	-0.2144	-0.0129	-0.0234	0.0446	-0.1111	-0.0841
3.5	-0.2558	0.1667	0.0198	-0.0635	-0.2582	0.0440	-0.0810	-0.0423	-0.0291	0.1024
5	0.0049	-0.1993	-0.1006	-0.0182	0.0221	-0.0011	0.0002	0.0562	0.0532	0.1840

TABLE:6.5.27: Correlation between every pair of lead – subject 4

CORRELATION BETWEEN EVERY PAIRS OF LEAD – SUBJECT 4										
	C3-CZ & C4-CZ	**C3-CZ & CZ-REF**	**C3-CZ & CH1**	**C3-CZ & CH2**	**C4-CZ & CZ-REF**	**C4-CZ & CH1**	**C4-CZ & CH2**	**CZ-REF & CH1**	**CZ-REF & CH2**	**CH1 & CH2**
0	0.9791	0.0328	0.0047	-0.0149	0.0871	0.0085	-0.0119	0.0015	0.0152	0.7562
0.5	0.9788	0.4001	-0.0458	-0.0150	0.5138	-0.0351	-0.0184	0.0207	-0.0066	0.6351
1	0.9753	-0.5724	0.0954	0.0271	-0.5115	0.1062	0.0313	-0.0372	-0.0361	0.5489
1.5	0.9273	-0.6438	0.0696	0.0672	-0.5766	0.0822	0.0591	-0.0309	-0.0297	0.4743
2	0.9565	-0.7458	-0.0027	0.0030	-0.6849	-0.0077	-0.0073	0.0144	-0.0024	0.4347
2.5	0.9771	-0.7075	-0.0347	0.0720	-0.6233	-0.0306	0.0775	0.0156	-0.1107	0.4468
3	0.7162	-0.7325	0.0181	0.0739	-0.4735	0.0114	0.0398	-0.0245	-0.0988	0.3728
3.5	0.9713	-0.4395	-0.0501	-0.0508	-0.3727	-0.0431	-0.0542	0.0044	-0.0203	0.3500
5	0.8171	0.1080	0.0406	-0.0161	0.0447	0.0470	-0.0208	-0.0265	0.0270	0.3251

TABLE:6.5.28 Correlation between every pair of lead – subject 5

CORRELATION BETWEEN EVERY PAIRS OF LEAD – SUBJECT 5										
	C3-CZ & C4-CZ	**C3-CZ & CZ-REF**	**C3-CZ & CH1**	**C3-CZ & CH2**	**C4-CZ & CZ-REF**	**C4-CZ & CH1**	**C4-CZ & CH2**	**CZ-REF & CH1**	**CZ-REF & CH2**	**CH1 & CH2**
0	0.1976	0.3541	-0.0193	0.0047	0.1367	-0.0039	0.0284	-0.0825	-0.0226	0.7626
0.5	0.2203	-0.7506	-0.0169	0.0004	-0.0197	-0.0768	-0.0362	-0.0758	-0.0519	0.7678
1	0.1400	-0.3424	-0.0345	0.0266	0.0566	-0.0312	-0.0172	0.0239	0.0292	0.7688
1.5	0.4925	-0.2219	-0.0226	0.0116	0.2701	-0.0126	0.0072	-0.0319	-0.0514	0.7961
2	0.1231	-0.5690	-0.0470	-0.0459	0.3404	-0.0412	-0.0873	0.0905	0.1042	0.7756
2.5	0.1481	-0.1036	0.0100	0.0607	0.0345	0.0613	0.0663	0.0059	-0.0105	0.7636
3	0.4210	0.1699	0.0440	0.0411	0.1260	-0.0010	0.0123	0.0356	0.0389	0.7784
3.5	0.5989	-0.2019	-0.0184	0.0412	0.0255	-0.0096	0.0182	0.0745	0.1001	0.7215
5	-0.0993	0.5834	-0.0144	-0.0091	-0.2021	-0.0050	-0.0098	0.0090	0.0257	0.7154

TABLE:6.5.29: Correlation between every pair of lead – subject 6

CORRELATION BETWEEN EVERY PAIRS OF LEAD – SUBJECT 6										
	C3-CZ & C4-CZ	**C3-CZ & CZ-REF**	**C3-CZ & CH1**	**C3-CZ & CH2**	**C4-CZ & CZ-REF**	**C4-CZ & CH1**	**C4-CZ & CH2**	**CZ-REF & CH1**	**CZ-REF & CH2**	**CH1 & CH2**
0	0.3870	-0.8414	-0.0253	-0.0225	0.0598	-0.0630	0.0470	0.0014	0.0449	-0.5284
0.5	-0.0328	-0.7579	-0.0374	0.0424	0.3291	-0.0056	0.0644	0.0228	-0.0528	-0.4130
1	0.1407	-0.8655	0.0047	0.0637	0.1838	0.01882	0.0038	-0.0060	-0.0420	-0.2664
1.5	-0.3924	-0.9071	0.0283	0.0581	0.6460	0.0789	-0.0305	0.0192	-0.0465	-0.2429
2	-0.4380	-0.9228	-0.0167	-0.0823	0.6121	0.0492	0.0512	0.0474	0.0938	-0.2116
2.5	0.0613	-0.7723	-0.0791	0.0526	0.3786	0.0620	0.0412	0.1114	0.0286	-0.2669
3	-0.3494	-0.8016	-0.0358	-0.0164	0.6669	0.0018	0.0124	0.01026	0.0248	-0.2254
3.5	0.0866	-0.8792	0.0296	0.0087	0.2376	0.0148	-0.0079	-0.0406	-0.0171	-0.1981
5	0.8820	-0.3923	-0.0252	-0.04432	0.00819	0.0328	-0.0112	0.0939	0.0935	-0.2620

TABLE:6.5.30: Correlation between every pair of lead – subject 7

CORRELATION BETWEEN EVERY PAIRS OF LEAD – SUBJECT 7										
	C3-CZ & C4-CZ	**C3-CZ & CZ-REF**	**C3-CZ & CH1**	**C3-CZ & CH2**	**C4-CZ & CZ-REF**	**C4-CZ & CH1**	**C4-CZ & CH2**	**CZ-REF & CH1**	**CZ-REF & CH2**	**CH1 & CH2**
0	0.0801	-0.3779	0.0660	0.0505	0.1148	-0.0054	-0.0227	-0.1056	-0.0602	0.6672
0.5	-0.0188	-0.3244	0.0037	-0.0161	0.2899	-0.0099	0.0012	0.0203	0.0486	0.6458
1	0.0805	-0.2227	-0.0441	-0.0127	0.3766	-0.0583	-0.0635	0.0273	0.0590	0.71487
1.5	0.2291	-0.3116	-0.0197	-0.0789	0.1541	-0.0767	-0.0703	-0.0408	-0.0167	0.6698
2	0.1266	-0.3211	0.0188	0.0518	0.2174	0.0266	0.0760	0.08482	0.0109	0.6544
2.5	0.0451	-0.4482	-0.0425	-0.0403	0.0933	-0.0214	0.0300	0.0290	0.0036	0.6379
3	-0.0041	-0.2607	-0.0052	-0.0141	0.1961	-0.0152	-0.0768	0.0171	0.0064	0.5860
3.5	0.0436	-0.3045	-0.0376	-0.0634	0.0947	-0.0549	-0.0464	0.0711	0.0402	0.6114
5	0.2644	-0.2459	0.0138	0.0268	0.0152	-0.01704	0.0165	-0.0706	-0.0611	0.8534

TABLE:6.5.31: Correlation between every pair of lead – subject 8

CORRELATION BETWEEN EVERY PAIRS OF LEAD – SUBJECT 8										
	C3-CZ & C4-CZ	**C3-CZ & CZ-REF**	**C3-CZ & CH1**	**C3-CZ & CH2**	**C4-CZ & CZ-REF**	**C4-CZ & CH1**	**C4-CZ & CH2**	**CZ-REF & CH1**	**CZ-REF & CH2**	**CH1 & CH2**
0	0.2854	-0.1395	-0.0342	0.0067	-0.0475	0.0185	-0.0291	0.0377	0.0113	0.1226
0.5	-0.1429	0.2071	0.0895	-0.0995	-0.6333	-0.0052	0.0539	-0.0136	-0.0116	0.2411
1	-0.4397	-0.3367	0.0118	-0.0716	0.3358	0.0021	0.0455	-0.0313	-0.0675	0.2012
1.5	-0.5277	-0.2821	-0.0442	-0.0497	0.0642	-0.0073	0.0096	0.0403	0.0107	0.0949
2	-0.4603	-0.0715	-0.0021	0.0423	0.2007	0.0086	-0.0504	0.1033	-0.0523	0.0648
2.5	-0.2889	0.0487	0.0491	-0.0500	-0.3675	-0.0152	0.0012	0.0287	-0.0068	0.2502
3	0.1105	-0.3045	0.0148	0.0502	-0.0952	0.0259	0.0245	0.0577	0.0034	0.1452
3.5	-0.4328	-0.0499	0.0485	0.0349	-0.3493	0.0662	0.0185	-0.0011	-0.0199	0.0335
5	-0.6026	-0.0380	0.0868	-0.0139	0.2385	-0.0800	0.0536	0.0213	-0.0746	0.0098

6.6 ANOVA RESULT FOR AVERAGE CORRELATION:

TABLE:6.6.32: ANOVA on average correlation

SUMMARY

Groups	*Count*	*Sum*	*Average*	*Variance*
0.348129	8	1.566361	0.195795125	0.0029585
-0.26146	8	-2.67835	-0.33479375	0.010098013
-0.00538	8	-0.019223	-0.002402875	0.00
-0.01182	8	-0.048124	-0.0060155	0.000445189
0.002408	8	-0.64641	-0.08080125	0.003155279
-0.01113	8	-0.023252	-0.0029065	0.00037566
-0.00455	8	-0.018137	-0.002267125	0.000369236
-0.01815	8	0.117819	0.014727375	0.000192244
0.009294	8	0.025717	0.003214625	0.000613838
0.053279	8	0.874593	0.109324125	0.000860055

ANOVA

Source of Variation	*SS*	*df*	*MS*	*F*	*P-value*	*F crit*
Between Groups	1.344477615	9	0.149386402	78.16646634	0.00	2.01660069
Within Groups	0.13377921	70	0.001911132			
Total	1.478256825	79				

The findings from the above ANOVA testing: -

- The p-value was less than 0.05, the significant level which accepts the alternative hypothesis and rejects the null hypothesis indicating that a significant variation exists between the electrode pairs.

CHAPTER 7

DISCUSSION

This chapter will throw light upon the above-mentioned experimental output in intricate and detailed manner. The interpretation from previous results is discussed. This experimentation was initiated from acquired EEG and EMG signal.

- **Discussion about denoising and analysis of Power spectral density:**

The first step in any bio signal analysis process is to remove artifacts from the signal. Signal denoising can be performed using various methods. But signal denoising using Wavelet Transform is a well-established and robust method to clean bio signals from unwanted noise. Here 1-D signals are used that is why wavelet transform method has been chosen as denoising method because wavelet transform deals with 1-D signal. Fourier transform is used only in frequency domain signals, but wavelet is used for both time and frequency domain. Here, Daubechies mother wavelet has been used for filtering those signals. In this experiment db6 wavelet and decomposition level 10 is used to remove noise from the signals. The objective of the denoising process was to suppress high frequency components and eliminates unwanted noise from the signal. Manual thresholding was used, and the thresholds were selected based on trial and error. The signals were visually inspected and the threshold values corresponding to minimal noise and maximal signal quality were selected. Power Spectral Density (PSD) were plotted before and after the denoising process to ensure high frequency components are suppressed in the denoised signal. The major components of the EEG signal are concerned in the low frequency region. Hence, the low frequency components carry the more information and higher frequency components can be noise. By performing power spectral density before and after removing denoising we can see that after denoising, the power of high frequency components has been reduced, without hampering the signal quality. Hence, the denoising process can be successful. Corresponding, graphs were given in the results section.

❖ **Discussion about EMG muscles band power variation due to changing weights:**

- The average EMG band power variation from channel 1 with respect to varying load is seen in fig.6.19. Here, it is clearly visible that when the weight varies from 0 kg to 5 kg, the band power of the muscles increases gradually. After 3.5 kg when 5 kg weight is applied then suddenly muscles feels more stressed which is signified by the shape increase in band power from 3.5 kg to 5 kg. Overall average muscle band power variation for channel 1, as seen from the graph in result section follows a 3^{rd} order polynomial equation and R-Square value obtained from the graph fits the muscle band power graph into a 3^{rd} order polynomial equation.
- The average muscle band power variation with respect to varying load for channel 2 is seen in fig.6.20**.** Here, it is clearly visible that when weight varies from 0 kg to 5 kg, the muscles feel stressed and band power increases. Overall, average muscle band power variation for channel 2, as seen from the graph in result section follows a 6^{th} order polynomial equation and R-Square value obtained from the graph fits the muscle band power graph into a 6^{th} order polynomial equation.
- Thus, from the muscle band power variation it is observed that when subjects were lifting different load, that time biceps muscle and forearm muscles feel stressed and the band power gradually increased. Also, the biceps muscles were more stressed while lifting a heavy weight so a sharp increase in band power is observed when the weight changed from 3.5 kg to 5 kg.

❖ **Discussion about EEG alpha band, beta band power variation due to changing weights:**

- The average alpha band power showed that the power is increasing from 0 kg to 5 kg. There are fluctuations present in the graph for the weights of 0.5 kg, 1 kg, 1.5 kg, 2 kg, 2.5 kg, 3 kg, 3.5 kg. Overall, alpha band power variation, as seen from the graph in result section follows a 6^{th} order polynomial equation and R-Square value obtained from the graph fits the alpha band power graph into a 6^{th} order polynomial equation.

- An increasing alpha power signified that for all the subjects there is no direct connection between the alpha power and the lifting of weight. But there is obviously some indirect connection between the alpha power and the lifting of weight.
- The average beta band power graph showed that the power is increasing from 0 kg to 5 kg. There are fluctuations present in the graph for the weights of 0.5 kg, 1 kg, 1.5 kg, 2 kg, 2.5 kg, 3 kg, 3.5 kg. Overall, beta band power variation, as seen from the graph in result section follows a 6^{th} order polynomial equation and R-Square value obtained from the graph fits the beta band power graph into a 6^{th} order polynomial equation.
- An increasing beta power signified that for all the subjects the lifting of weights required same force. The application of force was not subjective in nature.

❖ **Discussion about the change in fractal dimension with respect to varying load:**

As human body is nonlinear, the fractal analysis which is totally based on nonlinear studies is done. The change of fractal dimension of EMG and EMG signal with varying load is discussed.

❖ **Discussion about the change in fractal dimension with respect to varying load for EEG signal:**

- The average fractal dimension variation for EEG signal from transverse bipolar montage (lead C3-CZ, C4-CZ) with respect to varying load is seen in fig. 6.59, fig.6.60. Here, it is clearly visible that when weight increases from 0 kg to 5 kg fractal dimension decreases. Overall, fractal dimension variation, as seen from the graph in result section follows a 6^{th} order polynomial equation and R-Square value obtained from the graph fits the fractal dimension variation graph into a 6^{th} order polynomial equation.

- The average fractal dimension variation for EEG signal from referential montage (lead CZ-REF) with respect to varying load is seen in fig.6.61. Here, it is clearly visible that when weight increases from 0 kg to 5 kg fractal dimension increases. Overall, fractal dimension variation, as seen from the graph in result section follows a

6^{th} order polynomial equation and R-Square value obtained from the graph fits the fractal dimension variation graph into a 6^{th} order polynomial equation.

- In case of transverse bipolar montage, due to the varying weights the underlying center of brain gets activated for working based on the weight stimulus. For this the fractal dimension decreased in complexity.

- In case of referential montage, due to the varying weights the underlying center of brain sends various messages to the other centers for working based on the weight stimulus. For this the fractal dimension rose in complexity.

❖ **Discussion about the change in fractal dimension with respect to varying load for EMG signal:**

- The average fractal dimension with respect to varying load for channel 1 is seen in fig.6.78. Here, it is clearly visible that when weight increases from 0 kg to 5 kg fractal dimension decreases. Overall, fractal dimension variation, as seen from the graph in result section follows a 4^{th} order polynomial equation and R-Square value obtained from the graph fits the fractal dimension variation graph into a 4^{th} order polynomial equation.

- The average fractal dimension with respect to varying load for channel 2 is seen in fig.6.79. Here, it is clearly visible that when weight increases from 0 kg to 5 kg fractal dimension decreases. Overall, fractal dimension variation, as seen from the graph in result section follows a 6^{th} order polynomial equation and R-Square value obtained from the graph fits the fractal dimension variation graph into a 6^{th} order polynomial equation.

- Due to varying weights the muscles of forearm and biceps act in a coordinated manner under the action of the weight stimulus and do not perform any random activity. For this fractal dimension shows a decreasing complexity.

❖ **Discussion about the statistical analysis part:**

- To statistical analysis, a correlation between every pair of electrodes is made and it is seen that some pairs of electrodes show null correlation, whereas some are highly correlated, and some are negatively correlated. Now, we can link certain electrodes to specific methods using this methodology, but it would take considerably more analysis with far bigger data sets. As the correlation value is zero so it means that there exists a variation.

- For finding this variation ANOVA was performed between the electrode pairs. The p-value was less than 0.05 the significant level which accepts the alternative hypothesis and rejects the null hypothesis indicating that a significant variation exists between the electrode pairs.

CHAPTER 8

CONCLUSION

The objective of this work is to study the dynamics of brain and arm muscles when different weights are applied on the arm. For this purpose, EEG signals and EMG signals are analyzed in different domains, namely frequency, time domain and using non-linear techniques like fractal analysis.

This thesis is modeled to perceive how the activity of the brain and hand muscles perform when the load gradually increases. Preparatory to the analysis part, wavelet transform was studied. With the help of this, the higher frequency amplitude was suppressed which means that noise was removed from these signals. PSD was calculated for all channels in both signals. From PSD it is observed that the higher frequency has been suppressed. It is ensuring that the removal of the noise has been carried out from the signal.

Then EMG muscles band power was calculated. From average muscles band power variation for both channels it is observed that when subjects were lifting different load, that time biceps muscle and forearm muscles feel stressed and the band power gradually increased. Also, the biceps muscles were more stressed while lifting a heavy weight so a sharp increase in band power is observed when the weight changed from 3.5 kg to 5 kg.

Then in the next analysis part which is the change of EEG alpha and beta band power, when the load gradually increases from lower to higher. From the average alpha band power variation for leads it is observed that alpha power increased. This signifies that for all the subjects there is no direct connection between the alpha power and the lifting of weight. But there is obviously some indirect connection between the alpha power and the lifting of weight.

From the average beta band power variation for leads it is observed that beta power increased. An increasing beta power signified that for all the subjects the lifting of weights required same force. The application of force was not subjective in nature.

In fractal analysis basically, nonlinear dynamics was studied because human body is nonlinear. Here, Higuchi's algorithm was used for calculating this fractal dimension for both signals.

For nonlinear analysis of EEG signal fractal dimension is done. It is observed that in case of transverse bipolar montage, the fractal dimension decreased in complexity. This is because the underlying center of brain gets activated for working based on the weight stimulus. In case of referential montage, the fractal dimension rose in complexity. This is because the underlying center of brain sends various messages to the other centers for working based on the weight stimulus.

For nonlinear analysis of EMG signal fractal dimension is done. For both the channels fractal dimension value decreases. This is because the muscles of forearm and biceps act in a coordinated manner under the action of the weight stimulus and do not perform any random activity. For this fractal dimension shows a decreasing complexity.

From the ANOVA results of correlation analysis, it is evident that there is a significant change between the electrode pairs with varying weights.

CHAPTER 9

FUTURE SCOPE

In biomedical industry grows gradually as well as biomedical related product price also decreases gradually which is more pocket friendly for all. Similarly in clinical application lots of medicine designed with the help of previous record of work. Now a day highly demandable biomedical instrument is prosthetic hand or leg etc. Prosthetic related instruments also be upgraded gradually by the help of previous and ongoing project data. So that's why from this study some important pattern has been found which is good for upgraded prosthetic arm making software which price is also cheap and easy way to use. In future machine learning or artificial intelligence can be used on this data for getting success.

References:

[1] Brooks, A. (2018). An HCI Approach in Contemporary Healthcare and (Re) habilitation. *The Wiley Handbook of Human Computer Interaction*, *2*, 923-944.

[2] Soderberg, G.L. and Cook, T.M., 1984. Electromyography in biomechanics. Physical Therapy, 64(12), pp.1813-1820.

[3] Wang, M.H., Chen, N. and Wang, J.H., 2014. The coupling features of electrical synapses modulate neuronal synchrony in hypothalamic superachiasmatic nucleus. *Brain research*, *1550*, pp.9-17.

[4] Kumar, P., Kumar, D., Jha, S.K., Jha, N.K. and Ambasta, R.K., 2016. Ion channels in neurological disorders. Advances in protein chemistry and structural biology, 103, pp.97-136.

[5] Segel, L.A. and Edelstein-Keshet, L., 2013. Dynamic behavior of neuronal membranes. In Primer On Mathematical Models In Biology (pp. 195-225). The Weizmann Institute of Science.

[6] https://en.wikipedia.org/wiki/Action_potentia.

[7] https://faculty.washington.edu/chudler/ap.html

[8] Schneider, S.P., 1992. Slow potentials activated by afferent and direct stimulation in spinal interneurons of laminae III–V. Brain research, 599(1), pp.129-134.

[9] Coates, S.D., 2008. Neural Interfacing: Forging the Human-Machine Connection. Synthesis Lectures on Biomedical Engineering, 3(1), pp.1-112.

[10] https://faculty.washington.edu/chudler/ap.html

[11] Brewster, K., Love, R.J. and Webb, W.G., 1999. Neurology for the Speech-Language Pathologist.

[12] Patri, M., 2019. Synaptic transmission and amino acid neurotransmitters. In Neurochemical Basis of Brain Function and Dysfunction. IntechOpen.

[13] Silva, I.G.R.D., Pantoja, B.T.D.S., Almeida, G.H.D.R., Carreira, A.C.O. and Miglino, M.A., 2022. Bacterial Cellulose and ECM Hydrogels: An Innovative Approach for

Cardiovascular Regenerative Medicine. *International Journal of Molecular Sciences*, *23*(7), p.3955.

[14] Wali, M.K., Murugappan, M. and Ahmmad, R.B., 2013. Development of EEG data acquisition device by using single board computer. International Journal of Medical Engineering and Informatics, 5(3), pp.191-200.

[15] Kodagoda, S., Hemachandra, E.A.S.M., Pannipitiya, P.A.A.R., Bartholomeuz, L.S. and Pasqual, A.A., 2006, December. Minimal Invasive Headband for Brain Computer Interfacing and Analysis. In 2006 International Conference on Information and Automation (pp. 109-114). IEEE.

[16] https://www.emotiv.com/glossary/eeg-machine

[17] https://www.pinterest.com/pin/706502878933803 50/Photoby Snapgalleria on dreamstime.

[18] Ferri, R., Stam, C.J., Lanuzza, B., Cosentino, F.I., Elia, M., Musumeci, S.A. and Pennisi, G., 2004. Different EEG frequency band synchronization during nocturnal frontal lobe seizures. *Clinical neurophysiology*, *115*(5), pp.1202-1211.

[19] Tallon-Baudry, C., 2009. The roles of gamma-band oscillatory synchrony in human visual cognition. Front Biosci, 14(321-332), p.26.

[20] Suh, Y.A. and Yim, M.S., 2018. “High risk non-initiating insider” identification based on EEG analysis for enhancing nuclear security. Annals of Nuclear Energy, 113, pp.308-318.

[21] https://chemoton.wordpress.com/2012/08/11/brain-wave-patterns

[22] Wang, X.L., Bao, J.X., Deng, Y.C., Zhao, G., Swa, B. and Liu, Y.H., 2014. Jeavons syndrome in China. Epilepsy & Behavior, 32, pp.64-71.

[23] Bucci, P., Mucci, A. and Galderisi, S., 2011. Normal EEG Patterns and Waveforms. Standard Electroencephalography in Clinical Psychiatry: A Practical Handbook, pp.33-57.

[24] https://chemoton.wordpress.com/2012/08/11/brain-wave-patterns

[25] Lv, B., Su, C., Yang, L., Xie, Y. and Wu, T., 2014, August. Whole brain EEG synchronization likelihood modulated by long term evolution electromagnetic fields

exposure. In 2014 36th Annual International Conference of the IEEE Engineering in Medicine and Biology Society (pp. 986-989). IEEE.

[26] Aminoff, M.J., 2012. Aminoff's Electrodiagnosis in Clinical Neurology: Expert Consult-Online and Print. Elsevier Health Sciences.

[27] https://chemoton.wordpress.com/2012/08/11/brain-wave-patterns

[28] Watanabe, K., Hayakawa, F. and Okumura, A., 1999. Neonatal EEG: a powerful tool in the assessment of brain damage in preterm infants. Brain and Development, 21(6), pp.361-372.

[29] https://chemoton.wordpress.com/2012/08/11/brain-wave-patterns

[30] Jasper, H., 1958. Report of the committee on methods of clinical examination in electroencephalography. Electroencephalogr Clin Neurophysiol, 10, pp.370-375.

[31] https://www.tdcs.com/improving-insightfulness

[32] https://www.tdcs.com/improving-insightfulness

[33] Foldvary-Schaefer, N. and Grigg-Damberger, M.M., 2012. Identifying interictal and ictal epileptic activity in polysomnograms. Sleep Medicine Clinics, 7(1), pp.39-58.

[34] Chae, Y.S., Song, K.I., Park, J.W. and Youn, I., 2017. Development and verification of circular array electromyography system for the selective electromyography signal detection. Journal of Biomechanical Science and Engineering, pp.16-00594.

[35] Acharya, J.N. and Acharya, V.J., 2019. Overview of EEG montages and principles of localization. Journal of Clinical Neurophysiology, 36(5), pp.325-329.

[36] Kane, N., Acharya, J., Beniczky, S., Caboclo, L., Finnigan, S., Kaplan, P.W., Shibasaki, H., Pressler, R. and van Putten, M.J., 2017. A revised glossary of terms most used by clinical electroencephalographers and updated proposal for the report format of the EEG findings. Revision 2017. Clinical neurophysiology practice, 2, p.170.

[37] Frey, L. C. and Spitz, M. C. (n.d.) “Electroencephalography,” In chapter, pp. 442–458.

[38] Koo, D.L., Kim, W.J., Lee, S.A., Kim, J.M., Kim, J. and Park, S., 2017. Fundamental requirements for performing electroencephalography. Annals of Clinical Neurophysiology, 19(2), pp.113-117.

[39] https://openbci.com/forum/index.php?p=/discussion/1840/cyton-bipolar-montage

[40] https://www.medicine.mcgill.ca/physio/vlab/biomed_signals/eeg_n.htm

[41] Yang, S.C., Lan, S.H., Chang, H.Y. and Chung, P.C., 2015. Epileptiform discharges detection from eeg signals using grouped-channel restricted band analysis. *Biomedical Engineering: Applications, Basis and Communications*, *27*(02), p.1550014.

[42] Lemoyne, R., Coroian, C., Mastroianni, T. and Grundfest, W., 2008. Accelerometers for quantification of gait and movement disorders: a perspective review. Journal of Mechanics in Medicine and Biology, 8(02), pp.137-152.

[43] Benbadis, S.R., 2006. Introduction to sleep electroencephalography. Sleep: A comprehensive handbook, pp.989-1024.

[44] Gupta, S.D., Al Yusuf, S., Ammar, J.K. and Hasan, K., 2012, August. An analysis to generate EMG signal and its perspective: A panoramic approach. In 2012 International Conference on Advances in Power Conversion and Energy Technologies (APCET) (pp. 1-5). IEEE.

[45] Nadin, M., 2008. Analyzing motoric and physiological data in describing upper extremity movement in the aged.

[46] Legg, A.J., Stevens, R., Oakes, N.O. and Shahane, S.A., 2016. A comparison of nonoperative vs. Endobutton repair of distal biceps ruptures. Journal of Shoulder and Elbow Surgery, 25(3), pp.341-348.

[47] Crosby, J.W., 1957. Course on Upper Extremity Prosthetics. Canadian Journal of Occupational Therapy, 24(3), pp.93-98.

[48] https://www.kingofthegym.com/biceps-anatomy

[49] Duhan, M., Sharma, C. and Bhatia, D., 2011. Study of signal processing techniques for EMG analysis. International Journal of Biomechatronics and Biomedical Robotics, 1(3), pp.141-148.

[50] Amirmazlaghani, M. and Amindavar, H., 2009, April. EMG signal denoising via Bayesian wavelet shrinkage based on GARCH modeling. In 2009 IEEE International Conference on Acoustics, Speech and Signal Processing (pp. 469-472). IEEE.

[51] Reaz, M.B.I., Hussain, M.S. and Mohd-Yasin, F., 2006. Techniques of EMG signal analysis: detection, processing, classification and applications. Biological procedures online, 8(1), pp.11-35.

[52] Shi, L., Liu, Z. and Wang, Q., 2013, December. A Novel Method of sEMG Signal Segmentation. In 2013 IEEE 9th International Conference on Mobile Ad-hoc and Sensor Networks (pp. 515-520). IEEE.

[53] Duhan, M., Sharma, C. and Bhatia, D., 2011. Study of signal processing techniques for EMG analysis. International Journal of Biomechatronics and Biomedical Robotics, 1(3), pp.141-148.

[54] Santello, M. and McDONAGH, M.J., 1998. The control of timing and amplitude of EMG activity in landing movements in humans. Experimental Physiology, 83(6), pp.857-874.

[55] Zadeh, A.E. and Khazaee, A., 2011. High efficient system for automatic classification of the electrocardiogram beats. Annals of biomedical engineering, 39(3), pp.996-1011.

[56] Al-Barazanchi, K.K., Al-Neami, A.Q. and Al-Timemy, A.H., 2017, October. Ensemble of bagged tree classifier for the diagnosis of neuromuscular disorders. In 2017 Fourth International Conference on Advances in Biomedical Engineering (ICABME) (pp. 1-4). IEEE.

[57] Cast of human lungs, showing blood vessels on one side. Photo courtesy Ewald Weibel, Institute of Anantomy, University of Berne.

[58] Bialer, M., Johannessen, S.I., Levy, R.H., Perucca, E., Tomson, T., White, H.S. and Koepp, M.J., 2017. Seizure detection and neuromodulation: A summary of data presented at the XIII conference on new antiepileptic drug and devices (EILAT XIII). Epilepsy research, 130, pp.27-36.

[59] Harper, K., 2019. Alexander bain's mind and body (1872): An underappreciated contribution to early neuropsychology. Journal of the History of the Behavioral Sciences, 55(2), pp.139-160

[60] Borck, C., 2017. Vital brains: On the entanglement of media, minds, and models. Progress in Brain Research, 233, pp.1-24.

[61] Klonowski, W., 2016. Fractal analysis of electroencephalographic time series (eeg signals). In The fractal geometry of the brain (pp. 413-429). Springer, New York, NY.

[62] Walker, A.J. and Mashour, G.A., 2008. A brief history of sleep and anesthesia. International Anesthesiology Clinics, 46(3), pp.1-10.

[63] Atasoy, S., Vohryzek, J., Deco, G., Carhart-Harris, R.L. and Kringelbach, M.L., 2018. Common neural signatures of psychedelics: frequency-specific energy changes and repertoire expansion revealed using connectome-harmonic decomposition. Progress in Brain Research, 242, pp.97-120.

[64] Minati, L., 2006, June. Neuroimaging techniques: A conceptual overview of physical principles, contribution and history. In AIP Conference Proceedings (Vol. 839, No. 1, pp. 503-519). American Institute of Physics.

[65] Al-Kadi, M.I., Reaz, M.B.I. and Ali, M.A.M., 2013. Evolution of electroencephalogram signal analysis techniques during anesthesia. Sensors, 13(5), pp.6605-6635.

[66] Moreira, T., 2000. Translation, difference and ontological fluidity: Cerebral angiography and neurosurgical practice (1926-45). Social Studies of Science, 30(3), pp.421-446.

[67] Al-Kadi, M.I., Reaz, M.B.I. and Ali, M.A.M., 2013. Evolution of electroencephalogram signal analysis techniques during anesthesia. Sensors, 13(5), pp.6605-6635.

[68] Rao, V.P., Puwakpitiyage, C.H., Azizi, M.M., Tee, W.J., Murugesan, R.K. and Hamzah, M.D., 2018, October. Emotion recognition in e-commerce activities using eeg-based brain computer interface. In 2018 Fourth International Conference on Advances in Computing, Communication & Automation (ICACCA) (pp. 1-5). IEEE.

[69] Liu, J., Billings, S.A., Zhu, Z.Q. and Shen, J., 2002. Enhanced frequency analysis using wavelets. International Journal of Control, 75(15), pp.1145-1158.

[70] Arthur, N. and Penman, J., 1998. Condition monitoring with non-linear signal processing.

[71] Coelho, A.L. and Lima, C.A., 2014. Assessing fractal dimension methods as feature extractors for EMG signal classification. Engineering Applications of Artificial Intelligence, 36, pp.81-98.

[72] Farshchi, S.M. and Fard, A.J., 2011. RETRACTED: A Novel Fractal Approach for Persian/Arabic Identification based on Handwriting Recognition. Journal of Computer Science, 7(4), p.543.

[73] Gu, Q. and Zhou, J., 2009, April. Regular simplex criterion: A novel feature extraction criterion. In 2009 IEEE International Conference on Acoustics, Speech and Signal Processing (pp. 1581-1584). IEEE.

[74] Mustafa, Z.A., Abrahim, B.A. and Kadah, Y.M., 2012, April. K11. Modified Hybrid Median filter for image denoising. In 2012 29th National Radio Science Conference (NRSC) (pp. 705-712). IEEE.

[75] Reaz, M.B.I., Hussain, M.S. and Mohd-Yasin, F., 2006. Techniques of EMG signal analysis: detection, processing, classification and applications. Biological procedures online, 8(1), pp.11-35.

[76] Howe, T., Petterson, T., Smith, G., Tallis, R. and Oldham, J., 1993. Electrotherapy for muscles: time for a new start? Clinical rehabilitation, 7(1), pp.73-77.

[77] Sadikoglu, F., Kavalcioglu, C. and Dagman, B., 2017. Electromyogram (EMG) signal detection, classification of EMG signals and diagnosis of neuropathy muscle disease. Procedia computer science, 120, pp.422-429.

[78] Knaflitz, M. and Balestra, G., 1991. Computer analysis of the myoelectric signal. IEEE Micro, 11(5), pp.12-15.

[79] Gupta, S.D., Al Yusuf, S., Ammar, J.K. and Hasan, K., 2012, August. An analysis to generate EMG signal and its perspective: A panoramic approach. In 2012 International Conference on Advances in Power Conversion and Energy Technologies (APCET) (pp. 1-5). IEEE.

[80] Gupta, S.D., Al Yusuf, S., Ammar, J.K. and Hasan, K., 2012, August. An analysis to generate EMG signal and its perspective: A panoramic approach. In 2012 International Conference on Advances in Power Conversion and Energy Technologies (APCET) (pp. 1-5). IEEE.

[81] Russo, A., 2016. Kim's dilemma: why mental causation is not productive. Synthese, 193(7), pp.2185-2203.

[82] Farley, A., Johnstone, C., Hendry, C. and McLafferty, E., 2014. Nervous system: part 1. Nursing standard, 28(31).

[83] Zhao, Y., Malik, N. and Westphal, H., 2006. Functions of LIM-homeodomain proteins in the development of the nervous system. Transcription Factors in the Nervous System, pp.75-94.

[84] VanWessum, R., Sloet van Oldruitenborgh-Oosterbaan, M.M. and Clayton, H.M., 1999. Electromyography in the horse in veterinary medicine and in veterinary research a review. Veterinary quarterly, 21(1), pp.3-7.

[85] Gideiri, Y.A., 1971. The development of locomotory mechanisms in Bufo regularis. Behaviour, pp.121-131.

[86] Messa, G.A., Piasecki, M., Rittweger, J., McPhee, J.S., Koltai, E., Radak, Z., Simunic, B., Heinonen, A., Suominen, H., Korhonen, M.T. and Degens, H., 2020. Absence of an aging-related increase in fiber type grouping in athletes and non-athletes. Scandinavian journal of medicine & science in sports, 30(11), pp.2057-2069.

[87] Wakeling, J.M. and Rozitis, A.I., 2004. Spectral properties of myoelectric signals from different motor units in the leg extensor muscles. Journal of Experimental Biology, 207(14), pp.2519-2528.

[88] Yeung, S.S. and Evans, O., 1998. Relationships of vibromyographic and electromyographic signals during isometric voluntary contraction. Physiotherapy, 84(11), pp.541-546.

[89] LeFever, R.S., Xenakis, A.P. and De Luca, C.J., 1982. A procedure for decomposing the myoelectric signal into its constituent action potentials-part II: execution and test for accuracy. IEEE transactions on biomedical engineering, (3), pp.158-164.

[90] Wheeler, K., Kumar, D.K., Shimada, H. and Weghorn, H., 2011, January. Implementing a surface EMG model with accurate parameters and a force output. In ISSNIP Biosignals and Biorobotics Conference 2011 (pp. 1-5). IEEE.

[91] Rota, S., Hautier, C., Creveaux, T., Champely, S., Guillot, A. and Rogowski, I., 2012. Relationship between muscle coordination and forehand drive velocity in tennis. Journal of electromyography and kinesiology, 22(2), pp.294-300.

[92] Turpin, N.A. and Watier, B., 2020. Cycling biomechanics and its relationship to performance. Applied Sciences, 10(12), p.4112.

[93] Reaz, M.B.I., Hussain, M.S. and Mohd-Yasin, F., 2006. Techniques of EMG signal analysis: detection, processing, classification and applications. Biological procedures online, 8(1), pp.11-35.

[94] Gokgoz, E. and Subasi, A., 2014. Effect of multiscale PCA de-noising on EMG signal classification for diagnosis of neuromuscular disorders. Journal of medical systems, 38(4), pp.1-10.

[95] Reaz, M.B.I., Hussain, M.S. and Mohd-Yasin, F., 2006. Techniques of EMG signal analysis: detection, processing, classification and applications. Biological procedures online, 8(1), pp.11-35.

[96] Chowdhury, R.H., Reaz, M.B., Ali, M.A.B.M., Bakar, A.A., Chellappan, K. and Chang, T.G., 2013. Surface electromyography signal processing and classification techniques. Sensors, 13(9), pp.12431-12466.

[97] Reaz, M.B.I., Hussain, M.S. and Mohd-Yasin, F., 2006. Techniques of EMG signal analysis: detection, processing, classification and applications. Biological procedures online, 8(1), pp.11-35.

[98] James, C.J., Jones, R.D., Bones, P.J. and Carroll, G.J., 1996. The self-organising feature map in the detection of epileptiform transients in the EEG. In Proceedings of 18th Annual International Conference of the IEEE Engineering in Medicine and Biology Society (Vol. 3, pp. 913-914). IEEE.

[99] Banica, F.G., 2012. Chemical sensors and biosensors: fundamentals and applications. John Wiley & Sons.

[100] Gordon, M., 1980. Artifacts created by imbalanced electrode impedance. American Journal of EEG Technology, 20(4), pp.149-160.

[101] Young, J.J., Friedman, J.S., Oxley, T.J., Palmese, C., Panov, F., Ghatan, S., Fifi, J.T. and Marcuse, L.V., 2018. Intracarotid amobarbital disrupts synchronous and nested oscillatory activity ipsilateral to injection. Epilepsy & behavior case reports, 10, pp.25-28.

[102] Luo, H., Ni, J.T., Li, Z.H., Li, X.O., Zhang, D.R., Zeng, F.G. and Chen, L., 2006. Opposite patterns of hemisphere dominance for early auditory processing of lexical tones and consonants. Proceedings of the National Academy of Sciences, 103(51), pp.19558-19563.

[103] Gargiulo, G., Bifulco, P., Calvo, R.A., Cesarelli, M., Jin, C., McEwan, A. and Van Schaik, A., 2010. Non-invasive electronic biosensor circuits and systems. Intelligent and biosensors.

[104] Mutz, J., Vipulananthan, V., Carter, B., Hurlemann, R., Fu, C.H. and Young, A.H., 2019. Comparative efficacy and acceptability of non-surgical brain stimulation for the acute treatment of major depressive episodes in adults: systematic review and network meta-analysis. bmj, 364.

[105] Lee, W.R., 1970. The hazard of electrocution during patient monitoring. Postgraduate Medical Journal, 46(536), p.355.

[106] Karagiannis, A., Constantinou, P. and Vouyioukas, D., 2011. Biomedical time series processing and analysis methods: the case of empirical mode decomposition. In Advanced Biomedical Engineering. IntechOpen.

[107] Li, J., Yu, B., Zhao, W. and Chen, W., 2014. A review of signal enhancement and noise reduction techniques for tunable diode laser absorption spectroscopy. Applied Spectroscopy Reviews, 49(8), pp.666-691.

[108] Shapley, R. and Lennie, P., 1985. Spatial frequency analysis in the visual system. Annual review of neuroscience, 8(1), pp.547-581.

[109] Hamarsheh, M.M., Abdullah, M.K., Mahdi, M.A., Khatun, S. and Shalaby, H.M., 2005, November. Dynamic optical code division multiple access communication system analysis and performance enhancement by signal clipping. In 2005 1st International Conference on

Computers, Communications, & Signal Processing with Special Track on Biomedical Engineering (pp. 125-129). IEEE.

[110] Shi, W., Johansson, C. and Sundbäck, U., 1997. An investigation of the characteristics of impact sound sources for impact sound insulation measurement. Applied Acoustics, 51(1), pp.85-108.

[111] Lokesha, M., Majumder, M.C., Ramachandran, K.P. and Raheem, K.F.A., 2011. Fault diagnosis in gear using wavelet envelope power spectrum. International Journal of Engineering, Science and Technology, 3(8), pp.156-167.

[112] Gentile, A. and Messina, A., 2003. On the continuous wavelet transforms applied to discrete vibrational data for detecting open cracks in damaged beams. International Journal of Solids and Structures, 40(2), pp.295-315

[113] Domínguez, R. and Muñoz, R., 1999, October. Myoelectric patterns identification using wavelets. In *Proceedings of the First Joint BMES/EMBS Conference. 1999 IEEE Engineering in Medicine and Biology 21st Annual Conference and the 1999 Annual Fall Meeting of the Biomedical Engineering Society (Cat. N* (Vol. 2, pp. 964-vol). IEEE.

[114] Yu, I.K. and Song, Y.H., 1998. Wavelet transform and neural network approach to developing adaptive single-pole auto-reclosing schemes for EHV transmission systems. IEEE Power Engineering Review, 18(11), pp.62-64.

[115] Truchetet, F. and Laligant, O., 2008. Review of industrial applications of wavelet and multiresolution-based signal and image processing. Journal of Electronic Imaging, 17(3), p.031102.

[116] Aram, P., Freestone, D.R., Dewar, M., Scerri, K., Jirsa, V., Grayden, D.B. and Kadirkamanathan, V., 2013. Spatiotemporal multi-resolution approximation of the Amari type neural field model. Neuroimage, 66, pp.88-102.

[117] Sweldens, W. and Piessens, R., 1993. Calculation of the wavelet decomposition using quadrature formulae. In Wavelets: an elementary treatment of theory and applications (pp. 139-160).

[118] Sweldens, W. and Piessens, R., 1993. Calculation of the wavelet decomposition using quadrature formulae. In Wavelets: an elementary treatment of theory and applications (pp. 139-160).

[119] Wang, L., Xue, W., Li, Y., Luo, M., Huang, J., Cui, W. and Huang, C., 2017. Automatic epileptic seizure detection in EEG signals using multi-domain feature extraction and nonlinear analysis. Entropy, 19(6), p.222.

[120] Majumder, B., Das, S., Pan, I., Das, S. and Gupta, A., 2011, March. Denoising SPND signal by discrete wavelet analysis for efficient power feedback in regulating system of PHWRs under noisy environment. In 2011 2nd National Conference on Emerging Trends and Applications in Computer Science (pp. 1-5). IEEE.

[121] Sharbati, R., Khoshnoudian, F., Koopialipoor, M. and Tahir, M.M., 2021. Applying dual-tree complex discrete wavelet transform and gamma modulating function for simulation of ground motions. Engineering with Computers, 37(2), pp.1519-1535.

[122] Al-kadi, M.I., Reaz, M.B.I. and Ali, M.M., 2012, December. Compatibility of mother wavelet functions with the electroencephalographic signal. In 2012 IEEE-EMBS Conference on Biomedical Engineering and Sciences (pp. 113-117). IEEE.

[123] Kaur, C. and Singh, P., 2017. Toward EEG spectral analysis of tomographic neurofeedback for depression. In Proceeding of International Conference on Intelligent Communication, Control and Devices (pp. 97-103). Springer, Singapore.

[124] Dingli, K., Assimakopoulos, T., Fietze, I., Witt, C., Wraith, P.K. and Douglas, N.J., 2002. Electroencephalographic spectral analysis: detection of cortical activity changes in sleep apnoea patients. European Respiratory Journal, 20(5), pp.1246-1253.

[125] Kesić, S. and Spasić, S.Z., 2016. Application of Higuchi's fractal dimension from basic to clinical neurophysiology: a review. Computer methods and programs in biomedicine, 133, pp.55-70.

[126] Parbat, D. and Chakraborty, M., 2021. A novel methodology to study the cognitive load induced eeg complexity changes: Chaos, fractal and entropy-based approach. *Biomedical Signal Processing and Control*, *64*, p.102277.

[127] Parbat, D. and Chakraborty, M., 2021. A novel methodology to study the cognitive load induced eeg complexity changes: Chaos, fractal and entropy-based approach. *Biomedical Signal Processing and Control*, *64*, p.102277.

[128] Lin, B., Wong, S.F. and Baca, A., 2018. Comparison of Different Time-Frequency Analyses Techniques Based on sEMG-Signals in Table Tennis: A Case Study. International Journal of Computer Science in Sport, 17(1), pp.77-93.

[129] Dey, N., Dey, G., Chakraborty, S. and Chaudhuri, S.S., 2014. Feature analysis of blind watermarked electromyogram signal in wireless telemonitoring. In Concepts and trends in healthcare information systems (pp. 205-229). Springer, Cham.

[130] Parbat, D. and Chakraborty, M., 2021. A novel methodology to study the cognitive load induced eeg complexity changes: Chaos, fractal and entropy-based approach. *Biomedical Signal Processing and Control*, *64*, p.102277.